ISTANBUL TECHNICAL UNIVERSITY ★ GRADUATE SCHOOL OF SCIENCE ENGINEERING AND TECHNOLOGY

NON-ORTHOGONAL MULTI-CARRIER MODULATION SCHEMES FOR FUTURE WIRELESS COMMUNICATION SYSTEMS

Ph.D. THESIS

Ersin ÖZTÜRK

Electronics and Communications Engineering Department

Telecommunications Engineering Programme

JANUARY 2019

ISTANBUL TECHNICAL UNIVERSITY ★ GRADUATE SCHOOL OF SCIENCE ENGINEERING AND TECHNOLOGY

NON-ORTHOGONAL MULTI-CARRIER MODULATION SCHEMES FOR FUTURE WIRELESS COMMUNICATION SYSTEMS

Ph.D. THESIS

Ersin ÖZTÜRK
(504112302)

Electronics and Communications Engineering Department

Telecommunications Engineering Programme

Thesis Advisor: Prof. Dr. Hakan Ali ÇIRPAN

JANUARY 2019

İSTANBUL TEKNİK ÜNİVERSİTESİ ★ FEN BİLİMLERİ ENSTİTÜSÜ

GELECEK NESİL TELSİZ HABERLEŞME SİSTEMLERİ İÇİN ORTOGONAL OLMAYAN ÇOK TAŞIYICILI MODÜLASYON YAPILARI

DOKTORA TEZİ

Ersin ÖZTÜRK
(504112302)

Elektronik ve Haberleşme Mühendisliği Anabilim Dalı

Telekomünikasyon Mühendisliği Programı

Tez Danışmanı: Prof. Dr. Hakan Ali ÇIRPAN

OCAK 2019

Ersin ÖZTÜRK, a Ph.D. student of ITU Graduate School of Science Engineering and Technology 504112302 successfully defended the thesis entitled "NON-ORTHOGONAL MULTI-CARRIER MODULATION SCHEMES FOR FUTURE WIRELESS COMMUNICATION SYSTEMS", which he/she prepared after fulfilling the requirements specified in the associated legislations, before the jury whose signatures are below.

Thesis Advisor :	**Prof. Dr. Hakan Ali ÇIRPAN** Istanbul Technical University	.....
Jury Members :	**Doç. Dr. Güneş Z. KARABULUT KURT** Istanbul Technical University	.....
	Prof. Dr. İbrahim ALTUNBAŞ Istanbul Technical University	.....
	Prof. Dr. Hüseyin ARSLAN Medipol University	.....
	Doç. Dr. Ertuğrul BAŞAR Koç University	.....

Date of Submission : **10 December 2018**
Date of Defense : **11 January 2019**

To my spouse and children,

FOREWORD

The work presented in this thesis was conducted during my Ph.D. study at Telecommunication Engineering Program of Electronics and Communication Engineering Department in Istanbul Technical University Graduate School of Science Engineering and Technology. I would like to take this opportunity to acknowledge all the people who have supported me.

First and foremost, I would like to express my gratitude to my supervisor Prof. Dr. Hakan Ali ÇIRPAN for giving me a chance to be a doctoral student. I greatly appreciate his excellent guidance, trust and support during my doctoral process. I also want to express my gratitude to Doç. Dr. Ertuğrul BAŞAR for steering me into this interesting research topic and continuous support throughout this research work. I am grateful to him for his generosity in sharing his expertise and time in our frequent discussions. I would like to thank Prof. Dr. Hüseyin ARSLAN for encouraging me to work in this challenging research area and helping me to build a strong research mindset with his continuous pushing and high expectations along with valuable feedbacks and contributions. I would also like to thank Doç. Dr. Güneş Zeynep KARABULUT KURT for her valuable feedbacks and contributions which inspire me with new ideas. Furthermore, I would like to thank NETAŞ for their support. Last, but not least, I want to express my utmost gratitude to my family.

The studies conducted in this thesis have been published as two international journal papers and three international conference papers. In addition, one US patent application and one international journal paper were submitted. The proposed techniques in this thesis have recently attracted significant attention from the researchers and these mentioned papers got more than thirty citations in two years.

I hope that this thesis would be helpful to researchers working on non-orthogonal multicarrier modulation schemes.

January 2019 Ersin ÖZTÜRK

TABLE OF CONTENTS

Page

ABBREVIATIONS

1G	**:** First Generation
2G	**:** Second Generation
3G	**:** Third Generation
3GPP	**:** Third Generation Partnership Project
4G	**:** Fourth Generation
5G	**:** Fifth Generation
AWGN	**:** Additive White Gaussion Noise Channel
BER	**:** Bit Error Ratio
BLAST	**:** Bell Laboratories Layered Space-Time
BLER	**:** Block Error Rate
BPSK	**:** Binary Phase Shift Keying
ceCPM-SC	**:** Constraint Envelope Continuous Phase Modulation-Single Carrier
cFBMC	**:** Circular Filterbank Multicarrier
CFO	**:** Carrier Frequency Offset
CM	**:** Complex Multiplication
CP	**:** Cyclic Prefix
CPEP	**:** Conditional Pairwise Error Probability
CPM-SC-FDMA	**:** Continuous Phase Modulation-Single Carrier-Frequency Division Multiple Access
D-QAM-SC	**:** Differentail-Quadrature Amplitude Modulation-Single Carrier
DFT	**:** Discrete Fourier Transform
DMIM	**:** Dual Mode Index Modulation
EM	**:** Electramagnetic
EPA	**:** Extended Pedestrian A
f-DFT-S-OFDM	**:** Filtered-Discrete Fourier Transform-Spread-Orthogonal Frequency Division Multiplexing
f-OFDM	**:** Filtered-Orthogonal Frequency Division Multiplexing
FBMC	**:** Filter Bank Multicarrier
FCP-OFDM	**:** Flexible Cyclic Prefix-Orthogonal Frequency Division Multiplexing
FDE	**:** Frequency Domain Equalization
FFT	**:** Fast Fourier Transform
FIM	**:** Flexible Index Modulation
GFDM	**:** Generalized Frequency Division Multiplexing
GT	**:** Guard Time
IAI	**:** Inter-Antenna Interference
IAS	**:** Inter-Antenna Synchronization
ICI	**:** Inter-Carrier Interference
IFFT	**:** Inverse Fast Fourier Transform
IM	**:** Index Modulation
ITU	**:** International Telecommunication Union

JDD : Joint Detection and Demodulation
LLR : Log Likelihood Ratio
LOS : Line of Sight
MF : Matched-Filter
MIMO : Multiple-Input Multiple-Output
ML : Maximum Likelihood
MMSE : Minimum Mean-Squared Error
MMSE-QRD : Minimum Mean-Squared Error-Bell Laboratories Layered Space-Time with QR Decomposition
mTC : Machine Type Communications
NOMA : Non-Orthogonal Multiple Access
OFDM : Orthogonal Frequency Division Multiplexing
OFDM-IM : Orthogonal Frequency Division Multiplexing with Index Modulation
OOB : Out-of-Band
P-OFDM : Pulse-Shaped Orthogonal Frequency Division Multiplexing
PA : Power Amplifier
PAM : Pulse Amplitude Modulation
PAPR : Peak-to-Average Power Ratio
PEP : Pairwise Error Probability
PHY : Physical Layer
PIC : Parallel Interference Cancellation
PRB-ZT-DFT-S-OFDM : Physical Resource Block-Specific Zero Tail-Discrete Fourier Transform Spread-Orthogonal Frequency Division Multiplexing
PRCC : Phase Rotated Conjugate Cancellation
PSK : Phase Shift Keying
Q-QAM : Q-ary Quadrature Amplitude Modulation
QAM : Quadrature Amplitude Modulation
QRD : QR Decomposition
QSFDMIM : Quadrature Space Frequency Dual Mode Index Modulation
QSFIM : Quadrature Space Frequency Index Modulation
QSM : Quadrature Spatial Modulation
RAT : Radio Access Technology
RC : Raised Cosine
RF : Radio Frequency
S/P : Serial-to-Parallel
SC-FDE : Single Carrier Frequency Domain Equalization
SC-FDM : Single Carrier Frequency Domain Multiplexing
SD : Sphere Decoding
SDD : Separate Detection and Demodulation
SFDMIM : Space and Frequency Dual Mode Index Modulation
SFIM : Space and Frequency Index Modulation
SIC : Successive Interference Cancellation
SISO : Single-Input Single-Output
SM : Spatial Modulation
SMX : Spatial Multiplexing
SNR : Signal-to-Noise Ratio

SSK : Space-Shift Keying
STC : Space-Time Coding
STSK : Space-Time Shift Keying
UF-OFDM : Universal Filtered-Orthogonal Frequency Division Multiplexing
UFMC : Universal Filtered Multicarrier
UPEP : Unconditional Pairwise Error Probability
US : United States
UW : Unique Word
UW-DFT-S-OFDM : Unique-Word Discrete Fourier Transform-Spread-Orthogonal Frequency Division Multiplexing
UW-DFT-S-W-OFDM : Unique Word Discrete Fourier Transform Spread Windowed Orthogonal Frequency Division Multiplexing
UW-OFDM : Unique-Word Orthogonal Frequency Division Multiplexing
V-BLAST : Vertical-Bell Laboratories Layered Space-Time
W-DFT-S-OFDM : Windowed-Discrete Fourier Transform-Spread-Orthogonal Frequency Division Multiplexing
W-OFDM : Windowed-Orthogonal Frequency Division Multiplexing
WRAN : Wireless Regional Area Networks
ZF : Zero-Forcing
ZF-QRD : Zero-Forcing Bell Laboratories Layered Space-Time with QR Decomposition
ZT-DFT-S-OFDM : Zero-Tail Discrete Fourier Transform-Spread-Orthogonal Frequency Division Multiplexing

SYMBOLS

$(\cdot)^{\mathbf{T}}$	: Transposition of a vector or a matrix
$(\cdot)^{\mathbf{H}}$	: Hermitian transposition of a vector or a matrix
$(\cdot)^{-1}$	: Inverse of a matrix
$(\cdot)^{+}$	: Pseudo-inverse of a matrix
$C(u,v)$	: The binomial coefficient
$\lfloor \cdot \rfloor$	: The floor function
$\Re\{X\}$	: The real part of a complex variable X
$\Im\{X\}$	: The imaginary part of a complex variable X
$\mathrm{diag}(\cdot)$	: A diagonal matrix
$\|\cdot\|$	: The Euclidean norm
$\|\cdot\|_F$	: The Frobenius norm
$\mathscr{S}$	: Q-ary signal constellation
$\mathbf{x}(a:b)$	: All elements of $\mathbf{x}$ with indices from a to b, inclusive of a and b
$N_{\mathbf{CP}}$	: Length of cyclic prefix
$N_{\mathbf{Ch}}$	: Tap length of the communication channel
E_b	: The average transmitted energy per bit
E_s	: The average transmitted energy per symbol
N_0	: The noise power spectral density
B	: The channel bandwidth
$QR(\cdot)$	: QR decomposition
$\mathbf{X} \sim \mathscr{CN}(0, \sigma_X^2)$	: The distribution of a circularly symmetric complex Gaussian random variable $\mathbf{X}$ with variance σ_X^2
$\mathbf{I}_T$	: A $T \times T$ identity matrix
$\mathbf{mod}(\mu, \nu)$	: The modulo of μ with respect to ν
$\sim \mathscr{O}$	: Order of magnitude
$A \cap B$	: The intersection of two sets A and B
$\varnothing$	: The empty set

LIST OF TABLES

Page

LIST OF FIGURES

Page

NON-ORTHOGONAL MULTI-CARRIER MODULATION SCHEMES FOR FUTURE WIRELESS COMMUNICATION SYSTEMS

SUMMARY

The demand for wireless access continues to grow with the new applications which create a broad range of technical challenges. Although orthogonal frequency division multiplexing (OFDM) with multiple numerologies concept will likely address the current technical challenges of fifth generation (5G) wireless networks, the sufficiency of OFDM-based physical layer (PHY) is quite disputable due to massive growth trend on the number of wireless users and applications for future wireless networks. Therefore, enhanced radio access technologies (RATs) are needed to fulfill the technical requirements of beyond 5G networks. Generalized frequency division multiplexing (GFDM), which has attracted tremendous attention over the past few years, comes into prominence by providing advantages in terms of out-of-band (OOB) emission, spectral efficiency and latency due to digitally pulse shaping of each subcarrier, reduced overhead of cyclic prefix and block-based structure, respectively. Index modulation (IM) techniques convey digital information by utilizing transmission entities in an innovative way and offer attractive advantages such as energy and spectral efficiency without increasing the computational complexity. On the other hand, multiple-input multiple-output (MIMO)-friendliness is a key ability for a PHY scheme to satisfactorily match the foreseen requirements of future wireless networks. Therefore, tight integration of GFDM with the MIMO and IM concepts has a strong potential to fulfill the foreseen requirements of future wireless networks in a satisfactory manner. In the light of these assessments, in this thesis, the combination of MIMO and IM techniques with GFDM has been investigated and novel transceiver structures have been introduced. These transceiver structures has been optimized in terms of energy, spectral and computational efficiency.

In the first stage of the thesis, the combination of the IM technique with GFDM is investigated. The GFDM-IM system model is constructed and flexible IM numerology along with the near-optimum detector is proposed to improve OOB emission, error performance and computational complexity of the GFDM scheme. The main contribution of this stage is the combination of GFDM with IM about to provide coding gain due to enhanced distance spectrum of IM. In addition, in order to optimize OOB emission, spectral efficiency and latency jointly, sparse IM numerology is applied to the edge GFDM subsymbols. To the best of author's knowledge, this application would be the first attempt to exploit variable-sized IM subblocks with variable number of active subcarriers for GFDM. Besides, in order to enhance the error performance and reduce the computational complexity of the scheme, a new detector, which adapts a maximum likelihood (ML)-successive interference cancellation (SIC) based near-optimum detection, is developed for the single-input single-output (SISO) GFDM scheme considering the flexible IM numerology, and its theoretical error performance is analyzed. Furthermore, a new system model, which enables multi-layer

transmission through IM-bits and quadrature amplitude modulation (QAM)-bits, is presented. Thanks to this system model, the proposed scheme provides different error performances and spectral efficiencies for QAM and IM bits, and further benefits from enhanced distance spectrum of IM. The block error rate (BLER), OOB emission and computational complexity of the proposed GFDM-IM scheme are evaluated via computer simulations. It has been shown that the proposed GFDM-IM scheme achieves better error performance due to joint detection, GFDM and IM demodulation, and provides an interesting trade-off among OOB emission, spectral efficiency and latency.

In the second stage of the thesis, the integration of GFDM with space and frequency IM (SFIM) techniques is discussed in detail and a framework for the combination of GFDM with IM concept is presented. Then, by using this framework, a GFDM-based flexible IM (FIM) transceiver, which is capable of generating and decoding various IM schemes, is proposed. Thanks to FIM, switching between different IM schemes to adapt the channel conditions can be possible using a single transceiver structure. As a special case of FIM, a novel quadrature spatial modulation (QSM)-based GFDM scheme is proposed to enhance the spectral efficiency while preserving the advantages of spatial modulation (SM). To the best of author's knowledge, this contribution would be the first approach that exploits multi-carrier transmission for QSM. In addition, QSM transmission is combined with the SFIM scheme. For the receiver side, a near-optimum detection scheme, which is based on ML detection with SIC, is proposed and three different receiver structures using ML-SIC, zero-forced (ZF)-separate detection and demodulation (SDD) and minimum mean-squared error (MMSE) joint detection and demodulation (JDD) detectors are investigated. Bit error ratio (BER) performances of the proposed schemes are compared and their computational complexities and spectral efficiencies are analyzed. Based on the obtained results, a guideline for selecting the proper MIMO-GFDM scheme considering target performance criterion is given. It has been shown that GFDM-FIM has a strong potential to engineer the space-frequency structure according to channel conditions and use cases as well as it provides a great flexibility, which can be easily tuned to address the required performance criterion.

In the third stage of the thesis, a novel MIMO-GFDM scheme, which combines spatial multiplexing (SMX), GFDM and IM, is proposed in order to provide an efficient transmission scheme for beyond 5G wireless networks. The proposed scheme transmits independent GFDM-IM blocks through each transmit antenna and adapts MMSE Bell Laboratories Layered Space-Time (BLAST) with QR decomposition (MMSE-QRD)-based near-optimum detector at the receiver side. To the best of author's knowledge, this application would be the first attempt to exploit a near-optimum detector with SMX-GFDM-IM system. We analyze the uncoded and coded BER, OOB emission, spectral efficiency and computational complexity of the proposed scheme by comparing with classical SMX-OFDM and SMX-GFDM schemes via computer simulations. It has been demonstrated that the proposed SMX-GFDM-IM scheme achieves better error performance with respect to classical SMX-OFDM and SMX-GFDM schemes and has a lower OOB emission and better spectral efficiency advantages with respect to SMX-OFDM scheme because of digitally pulse shaping of each subcarrier and reduced overhead of cyclic prefix.

GFDM has a flexible structure which permits efficient management of time and frequency resources and is a prominent PHY technique due to its significant advantages such as low OOB emission, tolerance to time and frequency synchronization errors. In this thesis, the combination of GFDM with IM, SM and SMX has been demonstrated. Thanks to studies conducted during this thesis, GFDM has gained spectral and energy efficiency while preserving its inherent advantages. As a result, it has been considered that GFDM becomes a strong PHY candidate for future wireless networks.

GELECEK NESİL TELSİZ HABERLEŞME SİSTEMLERİ İÇİN ORTOGONAL OLMAYAN ÇOK TAŞIYICILI MODÜLASYON YAPILARI

ÖZET

Telsiz haberleşmeye olan talep, oldukça geniş bir kapsamda teknik açıdan zorluklara sahip yeni uygulamalar ile artmaya devam etmektedir. Her ne kadar çoklu parametre kümesine sahip dik frekans bölmeli çogullama (orthogonal frequency division multiplexing, OFDM) tabanlı bir fiziksel katman ile 5. nesil telsiz haberleşme ağlarının mevcut teknik zorluklarının karşılanacağı öngörülse de, telsiz haberleşme kullanıcıları ve uygulamaları sayılarında görülen sürekli ve yoğun artış eğilimi nedeniyle OFDM tabanlı bir fiziksel katmanın yeterliliği çok kuşkuludur. Bu nedenden dolayı 5. nesil sonrası telsiz haberleşme ağlarının teknik gereksinimlerini karşılamak için gelişmiş radyo erişim teknolojilerine ihtiyaç olduğu konusunda yaygın bir uzlaşı bulunmaktadır.

5. nesil ve sonrası ağlarda, tüm iletişim prosedürlerini yapısal olarak etkileyecek bazı yeni kullanım senaryoları öne çıkmaktadır. Bu kullanım senaryoları içinde en çok dikkat çekeni makineler arası iletişimdir. Bu yeni kavram ile şimdiye kadar insanlar arası iletişim merkezli olarak gelişen iletişim ağları artık makineler arası iletişim merkezli olarak da hizmet verebilecek şekilde tasarlanmak durumundadır. Makineler arası iletişimin tüm ağ yapılarını derinden etkileyecek bazı gereksinimleri bulunmaktadır. Enerji verimliliğini sağlayacak şekilde kısa ve eşzamanlamasız iletim bu gereksinimlerin en belirgin olanları arasında yer almaktadır. Makineler arası iletişimin bilhassa bu gereksinimleri nedeniyle şimdiye kadar yaygın olarak kullanılan ortogonal ve eş zamanlamalı çok taşıyıcılı iletim tekniklerinden, ortogonal olmayan ve eşzamanlamasız çalışan çok taşıyıcılı iletim tekniklerine doğru bir paradigma kayması yaşanmaktadır. Bununla birlikte ortogonal olmayan çok taşıyıcılı iletim tekniklerinin bir radyo iletişim teknolojisi olarak yerini alabilmesi için vericiden alıcıya değin her aşamada kapsamlı ve yoğun geliştirme ve optimizasyon çalışmalarının yapılmasına ihtiyaç duyulmaktadır.

Genelleştirilmiş Frekans Bölmeli Çoğullama (Generalized Frequency Division Multiplexing (GFDM), son yıllarda öne çıkmış ortogonal olmayan bir çok taşıyıcılı fiziksel katman tekniğidir. Özellikle gelecek nesil telsiz iletişim ağlarının gereksinimlerini karşılamada avantaj sağlayabilecek özellikleri nedeniyle araştırmacıların çok ilgisini çekmiştir. Bir GFDM sembolünde OFDM'e benzer olarak K adet alt taşıyıcı yer alır. Ancak OFDM'den farklı olarak her bir alt taşıyıcı üzerinde birden fazla olabilmek üzere M adet zaman dilimi (timeslot) yer almasına izin verilir. Böylelikle bir GFDM sembolü KM adet örnek içermiş olur. Tüm alt taşıycıların aynı numaralı zaman dilimleri bir GFDM alt sembolünü oluşturur. K ve M parametreleri uygulamanın gereksinimlerine göre ayarlanabilir. Özellikle iletim gecikmesinin azaltılması konusunda avantaj sağlayabilecek bu özellik sayesinde GFDM sembolü hedef uygulamaya göre zaman-frekans kaynağı planlamasının yapılabilmesine olanak sağlar. GFDM'de her bir alt taşıyıcı çevrimsel katlama işlemi ile bir süzgeçten geçirilir. Bu sayede GFDM'in bant dışı (out-of-band, OOB) yayınımı azalır ve parçalı frekans

spektrumlarının kullanımında ve bilişsel radyo uygulamalarında avantajlı hale gelir. GFDM, KM adet örnekten oluşan bir sembol için tek bir çevrimsel önek (cyclic prefix, CP) kullanır. Çevrimsel önek kullanımı frekans domeni dengelemesinin (frequency domain equalization, FDE) kullanılabilmesini sağlar. KM adet örnek için tek bir çevrimsel önek kullanılması spektral verimliliği artırır. Bu nedenlerden dolayı GFDM esnek özellikleri sayesinde yeni gereksinimleri karşılamak üzere kolay bir şekilde uyum sağlayabilecek yapıdadır.

İndis Modülasyonu (index modulation, IM) geçtiğimiz birkaç yılda çok büyük ilgi görmüş, hem spektrum, hem de enerji kullanımı açılarından oldukça verimli, aynı zamanda da oldukça basit bir sayısal modülasyon tekniğidir. İndis modülasyonu kullanıldığı haberleşme sisteminin yapıtaşlarının indislerini ilave bilgi iletimi için kullanır. Bu sayede indis modülasyonu sistemleri, sinüzoidal bir taşıyıcının faz, frekans ve genlik bilgilerini değiştirmeye dayanan geleneksel sayısal modülasyon tekniklerine alternatif yollar yaratır. IM, anten, alt taşıyıcı, zaman dilimi gibi iletim elemanlarının iletim için kullanılıp kullanılmama durumlarına bilgi bitlerini eşleme yeteneğine sahiptir. Örneğin uzaysal modülasyonda (spatial modulation, SM) iletim antenlerinin kullanımına bilgi bitlerine göre karar verilir ve alıcı tarafta alınan bilgi sembolüne ilave olarak iletimde kullanılan antenin tespit edilmesi ile de bilgi taşınır. Uzaysal modülasyon, uzaysal çoğullama (spatial multiplexing, SMX) ve uzay-zaman blok kodlama (space-time block coding, STBC) ile birlikte en yaygın kullanılan çok girişli çok-çıkışlı (multiple-input multiple-output, MIMO) iletim tekniklerinden biridir. Alt taşıyıcı IM tekniğinde ise çok taşıyıcılı yapıda kullanılacak alt taşıyıcılara bilgi bitlerine göre karar verilir, iletimde bazı alt taşıyıcılar kullanılmaz. Bu örneklerden görüldüğü üzere IM bilgi iletimi için tamamıyla yeni bir boyut yaratır. IM, iletim elemanlarının indislerinin var/yok şeklinde bir mekanizma ile bilgi iletiminde kullanılması sayesinde kullanılmayan iletim elemanlarından tasarruf edilen iletim enerjisini kullanılan iletim elemanlarına aktarma yeteneğine sahiptir. Bu sayede aynı enerji miktarı ile geleneksel yapılara göre daha iyi bir hata başarımı etme olanağı oluşur. Bu nedenlerden dolayı IM yapıları donanımsal bir karmaşıklık getirmeden, spektral verimlilik, enerji verimliliği ve hata başarımını iyileştirme avantajlarına sahiptir.

İkinci nesil telsiz iletişim sistemleri ile başlayan veri iletimi, uygulamaların günümüze kadar sürekli artan veri hızı talepleri nedeniyle ses iletişiminin yanında en az onun kadar önemli bir iletişim uygulaması olarak yerini almıştır. Özellikle frekans spektrumu kapasitesindeki sınırlar nedeniyle artan veri hızı talebini karşılayabilmek için spektral verimliliği artırma tekniklerine yönelinmiştir. 90'lı yılların sonlarında araştırmacıların gündemine giren MIMO iletim, spektral verimliliği artırmak için vazgeçilemez bir teknik haline gelmiştir. Bu nedenle MIMO iletim teknikleri ile uyum içerisinde çalışabilmek yeni nesil fiziksel katman teknikleri için olmazsa olmaz bir gereklilik olarak karşımıza çıkmaktadır.

Bu tezde, sayıları ve çeşitleri hızla artan telsiz iletişim kullanıcıları ve uygulamaları nedeniyle, gelecek nesil telsiz iletişim sistemlerine yönelik olarak ortaya çıkan teknik gereksinimleri karşılamak üzere yenilikçi fiziksel katman teknikleri üzerinde çalışılmıştır. Bu gereksinimlere yönelik olarak önemli avantajlara sahip çok taşıyıcılı ortogonal olmayan dalga biçimleri araştırılmıştır. Bu dalga biçimleri içerisinde öne çıkan GFDM yapısının ortogonal olmaması nedeniyle verici ve alıcı yapılarında karşılaşılan problemlere çözümler oluşturmak üzere çalışılmıştır. Bu bağlamda GFDM

yapısının, sağladığı spektral verimliliği nedeniyle öne çıkan MIMO, spektral ve enerji verimliliği nedeniyle öne çıkan IM iletim teknikleri ile etkin ve verimli bir şekilde birleştirilmesi konusu derinlemesine ele alınmıştır. Yeni verici-alıcı yapıları önerilmiş ve bu yapılar, enerji verimliliği, spektral verimlilik, işlemsel karmaşıklık ve hata başarımları açılarından ele alınıp optimize edilmiştir.

Tezin ilk aşamasında alt taşıyıcı IM tekniği ile GFDM'in etkin ve verimli bir şekilde birleştirilmesi üzerine çalışılmıştır. GFDM ve IM tekniklerini tümleştirmek üzere bir sistem modeli oluşturulmuştur. Bu sistem modeli temel alınarak esnek IM numerolojisi ve alıcıda kullanılacak optimuma yakın bir algılayıcı tekniği, GFDM 'in bant dışı yayınım, işlem karmaşıklığı ve hata performanslarını iyileştirmek üzere önerilmiştir. Bu aşamanın temel amacı, IM tekniğinin iyileşmiş semboller arası uzaklık spektrumu dolayısıyla sağladığı kodlama kazancını GFDM'e kazandırmaktır. Bu çalışmada esnek IM numerolojisi ile kenar GFDM alt sembollerine seyrek IM numerolojisi uygulayarak bant dışı yayınım, spektral verimlilik ve gecikme arasında optimizasyon yapılabilmesini sağlayan bir mekanizma kurulmuştur. Bilindiği kadarıyla bu çalışma ile alt taşıyıcı IM tekniği ve GFDM ilk kez bir araya getirilmiştir. Bu çalışmanın diğer bir katkısı ise, hata başarımını iyileştirmek ve işlem karmaşıklığını azaltmak üzere, sıfıra zorlama (zero-forcing, ZF) tabanlı QR ayrıştırma sonrası en büyük olabilirlik (maximum likelihood, ML) ve ardışıl girişim yoketme (successive interference cancellation, SIC) tekniklerine dayanan optimuma yakın bir algılayıcının esnek IM numerolojisi dikkate alınarak tek-girişli tek-çıkışlı (single-input single-output, SISO) GFDM uygulaması için geliştirilmesidir. Geliştirilen bu algılayıcı için teorik hata başarımı analizi de gerçekleştirilmiştir. Bundan başka, IM tekniği ile iletimin ve klasik dik genlik modülasyonu (quadrature amplitude modulation, QAM) ile iletimin bağımsız katmanlar halinde ele alındığı, bu katmanlar üzerinden iletilecek bitlerin bağımsız olarak seçilebildiği bir iletim modeli sunulmuştur. Bu yeni iletim modeli sayesinde QAM ve IM bitleri için farklı hata başarımı ve spektral verimlilikleri sunulması ve IM tekniğinin gelişmiş semboller arası uzaklık spektrumundan daha fazla yararlanılması mümkün olmuştur. Önerilen GFDM-IM yapısının blok hata başarımı, bant dışı yayınımı ve işlem karmaşıklığı bilgisayar simülasyonları aracılığıyla değerlendirilmiştir. Teorik hata başarımı analizi sonuçları ile bilgisayar simülasyonu sonuçlarının uyumlu olduğu gözlenmiştir. Geliştirilen GFDM-IM yapısının OFDM ve OFDM-IM'e nazaran daha iyi hata başarımına sahip olduğu ve önerilen yapının bant dışı yayınım, spektral verimlilik ve gecikme arasında ilgi çekici ödünleşimler sağladığı gösterilmiştir.

Tezin ikinci aşamasında GFDM'in uzay ve frekans IM teknikleri (space and frequency index modulation, SFIM) ile tümleştirilmesi detaylı bir şekilde incelenmiş ve GFDM'in SM ve alt taşıyıcı IM tekniği ile birleştirilmesi için bir çerçeve yapı sunulmuştur. Ardından bu yapı kullanılarak pek çok farklı IM yapısını üretme yeteneğine sahip SM-GFDM-IM verici-alıcı sistemi tasarlanmıştır. Tasarlanan bu yapı sayesinde tek bir verici-alıcı yapısı ile kanal koşullarına uyum sağlamak üzere farklı IM yapıları arasında geçiş yapmak mümkün olmaktadır. Bu yapının diğer bir özelliği de uzay, frekans ve zaman boyutlarını verimli bir şekilde kullanan çok katmanlı bir yapı sağlaması ve bu boyutları aynı anda kullanarak farklı kullanım senaryolarına hizmet edebilecek bir mimariye sahip olmasıdır. Önerilen yapının bir uygulaması olarak, SM'in sağladığı avantajları muhafaza ederek spektral verimliliği artırmak üzere yeni bir Dik Uzaysal Modülasyon (quadrature spatial modulation, QSM) tabanlı GFDM yapısı önerilmiştir. Bilindiği kadarıyla bu çalışma QSM tabanlı

ilk çok taşıyıcılı uygulamadır. Ayrıca yine literatürde ilk kez olmak üzere QSM iletimi SFIM ile birleştirilmiştir. Önerilen çerçeve yapının bir diğer uygulaması ise IM'de kullanılmayan alt taşıyıcılar nedeniyle yaşanan spektral verimlilik kaybını telafi etmek üzere önerilen çift modlu IM (dual-mode IM, DMIM) tekniğinin GFDM ile birleştirilmesidir. Böylelikle SM ve IM teknikleri GFDM özelinde birleştirilmiş ve bu tekniklerin QSM ve DMIM modlarının da GFDM için çalışabilirliği gösterilmiştir.

Tezin ikinci aşamasının bir diğer katkısı da ZF tabanlı QR ayrıştırma sonrası ML-SIC tekniğine dayanan optimuma yakın bir algılayıcının MIMO-GFDM-IM uygulaması için geliştirilmesidir. ML-SIC algılayıcı dışında ZF tabanlı ayrık algılama ve demodülasyon (separate detection and demodulation, SDD) ve minimum karesel ortalamalı hata (minimum mean-squared error, MMSE) tabanlı ortak algılama ve demodülasyon (joint detection and demodulation, JDD) olmak üzere iki ayrı alıcı yapısının da uzay ve frekans IM tabanlı GFDM uygulaması ile kullanılabilirliği gösterilmiştir. Önerilen yapıların hata başarımları, işlem karmaşıklıkları ve spektral verimlilikleri kanal kodlamalı ve kodlamasız durumlar için bilgisayar simülasyonları aracılığıyla incelenmiştir. Bu sonuçlarda ML-SIC tabanlı algılayıcı ile ZF-SDD ve MMSE-JDD tabanlı algılayıcılara göre işlem karmaşıklığının kısıtlı bir miktarda artmasına karşın hata performansında önemli oranda iyileşme elde edildiği görülmüştür. Bu artışın sebebi ML-SIC tekniği ile uzay ve frekans indisleri ile QAM sembollerine ortak bir şekilde karar verilmesidir. Böylece ML-SIC tekniğinin hata başarımı ile işlem karmaşıklığı arasında ödünleşimler sağlayabildiği gösterilmiştir. Öte yandan ML-SIC tabanlı GFDM alıcı ile karşı gelen ML tabanlı OFDM alıcılarının hata başarımları karşılaştırılmış ve GFDM alıcılarının performanslarının OFDM'e oldukça yakın ancak OFDM'den bir miktar kötü olduğu görülmüştür. Bunun nedeni ise GFDM'de alt taşıyıcıların ortogonal olmaması ve QR ayrıştırma nedeniyle oluşan hata yayılımıdır. Bununla birlikte aynı durum için GFDM ile OFDM'e nazaran azaltılmış CP oranı nedeniyle daha yüksek spektral verimlilik ve ortogonal olmayan alt taşıyıcı filtreleme nedeniyle daha düşük bant dışı yayınım avantajları elde edilmiştir. Sonuçlardan tespit edilen bir diğer durum ise QSM çalışma modunda aynı spektral verimlilikte, işlem karmaşıklığında artış getirmeden hata başarımında iyileşme sağlandığıdır. Benzer şekilde DMIM çalışma modu ile de aynı spektral verimlilikte artan işlem karmaşıklığı ile hata başarımında az miktarda iyileşme olduğu görülmüştür. SFIM yapıları ile ise spektral verimlilikte azalma ile ciddi hata başarımı iyileşmeleri sağlanabildiği görülmüştür. Ayrıca uzay ve frekans indislerinin birlikte kullanımı ile farklı hata başarımı ve spektral verimlilik sağlayabilen çok katmanlı bir iletim yapısı oluşturulmuştur. Böylece SFIM yapılarının ortak uzay, frekans ve zaman kaynaklarını kullanarak farklı kullanım senaryolarını destekleme potansiyeline sahip olduğu gösterilmiştir. Elde edilen sonuçlar ışığında hedef performans kriterlerine göre uygun MIMO-GFDM-IM yapısının seçilebilmesini sağlayan bir kılavuz sunulmuştur.

Tezin üçüncü aşamasında GFDM'i SMX ve alt taşıyıcı IM ile birleştiren yeni bir SMX-GFDM-IM yapısı geliştirilmiştir. Bu yapıda tüm iletim antenlerinden bağımsız GFDM-IM blokları iletilmektedir. Alıcı kısmında ise MMSE Bell laboratuvarı katmanlı uzay-zaman iletimi QR ayrıştırma (MMSE Bell Laboratories Layered Space-Time with QR decomposition, MMSE-QRD) sonrası ML-SIC tekniğini kullanan optimuma yakın bir algılayıcı önerilmiştir. Bilindiği kadarıyla bu uygulama SMX-GFDM-IM için ilk optimuma yakın alıcı kullanımıdır. Ayrıca MMSE-JDD algılayıcı tabanlı alıcının SMX-GFDM-IM için de kullanılabilirliği gösterilmiştir. SMX-GFDM-IM yapısı, bilgisayar simülasyonları kullanılarak kanal kodlamalı

ve kanal kodlamasız hata başarımları, bant dışı yayınım, spektral verimlilik ve işlem karmaşıklığı açılarından incelenmiştir. Önerilen SMX-GFDM-IM yapısının SMX-OFDM ve SMX-GFDM'e göre daha iyi hata başarımına sahip olduğu, SMX-OFDM'e göre alt taşıyıcı filtreleme ve azaltılmış çevrimsel önek oranı nedeniyle daha iyi spektral verimlilik ve daha az bant dışı yayınım performansına sahip olduğu gösterilmiştir.

GFDM, zaman ve frekans kaynaklarını etkin, verimli ve esnek bir şekilde kullanıma izin veren yapısıyla gelecek nesil telsiz haberleşme sistemleri için düşük bant dışı yayınım, düşük gecikme, eşzamanlama hatalarını tolere edebilme gibi avantajları sunmaktadır. Bu tezde yapılan çalışmalarla GFDM'in SM ve SMX MIMO teknikleri ile çalışabilirliği gösterilmiştir. Bu sayede GFDM'in avantajlarına spektral verimlilik de eklenmiştir. Bunun yanında GFDM'in alt taşıyıcı IM teknikleri ile çalışabilirliği gösterilerek GFDM'in avantajları arasına enerji verimliliği de eklenmiştir. Yapılan bu çalışmalar sonrasında GFDM'in gelecek nesil telsiz haberleşme sistemleri için önemli bir aday teknik haline geldiği değerlendirilmektedir.

1. INTRODUCTION

Wireless communication has become an essential tool for everyday life and has significant impacts on all industries. As an indispensable part of daily activities, various types of information need to be obtained and shared in real-time by using fast and reliable voice and data communications. Wireless communications systems ease to access and sharing of information without being connected to fixed locations.

Starting from early 1980s, wireless communication systems have undergone significant changes. Cellular communication has been an important class of wireless networks which has rapidly progressed in a series of evolutions. First Generation (1G) cellular communication systems provided basic voice service with analog modulation techniques. Second Generation (2G) cellular communication systems have introduced the digitized voice along with the low-rate data service. Third Generation (3G) cellular communication systems provided data rates close to wired solutions of that time. Fourth Generation (4G) cellular communication systems have presented broadband wireless access which provides to access real-time high definition multimedia content anywhere and anytime. Nowadays, standardization activities for the cellular communication systems are moving towards fifth generation (5G). Considering the widespread usage of smartphones with advanced computing and storage capabilities, the thirst for higher throughput is sure to continue.

While wireless communication systems continue to progress evolutionary, there have been significant advancements in electronic circuit design methodologies which provide high processing capability consuming very low power in a very small area. These advancements pave the way for various type of remote sensing, monitoring and management applications which make the machines an integral part of wide area information networks. There are significant differences between the machine-centric information networks and human-centric information networks. First, machine-generated content will be short and bursty. Second, machine-generated content has to be delivered with high reliability and very low latency. Third, the

number of users in machine-cenctric information networks will be much higher than the number of users in human-centric informations networks and continues to increase exponentially. Consequently, future wireless networks will need to handle low data rate bursty traffic generated by 10s of billions of devices offering energy-efficient, highly-reliable and fast communication methods while serving for real-time ultra high definition multimedia demands.

In the light of these assessments, it is obvious that the demand for wireless communication continues to grow with the new applications which necessitate the capabilities beyond current ones. Therefore, adaptive, flexible, and efficient radio access technologies (RATs) are needed to serve future demands for wireless communication.

1.1 Purpose of Thesis

Owing to a broad range of applications spanning from wireless regional area networks (WRAN) to machine type communications (mTC), future wireless networks have challenging objectives such as very high spectral and energy efficiency, very low latency and very high data rate, which go beyond 4G wireless networks [4]. In this context, the vision and overall objectives of future wireless networks for 2020 and beyond have been defined by the International Telecommunication Union (ITU) [5] and standardization activities for 5G wireless networks have been started through discussions about scenarios and requirements by Third Generation Partnership Project (3GPP) [6].

Orthogonal frequency division multiplexing (OFDM) is the core of the physical layer of 4G wireless networks and fulfills the requirements and challenges of 4G scenarios. OFDM has attractive advantages such as simple implementation via fast Fourier transform (FFT)/inverse FFT (IFFT) blocks, robustness to frequency selective fading and simple equalization. However, considering the diverse applications of future wireless networks, the shortcomings of OFDM such as high peak-to-average power ratio (PAPR), high out-of-band (OOB) emission and sensitivity to time and frequency synchronization errors make difficult to address the requirements of the future radio access technologies satisfactorily [7, 8]. Thus, OFDM can fulfill the requirements of future wireless networks in a limited way. As a result, radically

new physical layer (PHY) technologies and modulation formats have been explored to fulfill the challenges of 5G wireless networks [7]. After years of discussion on the standardization of 5G, it was decided that none of the waveform alternatives were able to address all the requirements at the same time and an expanded version of OFDM with multiple numerologies, i.e., different parameterization of OFDM subframes, would provide the optimum results for the PHY of 5G [9, 10].

Taking account the massive growth trend from 1G to 5G, it is expected that the number of wireless users and applications will certainly continue to increase beyond 5G with expanded diverse requirements and technical challenges. For this reason, although OFDM with multiple numerologies concept will likely address the current technical challenges of 5G wireless networks, the sufficiency of OFDM-based PHY is quite disputable for beyond 5G. Therefore, new RATs are needed to fulfill the technical challenges of beyond 5G wireless networks. In this context, research efforts on the novel RATs including advanced waveforms and more flexible radio accessing schemes must continue for future wireless networks. The physical layer is the foundation of the networks. It comprises a complex set of techniques mainly related with efficient use of physical resources. Considering the short, bursty and asynchronous nature of the data traffic generated by the machine-centric networks, novel concepts for multi-carrier communication are researched and non-orthogonal techniques come into prominence due to their potential to fulfill the requirements of the new concepts. Therefore, there is a paradigm shift from orthogonal to non-orthogonal waveforms. However, the self-introduced interference of non-orthogonal techniques results much increased receiver complexity especially for multiple-input multiple-output (MIMO) transmission due to additional inter-antenna interference (IAI). Consequently, a major research effort is required to exploit and optimize the all aspects of the PHY.

In this thesis, the non-orthogonal filtered waveforms have been studied to provide significant enhancements to problems which are arised from non-orthogonal and asynchronous nature of the proposed schemes. The main aim is to contribute to design the physical layer of future wireless networks.

1.2 Literature Review

In recent years, several waveform proposals have been presented to overcome the limitations of OFDM. These proposals can be categorized into two main classes: cyclic prefix OFDM (CP-OFDM)-based and non-CP-OFDM-based. The proposals in the first class, such as filtered OFDM (f-OFDM) [11, 12] and windowed OFDM (W-OFDM) [13], are the attempts to resolve the aforementioned problems by keeping the orthogonality. The proposals in the second class initially dismiss orthogonality to obtain better temporal and spectral characteristics, thus, causes a major paradigm shift in the context of waveform design, which may yield some backward compatibility issues [7]. Amongst the waveforms in the second class, filter bank multi-carrier (FBMC) [14, 15], universal filtered multi-carrier (UFMC) [16] and generalized frequency division multiplexing (GFDM) [2] appear as promising candidates.

GFDM [2], which has attracted tremendous attention over the past few years, comes into prominence by providing advantages in terms of OOB emission, spectral efficiency and latency due to digitally pulse shaping of each subcarrier, reduced overhead of cyclic prefix and block-based structure, respectively. Unlike OFDM, GFDM permits to use more than one timeslot on the subcarriers and enables flexible time-frequency structuring which can be shaped according to corresponding scenario. Therefore, GFDM is one of the candidate schemes for beyond 5G wireless networks.

MIMO-friendliness is a key ability for a physical layer scheme to satisfactorily match the foreseen requirements of future wireless networks. Since GFDM is a generalized form of OFDM, one can expect that its combination with MIMO is feasible. In this sense, the combination of GFDM with space-time coding (STC) technique [2, 17–19] and spatial multiplexing (SMX) [20–28] have been investigated. In [20–22], iterative algorithms have been proposed for detecting spatially multiplexed GFDM signals. In [23], separate detection and demodulation (SDD) with linear MIMO detection algorithms such as minimum mean-squared error (MMSE) and zero-forcing (ZF) have been investigated. In [24], GFDM modulation and MIMO transmission have been combined as an equivalent MIMO-GFDM channel and QR decomposition-based sphere decoding (SD) with successive interference cancellation

(SIC) has been proposed. Coded performance analysis of QR decomposition-based SD-SIC receiver has been presented in [25]. In [26] and [27], an iterative MMSE with parallel interference cancellation (MMSE-PIC) detection has been proposed for MIMO-GFDM. Furthermore, a low complexity implementation of MMSE equalization was proposed and link level performance of MIMO-GFDM was analyzed along with the CP-OFDM-based counterparts in [28]. Among these studies, it has been reported that GFDM performed worse than OFDM in [23] and [25]. Based on these obtained results, while non-iterative MIMO-GFDM receivers generally performed worse than OFDM, iterative MIMO-GFDM receivers outperformed OFDM schemes at the cost of extra processing latency. Nevertheless, despite these advancements, non-orthogonality resulting from filtering each subcarrier individually prevents the frequency domain decoupling and makes the MIMO detection complicated.

The continuing demand for higher data rates motivates the researchers to seek spectral-efficient new modulation schemes. Spatial modulation (SM) is a MIMO transmission method, which considers the transmit antennas as spatial constellation points to carry additional information bits [29]. In SM, at each time interval, a single transmit antenna is activated by the input bit sequences and other antennas remain silent. For SM multi-carrier schemes, only one transmit antenna is activated at any subcarrier. As a result, activating single transmit antenna at a time or subcarrier eliminates IAI and reduces the receiver complexity. Moreover, SM techniques are more robust to channel imperfections and enhance the error performance.

SM-based modulation schemes have recently received a great deal of interest due to their attractive advantages over classical MIMO systems. Space-shift keying (SSK) is a special case of SM, where only active transmit antenna indices are used to convey information. In SSK, phase shift keying (PSK)/quadrature amplitude modulation (QAM) symbols are not used and active transmit antenna transmits a fixed non-data bearing signal. Space-time shift keying (STSK) is another SM-based modulation scheme, where both the indices of multiple pre-assigned dispersion matrices and signal constellation points are used to convey information. Additionally, the concept of SM is extended to include both the space and time dimensions. Quadrature Spatial Modulation (QSM) [30] expands the spatial constellation symbols to in-phase and quadrature components, and doubles the number of spatially carried bits with respect

to a conventional SM system. In QSM, signal constellation symbol is divided into its real and imaginary parts and their corresponding transmit antennas are determined by the input bit sequences in a separate fashion. It is demonstrated that QSM achieves the same error performance and spectral efficiency using 3 dB less signal power with respect to its SM counterpart without increasing the receiver complexity [30].

OFDM with index modulation (IM) is an extension of spatial modulation concept to subcarrier indices in multi-carrier systems [31–33]. In OFDM-IM, active subcarriers are selected by the input bit sequences and the information bits are conveyed through both the activated subcarrier indices and the conventional modulation symbols. While OFDM-IM scheme improves the error performance by conveying extra information bits through active subcarrier indices, it reduces throughput due to unused subcarriers. In [34], a dual-mode OFDM-IM (DMIM) scheme has been proposed to prevent throughput loss still using subcarrier indices to convey extra information. In DMIM scheme, based on the OFDM subblocks concept in [31], two different constellation modes have been used to modulate the subcarriers with selected indices and the remaining subcarriers. More recently, a multiple-mode DM-OFDM scheme is proposed in [35] by considering full permutation of modes. In order to improve the spectral efficiency, diversity and coding gains of OFDM-IM, several studies have been also performed in recent times [36–40]. Furthermore, in [41–44], combination of the OFDM-IM technique with MIMO methods has been investigated and significant performance gains have been reported. For a comprehensive overview of OFDM-IM and related literature, interested readers are referred to [45]. Taking account the prominent advantages of IM [3], combination of GFDM with IM techniques has been investigated in [46, 47]. In [46], the combination of Kalman algorithm-based channel estimation, turbo MMSE equalization and phase rotated conjugate cancellation (PRCC) algorithm has been proposed for MIMO-GFDM-IM scheme. In [47], a GFDM-IM transceiver structure has been introduced for multi-user networks and bit error ratio (BER) performance improvement with respect to classical GFDM and OFDM-IM has been reported. However, the combination of GFDM with IM considering optimum detection techniques remains an open as well as interesting research problem.

1.3 Original Contributions

During thesis proposal stage, motivation, key scenarios, key technical objectives, candidate technologies and expectations from the PHY for the future wireless communication systems were introduced. Current 4G methods, procedures, their shortcomings and advantages were discussed along with the new emerging trends such as machine type communications, heterogeneous networks and fragmented spectrum usage. Then, non-orthogonal multi-carrier modulation schemes were addressed to cope with the shortcomings of 4G methods. Amongst non-orthogonal multi-carrier modulation schemes, FBMC [15] and GFDM [2] were investigated. These two schemes were compared and deep investigation of GFDM was decided due to widespread studies about it.

MIMO transmission is an unquestionable method to increase the spectral efficiency. For this reason, applicability with MIMO techniques is mandatory for a candidate PHY scheme for future wireless networks. On the other hand, IM concept has appealing advantages over classical OFDM, such as flexible system design with adjustable number of active subcarriers, improved error performance for low-to-mid spectral efficiencies and simple transceiver design. Therefore, tight integration of GFDM with the MIMO and IM concepts has a strong potential to fulfill the foreseen requirements of future wireless networks in a satisfactory manner. In the light of these assessments, in this thesis, the combination of MIMO and IM techniques with GFDM has been investigated and novel transceiver structures have been introduced [48–53]. These transceiver structures have been optimized in terms of energy, spectral and computational efficiency.

In the first stage of the thesis, a GFDM-IM scheme, which uses flexible IM (FIM) numerology along with the near-optimum detector, is proposed to improve OOB emission, error performance and computational complexity of the GFDM scheme [52]. The contributions of the first stage of the thesis can be summarized as follows:

- The main contribution of this stage is the combination of GFDM with IM about to provide coding gain due to enhanced distance spectrum of IM.
- In order to optimize OOB emission, spectral efficiency and latency jointly, sparse IM numerology is applied to the edge GFDM subsymbols. To the best of author's

knowledge, this application would be the first attempt to exploit variable-sized IM subblocks with variable number of active subcarriers for GFDM.

- In order to enhance the error performance and reduce the computational complexity of the scheme, a new detector, which adapts a maximum likelihood (ML)-SIC based near-optimum detection, is developed for the single-input single-output (SISO) GFDM scheme considering the flexible IM numerology, and its theoretical error performance is analyzed.

- A new system model, which enables multi-layer transmission through IM-bits and QAM-bits, is presented. Thanks to this system model, the proposed scheme provides different error performances and spectral efficiencies for QAM and IM bits, and further benefits from enhanced distance spectrum of IM.

The block error rate (BLER), OOB emission and computational complexity of the proposed GFDM-IM scheme are evaluated via computer simulations. It has been shown that the proposed near-optimum, flexible, multi-layer GFDM-IM scheme is a strong alternative for future wireless networks due to its improved BLER and computational complexity performance.

In the second stage of the thesis, a framework for the combination of GFDM with IM concept is presented and integration of GFDM with space and frequency IM (SFIM) concept is discussed in detail to pave the way for innovative transceiver structures [51]. Then, by using this framework, novel transmitter and receiver schemes for MIMO-GFDM applications are proposed. BER performances of the proposed schemes are compared and their computational complexities and spectral efficiencies are analyzed. Based on the obtained results, a guideline for selecting the proper MIMO-GFDM scheme considering target performance criterion is given. The contributions of the second stage of this thesis can be summarized as follows:

- A GFDM-based FIM transceiver, which is capable of generating and decoding various IM schemes, is proposed. Thanks to FIM, switching between different IM schemes to adapt the channel conditions can be possible using a single transceiver structure.

- FIM provides a multi-layer transmission scheme by effectively using space, frequency, and time dimensions to adjust the BER performance and spectral efficiency, and enables to support different use cases by using common space, frequency, and time resources at the same time.

- A novel QSM-based GFDM scheme is proposed as a special case of FIM to enhance the spectral efficiency while preserving the advantages of SM. To the best of author's knowledge, this contribution would be the first approach that exploits multi-carrier transmission for QSM. In addition, QSM transmission is combined with the SFIM scheme.

- A near-optimum detection scheme, which is based on ML detection with SIC, is proposed.

- It is shown that ML-SIC detection scheme is also applicable for SISO, SM, IM, SFIM, and SSK-based GFDM systems.

In the third stage of the thesis, a novel MIMO-GFDM system, which combines SMX, GFDM and IM, is proposed in order to provide an efficient transmission scheme for beyond 5G wireless networks. The proposed scheme transmits independent GFDM-IM blocks through each transmit antenna and adapts MMSE Bell Laboratories Layered Space-Time (BLAST) with QR decomposition (MMSE-QRD)-based near-optimum detector at the receiver side. To the best of author's knowledge, this application would be the first attempt to exploit a near-optimum detector with SMX-GFDM-IM system. The uncoded and coded BER, OOB emission, spectral efficiency and computational complexity of the proposed scheme are analyzed by comparing with classical SMX-OFDM and SMX-GFDM schemes via computer simulations. It has been demonstrated that the proposed SMX-GFDM-IM scheme can be considered as a viable PHY scheme for beyond 5G wireless networks due to its improved BER, OOB emission and spectral efficiency.

The list of the journal and conference publications presenting the original contributions of this thesis to the wireless communication literature is given below.

- **Ozturk E.**, Basar E., Cirpan H. A., 2017. Generalized Frequency Division Multiplexing with Flexible Index Modulation. *IEEE Access*, 5, 24727-24746.

- **Ozturk E.**, Basar E., Cirpan H. A., 2018. Generalized Frequency Division Multiplexing with Flexible Index Modulation Numerology. *IEEE Signal Processing Lett.*, 26(10), 1480-1484.

- **Ozturk E.**, Basar E., Cirpan H. A., 2018. Multiple-Input Multiple Output Generalized Frequency Division Multiplexing with Index Modulation, submitted to journal of *Physical Communication*.

- **Ozturk E.**, Basar E., Cirpan H. A., 2017. Generalized Frequency Division Multiplexing with Space and Frequency Index Modulation. *5th Int. Black Sea Conf. Commun. Netw. (IEEE BlackSeaCom)*, June 5-8, 2017, Istanbul, Turkey.

- **Ozturk E.**, Basar E., Cirpan H. A., 2016. Generalized Frequency Division Multiplexing with Index Modulation. *IEEE GLOBECOM Workshops*, December 4-8, 2016, Washington, DC, USA.

- **Ozturk E.**, Basar E., Cirpan H. A., 2016. Spatial modulation GFDM: A Low Complexity MIMO-GFDM System for 5G Wireless Networks. *4th Int. Black Sea Conf. Commun. Netw. (IEEE BlackSeaCom)*, June 6-9, Varna, Bulgaria.

- **Ozturk E.**, Basar E., Cirpan H. A., 2018. Multiple-Input Multiple-Output Generalized Frequency Division Multiplexing with Flexible Index Modulation. PCT Patent Application Number: PCT/TR2018/050341.

The proposed techniques in this thesis have recently attracted significant attention from the researchers and these mentioned papers got more than thirty citations in two years.

The sections in this thesis are organized as follows. In Section 2, basic concepts about the subjects undertaking in this thesis are explained shortly. In Section 3, the combination of IM technique with GFDM is presented. The integration of GFDM with space and frequency IM techniques are analyzed in Section 4. In Section 5, a novel MIMO-GFDM system, which combines SMX, GFDM and IM is proposed. Section 6 presents the results of this thesis.

2. BASIC CONCEPTS

In this chapter, basic concepts related with the techniques investigated in this thesis are explained.

2.1 Wireless Communication Channels

2.1.1 Additive White Gaussian Noise channel

Additive White Gaussian Noise Channel (AWGN) is the most simple channel model for a digital communication system and it is used to model thermal noise in communication systems [54]. The basic characteristics of the AWGN channel model can be summarized as follows:

- The noise is additive, i.e., the noise is added to received signal directly, there is not any multiplication effect.
- The noise is white, i.e., its power spectral density is flat for all frequency values.
- The noise is statistically independent of the signal.
- The noise samples have a Gaussian distribution.

For a Gaussian random variable w, probability density function of w is given by

$$f(w) = \frac{1}{\sqrt{2\pi\sigma_w^2}} e^{-\frac{(w-m_w)^2}{2\sigma_w^2}}, \qquad -\infty \leq w \leq \infty, \tag{2.1}$$

where m_w is the mean value and σ_w^2 is the variance of the w.

2.1.2 Wireless channel and fading

Although AWGN channel model is suitable for many physical channels, it is not sufficient for communication channels whose transmission characteristics vary with time [55]. In such a situation, more sophisticated channel models are needed. The

most distinctive feature of the wireless channels is the multiple transmission paths between the transmitter and the receiver [56]. Because of these multiple transmission paths, more than one replica of the transmitted signal are reached to the receiver. If there is direct path between the transmitter and the receiver, it is called as line of sight (LOS). However, electramagnetic (EM) waves can travel from transmitter to receiver without LOS path. Meanwhile, EM waves are exposed to some destructive effects due to obstacles in the transmission medium. EM waves are reflected when they impinge to object which has a size larger than wavelength of the EM wave. Multiple replicas of the transmitted EM wave may reach to the receiver as a result of reflection around the large obstacles with different power levels at different times. Other destructive effects are scattering and diffraction. EM waves are scattered if the obstacle size is smaller than wavelength of the EM wave and EM waves are diffracted when they interact with sharp-edged objects in the transmission medium. As a result of these destructive effects, the received signal has some channel-specific properties. These properties are examined as large-scale fading and small-scale fading.

2.1.2.1 Large-scale fading

Large-scale fading appears as variations in received power that occur over relatively large distances due to effects of the propagation channel and has two different effects classified as path loss and shadowing. Path loss is caused by dissipation of the power radiated by the transmitter due to distance between the transmitter and the receiver. Shadowing is caused by obstacles between the transmitter and the receiver that attenuate signal power through absorbtion, reflection, scattering, and diffraction. Shadowing is experienced as fluctations on local-mean powers.

2.1.2.2 Small-scale fading

Small-scale fading is the rapid fluctation in signal strength over a small travel distance or time interval. The factors that affect small-scale fading are multi-path propagation, the relative speed between the transmitter and the receiver, speed of surrounding objects and transmission bandwidth of the signal.

Coherence bandwidth is the bandwidth of the multi-path channel and it is the bandwidth over which the channel transfer function remains virtually constant. In other words, it is a channel which passes all spectral components with approximately

equal gain and linear phase. The received signal will be distorted if the transmission bandwidth is greater than coherent bandwidth. Coherence time is the another important issue to classify fading effects. Coherence time is the time that the channel impulse reponse remain nearly unchanged. Small-scale fading channels are classified as frequency-flat and frequency-selective in terms of multi-path delay spread and fast and slow in terms of Doppler spread [56]. According to this classification, there are four different types of small-scale fading channels:

- Frequency-flat slow fading channel: Bandwidth of the signal is smaller than the coherence bandwidth and the modulation interval of the signal is smaller than the coherence time.
- Frequency-flat fast fading channel: Bandwidth of the signal is smaller than the coherence bandwidth and the modulation interval of the signal is greater than the coherence time.
- Frequency-selective slow fading channel: Bandwidth of the signal is greater than the coherence bandwidth and the modulation interval of the signal is smaller than the coherence time.
- Frequency-selective fast fading channel: Bandwidth of the signal is greater than the coherence bandwidth and the modulation interval of the signal is greater than the coherence time.

2.1.3 Rayleigh channel model

In a wireless communication system, statistical models are needed in order to investigate the variations of received signal power. For a frequency-flat, non-LOS, with J-transmission paths multi-path wireless channel, the received signal can be given as

$$r(t) = \sum_{j=1}^{J} a_j \cos\left(2\pi f_c t + \phi_j\right) + w(t), \tag{2.2}$$

where f_c is the carrier frequency, a_j and ϕ_j is the amplitude and the phase of the j-th component, respectively, and $w(t)$ is the Gaussian noise. After extracting cos term in equation 2.2, the received signal can be expressed as

$$r(t) = \cos(2\pi f_c t) \sum_{j=1}^{N} a_j \cos\left(\phi_j\right) - \sin(2\pi f_c t) \sum_{j=1}^{J} a_j \sin\left(\phi_j\right) + w(t). \tag{2.3}$$

Taking $A = \sum_{j=1}^{J} a_i \cos\left(\phi_j\right)$ and $B = \sum_{j=1}^{J} a_j \sin\left(\phi_j\right)$, equation 2.3 can be expressed in a more compact form as

$$r(t) = A\cos(2\pi f_c t) - B\sin(2\pi f_c t). \tag{2.4}$$

According to central limit theorem, for larger values of J, A and B are statistically independent and identically distributed Gaussian random variables. Thus, the envelope of the received signal becomes $\sqrt{A^2+B^2}$ and it has Rayleigh distribution. The probability density function of a Rayleigh random variable is given by

$$f(r) = \frac{r}{\sigma^2} e^{\frac{-r^2}{2\sigma^2}}, \qquad r \geq 0, \tag{2.5}$$

where σ^2 is the variance of A and B. The signal in equation 2.5 is related with the analog signal at the radio frequency (RF) Front-End. For baseband representation, the following transmisson model is used for the frequency-flat channels:

$$r_k = hs_k + w_k \tag{2.6}$$

Here, r_k is the matched-filter (MF) output after demodulation, h is the complex Gaussian random variable, s_k and w_k are the discrete versions of the transmitted signal $s(t)$ and noise signal $w(t)$, respectively. Since the real and the imaginer parts of the h are zero-mean Gaussian random variables, $|h|$ has Rayleigh distribution. Here $|h|$ is the path gain, w_k is Gauss noise. In this thesis Rayleigh fading channel model is used.

2.2 Waveform Design Criteria

RAT is the method for establishing physical connection to connect to a radio based communication network. The general building blocks of a RAT is shown in Fig. 2.1. Waveform is the shaping component of a RAT. Multiple Access determines the rules to manage the common resources such as spectrum, spreading code, etc. Frame Structure organizes the data transmission units. Coding is very crucial element to provide very low error probability. Modulation schemes impacts maximum achievable data rates. Duplex Mode is used to divide forward and reverse communication channels. Considering the continuing massive growth trend in number of wireless devices and applications, the following waveform design principles are essential for a new waveform in order to be able to meet the requirements of future wireless networks [1, 57–60]:

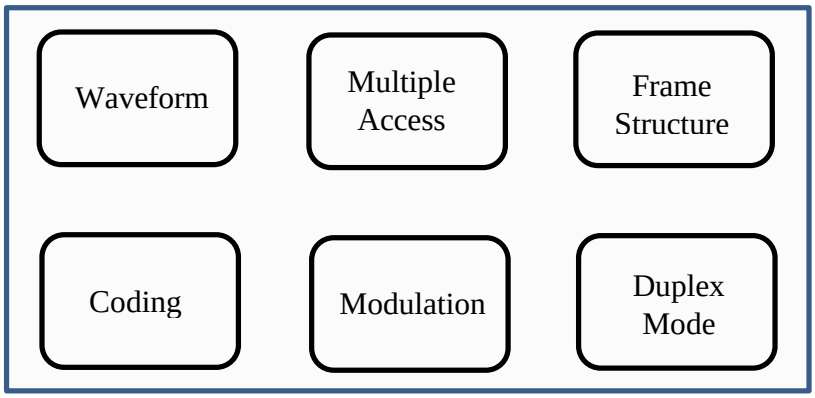

Figure 2.1 : Building blocks of a RAT.

- High spectral efficiency,
- Low processing latency,
- Good frequency localization, i.e., low OOB emission,
- Low PAPR,
- Low processing complexity for the generation/detection,
- Flexible waveform parametrization, such as CP and subcarrier spacing in multi-carrier schemes,
- Flexible and scalable bandwidth support,
- Efficient asynchronous communication with reduced signalling/access overhead,
- Good time localization,
- MIMO-friendliness,
- High order modulation support,
- Uniform waveform design for uplink and downlink,
- High power amplifier (PA) efficiency,
- Robustness to hardware impairments such as carrier frequency offset (CFO) and phase noise,
- Robustness to channel time-selectivity and frequency selectivity.

In Fig. 2.2, a common framework, that includes certain blocks to generate a waveform, is shown [1]. In the past decade, several waveforms have been proposed for wireless communications. Among these waveforms, the prominent ones are listed below.

OFDM based waveforms:

- Windowed OFDM (W-OFDM) [13, 61]
- Pulse-Shaped OFDM (P-OFDM) [62]
- Unique-Word OFDM (UW-OFDM) [63, 64]
- Universal Filtered Multicarrier (UFMC) [65]
- Universal Filtered OFDM (UF-OFDM) [66]
- Flexible CP-OFDM (FCP-OFDM) [67]
- Filtered OFDM (f-OFDM) [11, 12]

DFT spread OFDM based waveforms:

- Zero-Tail DFT Spread OFDM (ZT-DFT-S-OFDM) [59, 68]
- Filtered DFT Spread OFDM (f-DFT-S-OFDM) [11]
- Windowed DFT Spread OFDM (W-DFT-S-OFDM) [69]
- Unique-Word DFT Spread OFDM (UW-DFT-S-OFDM) [69]
- Unique-Word DFT Spread Windowed OFDM (UW-DFT-S-W-OFDM) [69]
- Physical Resource Block-specific Zero-Tail DFT Spread OFDM (PRB-ZT-DFT-S-OFDM [59]
- Continuous-Phase-Modulation Single Carrier Frequency Division Multiple Access (CPM-SC-FDMA) [70]

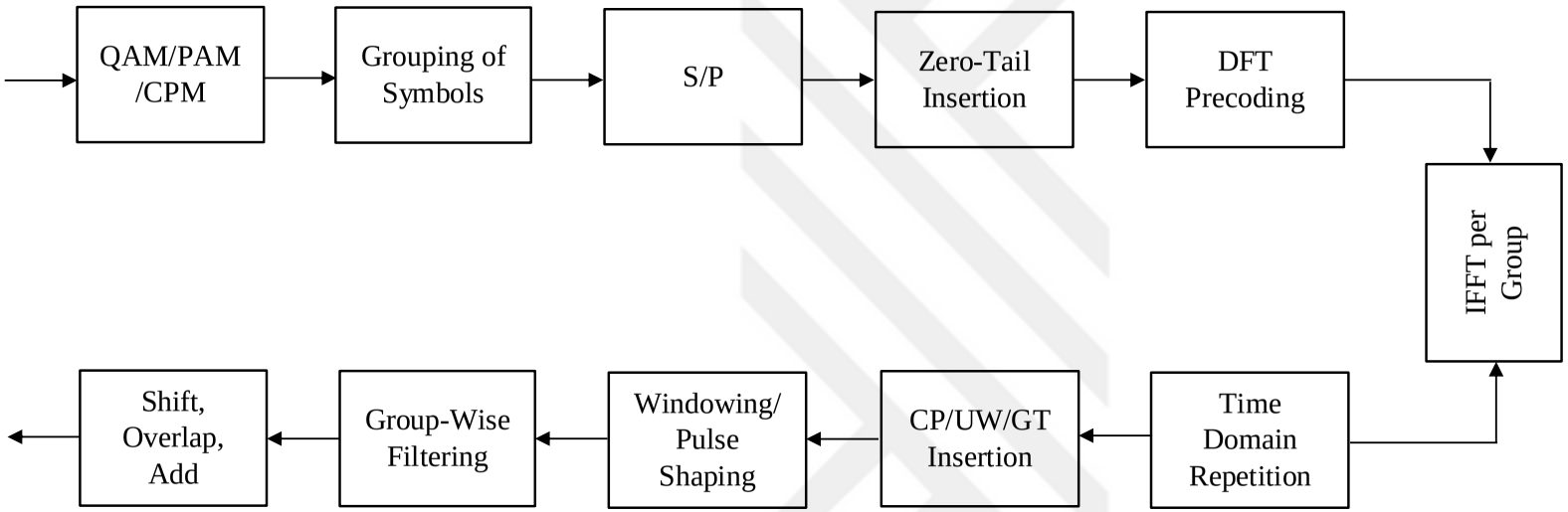

Figure 2.2 : Building blocks of a waveform [1].

Single carrier based waveforms:

- Constraint Envelope Continues Phase Modulation Single Carrier (ceCPM-SC) [71]
- Differentail QAM Single Carrier (D-QAM-SC) [72]

Non-orthogonal waveforms:

- Filterbank Multicarrier (FBMC) [14, 15]
- Generalized Frequency Domain Multiplexing (GFDM) [2]
- Circular Filterbank Multicarrier (cFBMC) [73]

2.3 Generalized Frequency Division Multiplexing

2.3.1 Basics of GFDM

GFDM [2] is one of the prominent non-CP-OFDM-based waveforms designed to overcome the major challenges of future wireless networks. These challenges can be listed as higher spectrum efficiency, higher energy efficiency and tolerance to synchronization errors. It has recently attracted significant attention from the researchers because of its beneficial properties to fulfill the requirements of future wireless networks. GFDM is a generalized form of OFDM in which a GFDM symbol has a block structure consisting of KM samples, where K subcarriers carry M timeslots each. Therefore, a GFDM symbol includes a group of OFDM symbols. The block structure of GFDM can be tuned to match the requirements of the application. Therefore GFDM has a flexibility to engineer the time-frequency structure according to corresponding scenario and the flexibility is the main strength of it. An important benefit of this flexibility is the possibility of reducing the latency on the physical layer of communications systems. In GFDM, circular pulse shaping is applied for each subcarrier by using adjustable pulse shaping filters. This reduces OOB emission significantly since the transmit signal has strong frequency localization per subcarrier. In this procedure, circular pulse shaping preserves the the block oriented structure and prevents rate loss that occur from filter tails. As a result, GFDM can serve for fragmented and opportunistic spectrum allocation purposes. In GFDM, variable pulse

shaping filters can be used and the transmit filter impulse response is not restricted to be rectangular. As a result, the orthogonality between the subcarriers is initially dismissed and self induced interference occurs. However, by using appropriate interference canceling algorithms in the receiver, self interference effects can be removed. As a benefit of being a non-orthogonal multi-carrier scheme, GFDM can tolerate loose time and frequency synchronization. GFDM uses only one CP per symbol, thus, spectral efficiency of GFDM is higher than that of OFDM. On the other hand, the insertion of CP enables low-complexity frequency domain equalization (FDE). To sum up, attractive claims of GFDM are listed below:

- A flexible time-frequency structuring,
- A lower OOB emission compared to OFDM,
- A lower synchronization need compared to OFDM,
- A higher spectral efficiency compared to OFDM,
- An efficient FFT-based equalization.

2.3.2 System model of GFDM transceiver

The block diagram of the GFDM transceiver is seen in Fig. 2.3. The binary vector $\mathbf{b}$ is provided by a data source and is encoded to obtain $\mathbf{b_c}$. In the mapper block, a form of QAM signalling is used to modulate each subcarrier individually. In this block, a QAM mapper maps the $\mathbf{b_c}$ to symbols from a 2^{μ}-valued complex constellation, where μ is the modulation order. The resulting vector $\mathbf{d}$ denotes a data block that contains N elements, which can be decomposed into K subcarriers with M subsymbols each according to $\mathbf{d} = [\mathbf{d}_0, \mathbf{d}_1, \ldots, \mathbf{d}_{M-1}]^{\mathrm{T}}$ and $\mathbf{d}_m = [d_{0,m}, d_{1,m}, \ldots, d_{K-1,m}]^{\mathrm{T}}$. Here, $d_{k,m}$ is the data transmitted on the k-th subcarrier of the m-th subsymbol of the block, $(\cdot)^T$ shows the transposition of a vector. The total number of symbols follows as $N = KM$. The details of the GFDM modulator are shown in Fig. 2.4.

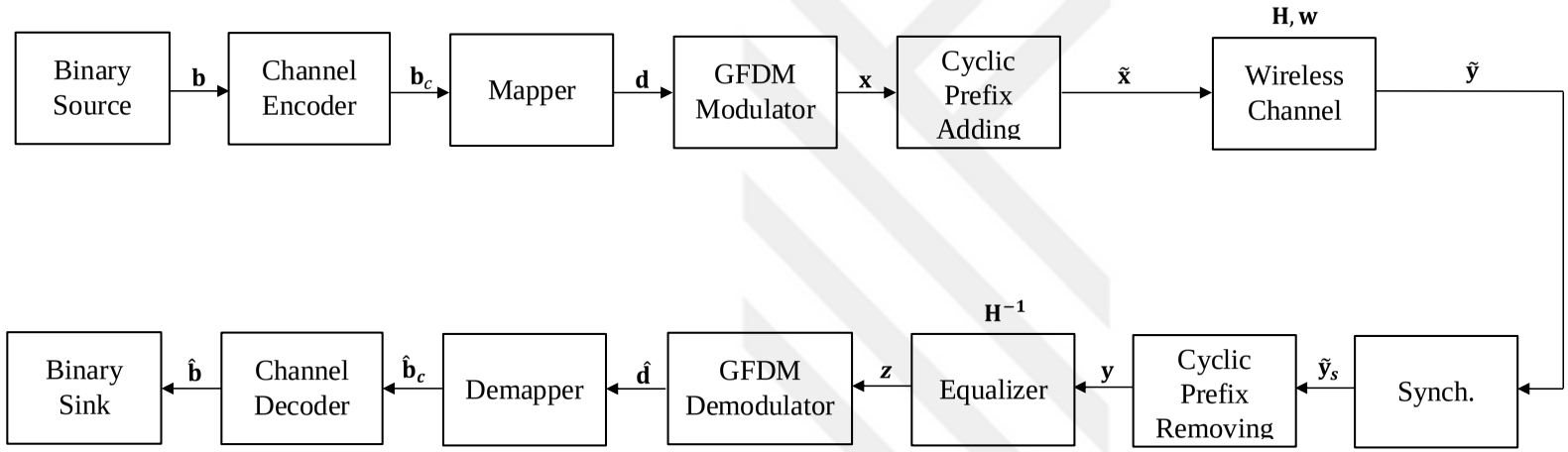

Figure 2.3 : Block diagram of the GFDM transceiver [2].

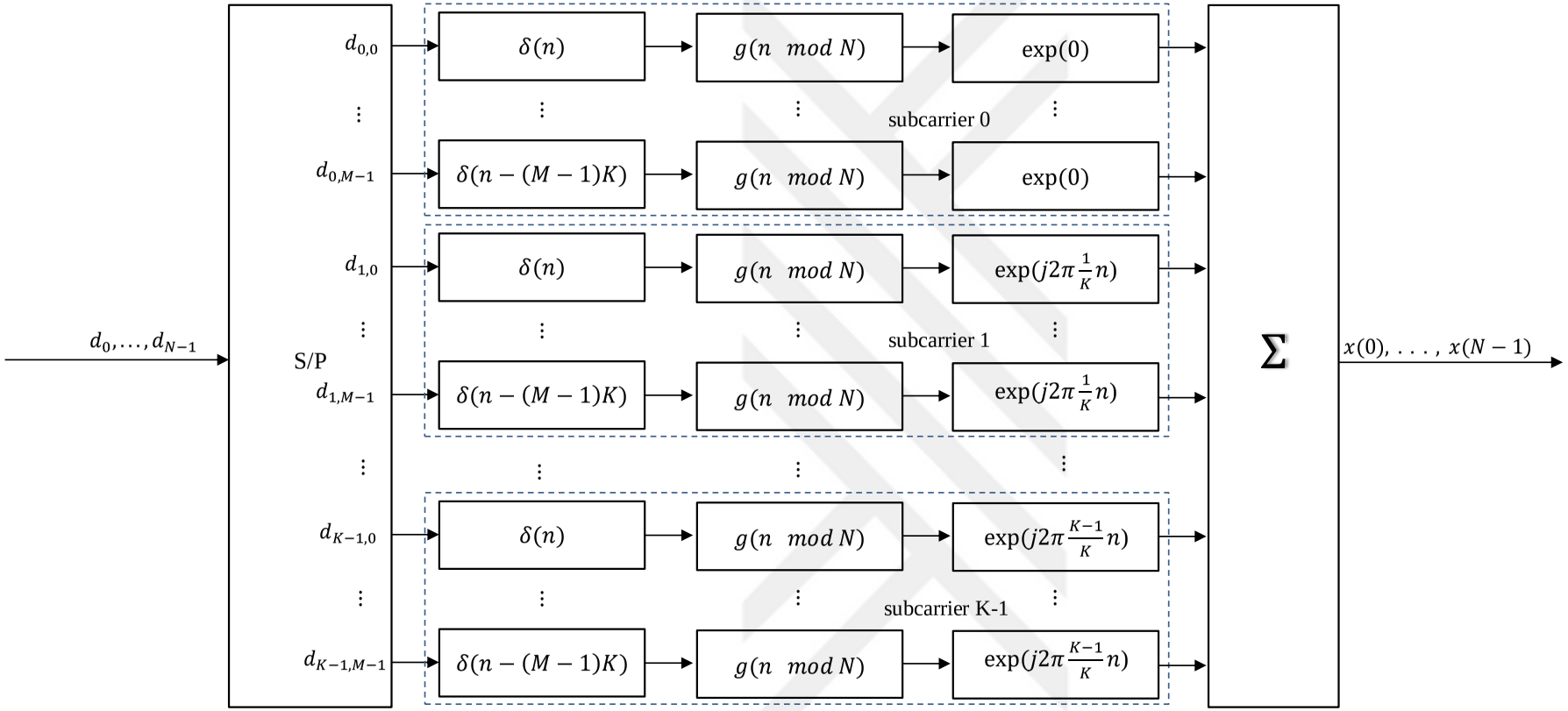

Figure 2.4 : Details of the GFDM modulator [2].

Each $d_{k,m}$ is individually filtered by using circular convolution with the pulse shape

$$g_{k,m}(n) = g\left((n-mK)_{\text{mod}N}\right)\exp\left(j2\pi\frac{kn}{K}\right), \tag{2.7}$$

where n is the sampling index. Each $g_{k,m}(n)$ is a time and frequency shifted version of a prototype filter $g(n)$, where the modulo operation makes $g_{k,m}(n)$ a circularly shifted version of $g_{k,0}(n)$ and the complex exponential performs the shifting operation in frequency. The transmit samples $\mathbf{x} = [x(n)]^{\text{T}}$ are obtained by superposition of all transmit symbols

$$x(n) = \sum_{k=0}^{K-1}\sum_{m=0}^{M-1} d_{k,m}g_{k,m}(n). \tag{2.8}$$

After collecting the filter samples in a vector $\mathbf{g}_{k,m} = \left[g_{k,m}(0),\ldots,g_{k,m}(N-1)\right]^{\text{T}}$, equation 2.8 can be rewritten as

$$\mathbf{x} = \mathbf{A}\mathbf{d}, \tag{2.9}$$

where $\mathbf{A}$ is a $KM \times KM$ transmitter matrix [2] with the following structure:

$$\mathbf{A} = \left[\mathbf{g}_{0,0},\ldots,\mathbf{g}_{K-1,0},\mathbf{g}_{0,1},\ldots,\mathbf{g}_{K-1,1},\ldots,\mathbf{g}_{K-1,M-1}\right]. \tag{2.10}$$

The last step at the transmitter side is the addition of a CP with length N_{CP} in order to make the convolution with the channel circular and the resulting vector

$$\widetilde{\mathbf{x}} = \left[\mathbf{x}(KM-N_{\text{CP}}+1:KM)^{\text{T}},\mathbf{x}^{\text{T}}\right]^{\text{T}} \tag{2.11}$$

is obtained. Here, $\mathbf{x}(a:b)$ shows the aAll elements of $\mathbf{x}$ with indices from a to b, inclusive of a and b. Finally, $\widetilde{\mathbf{x}}$ is transmitted over a frequency-selective Rayleigh fading channel.

At the receiver side, assuming that the wireless channel remains constant during the transmission of a GFDM block, CP is longer than the tap length of the channel (N_{Ch}) and perfect synchronization is ensured, the received signal vector $\mathbf{y}$ can be expressed as

$$\mathbf{y} = \mathbf{H}\mathbf{x} + \mathbf{w} = \mathbf{H}\mathbf{A}\mathbf{d} + \mathbf{w} \tag{2.12}$$

after the removal of CP. Here, $\mathbf{y} = [y(0),y(1),\ldots,y(N-1)]^{\text{T}}$ is the vector of received signals, $\mathbf{H}$ is the $N \times N$ circular convolution matrix constructed from the channel impulse response coefficients given by $\mathbf{h} = [h(1),h(2),\ldots,h(N_{\text{Ch}})]^{\text{T}}$, and $\mathbf{w}$ is an $N \times 1$ vector of AWGN samples. The elements of $\mathbf{h}$ and $\mathbf{w}$ follow $\mathscr{CN}(0,1)$ and $\mathscr{CN}(0,\sigma_w^2)$

distributions, respectively, where $\mathscr{CN}(\mu,\sigma^2)$ shows the distribution of a circularly symmetric complex Gaussian random variable with mean μ and variance σ^2. Equation 2.12 enables to use ZF-based channel equalization and the received signal after channel equalization can be expressed as

$$\mathbf{z} = \mathbf{H}^{-1}\mathbf{H}\mathbf{A}\mathbf{d} + \mathbf{H}^{-1}\mathbf{w} = \mathbf{A}\mathbf{d} + \widetilde{\mathbf{w}}. \tag{2.13}$$

Here, $(\cdot)^{-1}$ shows inverse of a matrix. Note that other equalization procedures can be employed as well. At this point, linear demodulation of the signal can be given as

$$\widetilde{\mathbf{d}} = \mathbf{B}\mathbf{z}, \tag{2.14}$$

where $\mathbf{B}$ is a $KM \times KM$ receiver matrix. There are mainly three options for the GFDM demodulator. The MF receiver $\mathbf{B}_{\text{MF}} = \mathbf{A}^{\text{H}}$, where $(\cdot)^{\text{H}}$ shows hermitian transposition of a vector or a matrix, maximizes the signal-to-noise ratio (SNR) per subcarrier, but it introduce self-interference when the pulse shaping filter is non-orthogonal. On the other hand, the ZF receiver $\mathbf{B}_{\text{ZF}} = \mathbf{A}^{-1}$ removes any self-interference completely but it enhances the noise. The linear MMSE receiver $\mathbf{B}_{\text{MMSE}} = \left(\mathbf{R}_w^2 + \mathbf{A}^{\text{H}}\mathbf{H}^{\text{H}}\mathbf{H}\mathbf{A}\right)^{-1}\mathbf{A}^{\text{H}}\mathbf{H}^{\text{H}}$ jointly equalizes the channel and makes a trade-off between self interference and noise enhancement. Here, $\mathbf{R}_w^2$ denotes the covariance matrix of the noise. For MMSE reception, ZF channel equalizer block is not required and $\widetilde{\mathbf{d}} = \mathbf{B}\mathbf{y}$. After that, original information bits are retrieved after demapping and decoding stages.

After investigating the transmitter and receiver structures, it can be stated that GFDM is a filtered multi-carrier system. Since it is more flexible than OFDM or single carrier frequency domain equalization (SC-FDE), it is named as "generalized". GFDM becomes OFDM when $M = 1$, $\mathbf{A} = \mathbf{F}_N^{\text{H}}$ and $\mathbf{B} = \mathbf{F}_N$, where $\mathbf{F}_N$ is a $N \times N$ Fourier matrix. When $K = 1$, SC-FDE is obtained and when $\mathbf{g}$ is a Dirichlet pulse single carrier frequency domain muliplexing (SC-FDM), a frequency division multiplexing of several SC-FDE signals, is obtained [74]. However, the prominent distinguishable property of GFDM is time-frequency partitioning into K subcarriers and M timeslots as depicted in Fig. 2.5. This feature enables to engineer the spectrum according to given requirements. Therefore, different configurations such as large number of narrow band subcarriers like in OFDM and small number of subcarriers of large individual bandwidth like in SC-FDM can be configured without changing the sampling rate.

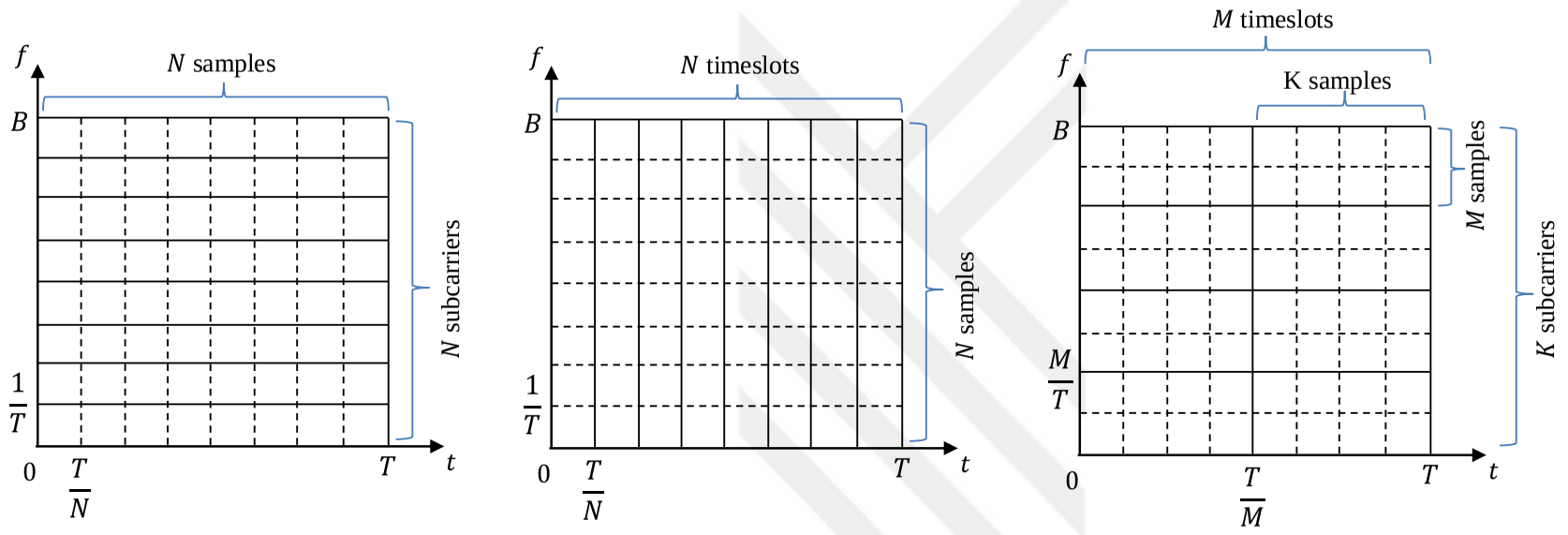

Figure 2.5 : Partitioning of time and frequency, where data occupies different resources depending on the chosen scheme. (a) with $K = N$ subcarriers and $M = 1$ subsymbols, (b) with $K = 1$ subcarriers and $M = N$ subsymbols and (c) with $K = 4, M = 3$ and $N = 12$. (a) OFDM; (b) SC-FDE; (c) SC-FDM and GFDM [2].

Furthermore, although the subcarriers are filtered individually, GFDM has block based structure which reveals advantages when targeting low latency transmissions [75].

2.4 Index Modulation

IM has attracted significant attention during recent times due to its appealing advantages over traditional digital modulation schemes which is based on modulating the frequency, phase and amplitude of a sinusoidal carrier. IM is a novel digital modulation technique that convey digital information by utilizing the indices of the transmission entities. It offers attractive advantages such as energy and spectral efficiency without increasing the computational complexity [45]. IM schemes transmit information through alternative ways. While the on/off status of the transmit antennas are altered according to information bits in SM [29], the on/off status of the subcarriers are altered in subcarrier index modulation [31–33]. Therefore IM schemes save the transmission energy by deactivating some transmit entities and have the ability to improve error performance by using saved transmission energy. In this section two variants of IM, namely SM and OFDM with Index Modulation (OFDM-IM), are investigated.

2.4.1 Index Modulation for transmit antennas: Spatial Modulation

SM is a novel MIMO scheme which transmits information through the indices of the transmit antennas in conjunction with the conventional Q-ary signal constellations. Unlike the conventional MIMO schemes, such as SMX, which intends to increase data rate, and spatial diversity, which intends to improve error performance, SM uses multiple transmit antennas for a different purpose. In SM, at each time interval, a single transmit antenna is activated by the input bit sequences and other antennas remain silent. For SM multi-carrier schemes, only one transmit antenna is activated at any subcarrier [29]. As a result, both indices of transmit antennas and Q-ary constellation symbols are used to carry information by SM. The block diagram of the SM scheme is shown in Fig. 2.6. For an SM system, a total of $\log_2 T + \log_2 Q$ bits enter the transmitter at each time interval as seen from Fig. 2.6, where T is the number of transmit antennas and Q is the size of the signal constellation. Here, while $\log_2 T$ bits of the incoming bit sequence are used to select the active transmit antenna, the remaining $\log_2 Q$ bits of

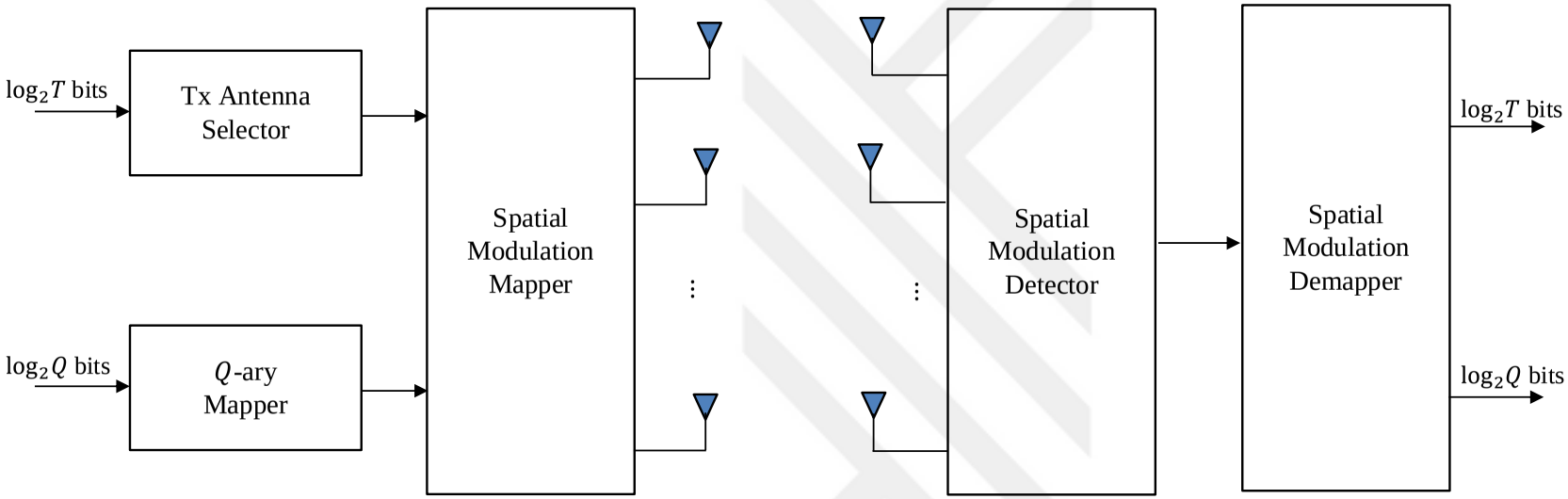

Figure 2.6 : Block diagram of SM transceiver.

the incoming bit sequence modulates the phase and/or amplitude of a carrier signal. Then, the selected antenna transmits the corresponding modulated signal(s) and the other transmits antennas remain silent.

At the receiver side, the active transmit antenna as well as the transmitted data symbol have to be detected to demodulate the index selecting bits and the bits mapped to Q-ary signal constellation, respectively. For this purpose, both optimum ML detection and suboptimal detection approaches can be applicable. Whereas the ML detector makes a joint search considering the transmit antennas and the constellation symbols, the suboptimal detector determines the activated transmit antenna at first and then it finds the data symbol transmitted over this antenna.

SM systems has significant advantages with respect to classical MIMO systems [76, 77]. The main advantages of SM are summarized below:

- SM simplifies the transceiver design. Activating single transmit antenna at a time or subcarrier eliminates IAI and the need for inter-antenna synchronization (IAS). In addition, the computational complexity of the receiver grows linearly with the number of transmit antennas and constellation size, rather than exponentially, as in SMX MIMO transmission.

- SM provides flexibility in terms of system configuration. In SM, the number of receive antennas can be lower than the number of transmit antennas.

- SM provides higher spectral efficiency with respect to SISO and orthogonal STC systems thanks to the use of the antenna indices to transmit additional information.

- SM provides higher energy efficiency since the consumed transmitter power does not related to the number of transmit antennas.

Although the SM systems have the mentioned attractive advangates, it has some disadvantages. Whereas the spectral efficiency of Vertical-Bell Laboratories Layered Space-Time (V-BLAST) based MIMO systems increases linearly with the number of transmit antennas, the spectral efficiency of SM systems increases logarithmically with the number of transmit antennas. Thus, SM systems need higher number of transmit antennas to obtain the same spectral efficiency with V-BLAST. In order to obtain better error performance, SM needs rich scattering environments, that is, different transmit

antennas have to experience sufficiently different channel coefficients. Unlike STC systems which are based on both spatial and time domains to transmit information, SM relies on only the spatial domain, therefore, it can not provide transmit diversity as STC systems.

Consequently, based on the investigations about the advantages and the disadvantages, SM systems provide an interesting trade-off amongst error performance, spectral efficiency and complexity, and it has been regarded as a prominent technique for spectral and energy-efficient future wireless communications systems.

2.4.2 Index Modulation for OFDM subcarriers: OFDM with Index Modulation

OFDM-IM concept has appealing advantages over classical OFDM such as flexible system design with adjustable number of active subcarriers and improved error performance for low-to-mid spectral efficiencies [3]. In OFDM-IM, the input bit stream is partitoned into Q-ary constellation and index selection bits. Then, by using the index selection bits, only a subset of available subcarriers are determined as active. The remaining inactive subcarriers are not used and set to zero. On the other hand, the active subcarriers are modulated as in classical OFDM according to the Q-ary constellation bits. As a result, the information bits are conveyed through both the activated subcarrier indices and the conventional modulation symbols. Consequently, OFDM-IM has better error performance due to the improved Euclidean distance spectrum of IM.

During OFDM-IM block creation, although the indices of active subcarriers can be selected directly, since an OFDM block can take very large number of subcarriers, OFDM-IM block is usually split into smaller subblocks to avoid complexity which will be created by the huge number of possible combinations. The block diagram of OFDM-IM transmitter is shown in Fig. 2.7. Considering an OFDM system with N subcarriers, an OFDM block is divided into L groups, each of $u = N/L$ subcarriers. Among the u subcarriers, only v subcarriers are used to transmit Q-QAM symbols. The different positions of the active subcarriers within an IM group can be used to convey additional information. As a result, each group can transmit a message of $v \log_2 Q$ bits carried by the Q-QAM symbols, in addition to $\log_2 c_m$ bits corresponding to IM, where $c_m = 2^{p_1}$ is the number of allowed combinations of the active subcarriers. Therefore,

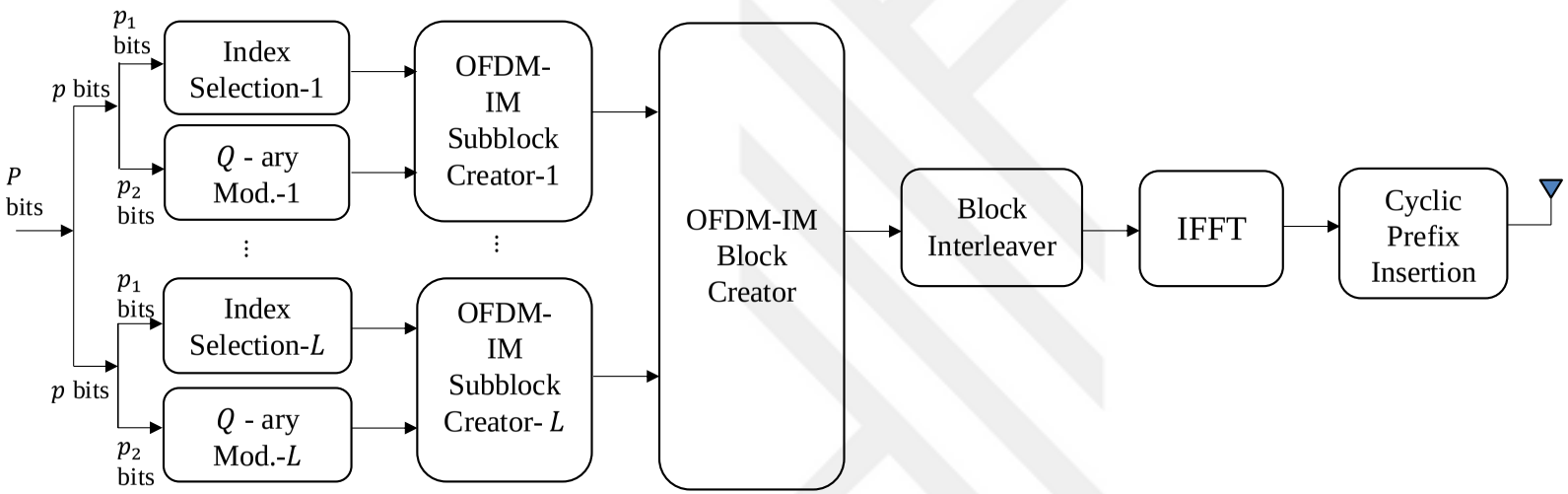

Figure 2.7 : Block diagram of the OFDM-IM transmitter [3].

the total bits which can be transmitted within the OFDM-IM scheme is given by

$$P = pL, \tag{2.15}$$

where $p = p_1 + p_2$, $p_1 = \lfloor C(u,v) \rfloor$, $p_2 = v \log_2 Q$ and $\lfloor \cdot \rfloor$ is the floor function. There are two index selection methods are available in the literature [31]. For smaller N values, reference look-up tables are used and for higher N values, combinatorial number theory method is preferred. In the OFDM-IM receiver, the active subcarriers as well as the corresponding data symbols have to be determined according to the index selection procedure executed at the transmitter. The block diagram of the OFDM-IM receiver is shown in Fig. 2.8. Since the OFDM-IM transmitter works on the IM subblocks independently, the OFDM-IM receiver can handle the detection of different subblocks independently. Similar to SM, both high-complexity ML detector and low-complexity log-likelihood ratio (LLR) based near-optimum detector can be carried out. Whereas the ML detector executes a joint test over possible active subcarrier indices and data symbols, the LLR detector decides the active subcarrier indices first and then detects the corresponding data symbols. It has been recently proved in [43] that the combination of OFDM-IM and MIMO transmission techniques provides an interesting trade-off among error performance, spectral efficiency and decoding complexity. Furthermore, it has been demonstrated in [78] that OFDM-IM also provides improvements over classical OFDM in terms of ergodic achievable rate. However, the combination of GFDM with IM remains an open as well as interesting research problem.

Consequently, subcarrier IM concept has significant advantages such as energy-efficient flexible system design and it also has strong potential for future wireless networks.

2.5 Multiple-Input Multiple-Output Transmission

The demand for high data rate is one of the key elements which steers research in future wireless communication systems. Since frequency spectrum is a scarce resource, high spectral efficiency comes into prominence among various performance indicators. In this sense, MIMO transmission has attracted significant interest across the researchers and MIMO-friendliness becomes a key ability for a physical layer scheme to

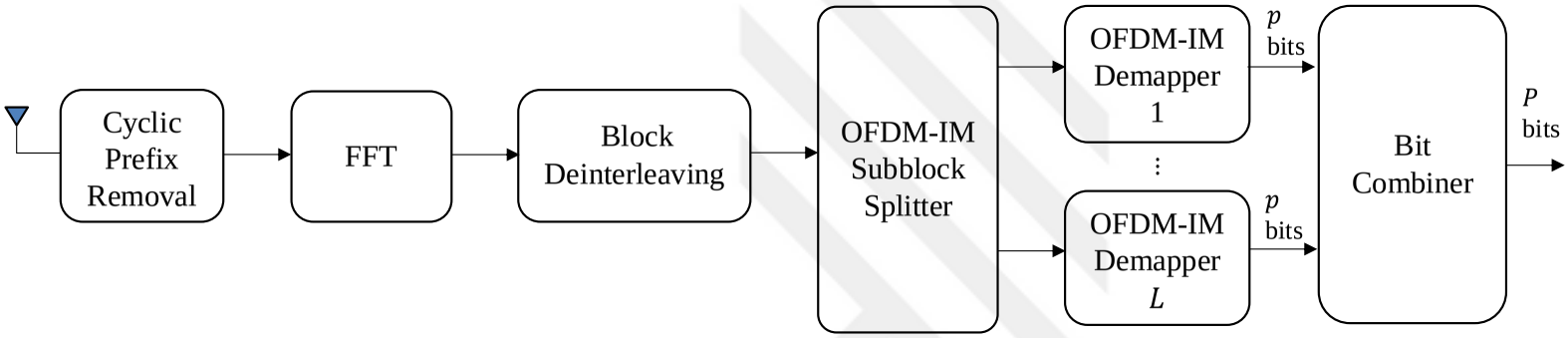

Figure 2.8 : Block diagram of the OFDM-IM receiver [3].

satisfactorily match the foreseen requirements of future wireless networks. For a $T \times R$ MIMO system, T signals are transmitted by T antennas using the same bandwidth at the same time. At the receiver, R signals received by R antennas are used to distinguish the different transmitted signals. In this communication scenario, the main task that is executed by the receiver is to cancel co-channel interference based on the collected multiple information. Thanks to effective processing techniques, this permits improving system capacity such as increasing the single link data rate or increasing the number of users.

2.5.1 MIMO system model

A MIMO system model with T transmit antennas and R receive antennas is shown in Fig. 2.9. Based on this system model, the overall received signal can be expressed as

$$\begin{bmatrix} y_1 \\ y_2 \\ \vdots \\ y_R \end{bmatrix} = \begin{bmatrix} h_{1,1} & h_{1,2} & \cdots & h_{1,T} \\ h_{2,1} & h_{2,2} & \cdots & h_{2,T} \\ \vdots & \vdots & \ddots & \vdots \\ h_{R,1} & h_{R,2} & \cdots & h_{R,T} \end{bmatrix} \begin{bmatrix} x_1 \\ x_2 \\ \vdots \\ x_T \end{bmatrix} + \begin{bmatrix} w_1 \\ w_2 \\ \vdots \\ w_R \end{bmatrix}. \tag{2.16}$$

Equation 2.16 can be rewritten in a more compact form as

$$\mathbf{y} = \mathbf{H}\mathbf{x} + \mathbf{w}, \tag{2.17}$$

where $\mathbf{y}$ is the $R \times 1$ vector of received signals, $\mathbf{x}$ is T-dimensional transmitted symbol, $\mathbf{H}$ is the $R \times T$ channel matrix constructed from the channel impulse response coefficients between the t-th transmit antenna and the r-th receive antenna given by $h_{r,t}$, $\mathbf{w}$ is an $R \times 1$ vector of AWGN samples with elements distributed as $\mathscr{CN}(0, \sigma_w^2)$, $\sigma_w^2 = N_0 B$, N_0 is the noise power spectral density and B is the channel bandwidth. In MIMO-OFDM, each subcarrier signal is subject to narrowband frequency-domain attenuation. Thus, equation 2.17 applies to each subcarrier. Thus, for a $T \times R$ MIMO channel and a transmit data vector $\mathbf{x}_k$ belonging to the k-th subcarrier, the received signal of the k-th subcarrier can be expressed as

$$\mathbf{y}_k = \mathbf{H}_k \mathbf{x}_k + \mathbf{w}_k, \quad k = 0, 1, \ldots, K-1, \tag{2.18}$$

where $\mathbf{H}_k$ is the channel matrix and $\mathbf{w}_k$ is the channel noise vector at the k-th subcarrier frequency. After that, an estimate of $\mathbf{x}_k$ can be obtained by applying ZF or MMSE equalization to equation 2.18.

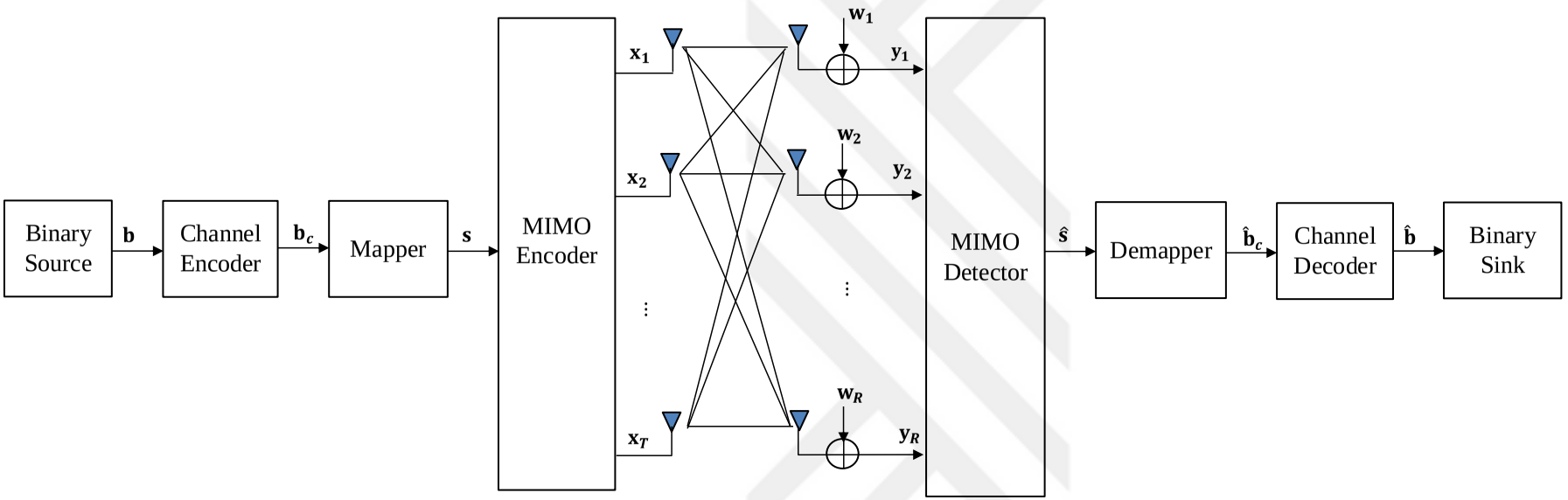

Figure 2.9 : MIMO system model.

2.5.2 MIMO techniques

MIMO techniques can be classified as four main categories: Diversity coding, precoding, SMX and SM. SM has already been investigated in scope of IM concept in this thesis. Diversity coding tries to improve power efficiency by increasing spatial diversity [79, 80]. In these techniques, a single stream is coded using a method named as STC. The coded signal is transmitted by each of the transmit antennas with full or near orthogonal coding. Diversity coding benefits from the independent fading in the multiple antenna links to improve signal diversity. The resulting diversity gain is used to enhance error performance for the same spectral efficiency. In the precoding techniques, the transmitter has the channel knowledge and this knowledge is used by the transmitter as prefilters to achieve capacity gain [81, 82]. In other words, the transmitter makes the all spatial processing. SMX divides a high-rate data stream into multiple lower-rate streams and transmits each stream through a different transmit antenna using the same frequency channel [83, 84]. At the the receiver, these multiplexed signals are decomposed into parallel channels exploiting the different spatial signatures that the streams experienced. SMX is a very efficient MIMO method to increase the data rate at higher SNR. This technique can be combined with precoding if the transmitter has the channel knowledge.

2.5.3 MIMO detection methods

2.5.3.1 ML MIMO detector

ML detector is the optimal detector to minimize the probability of error. The ML solution for the problem in equation 2.17 can be expressed as

$$\hat{\mathbf{x}} = \underset{\mathbf{x}\in\{\mathscr{X}\}}{\operatorname{argmin}} \|\mathbf{y} - \mathbf{H}\mathbf{x}\|^2, \tag{2.19}$$

where $\|\cdot\|$ is the Euclidean norm. Here, the minimization must be executed over all possible transmitted vectors. From equation 2.19, it is obvious that a straightforward solution to ML detection of SMX transmission is extremely complex. Therefore, low complexity solutions are needed.

2.5.3.2 Linear MIMO detection methods

Linear MIMO detection methods try to decouple the effects of the channel spatially. It involves multiplying the received signal with a MIMO equalization matrix $\mathbf{G}$. After equalization, parallel decision steps are executed on all streams. In the decision step, each element of the multiplication output vector $\hat{\mathbf{x}} = \mathbf{G}\mathbf{y}$ is mapped onto an element of the signal constellation by a minimum distance quantization. There are two common methods for linear MIMO equalization. These methods are ZF and MMSE detectors.

Linear ZF Detector

ZF detector uses the equalization matrix

$$\mathbf{G}_{\mathrm{ZF}} = \mathbf{H}^{+} = \left(\mathbf{H}^{\mathrm{H}}\mathbf{H}\right)^{-1}\mathbf{H}^{\mathrm{H}} \tag{2.20}$$

and tries to suppress the mutual interference between the layers. Here, it is assumed that $\mathbf{H}$ has full column rank and $(\cdot)^{+}$ shows the pseudo-inverse of a matrix. At the decision step, each element of the filter output vector

$$\widehat{\mathbf{x}}_{\mathrm{ZF}} = \mathbf{G}_{\mathrm{ZF}}\mathbf{y} = \mathbf{x} + \left(\mathbf{H}^{\mathrm{H}}\mathbf{H}\right)^{-1}\mathbf{H}^{\mathrm{H}}\mathbf{w} \tag{2.21}$$

is mapped onto an element of the symbol alphabet by a minimum distance quantization [85].

Linear MMSE Detector

MMSE detector uses

$$\mathbf{G}_{\mathrm{MMSE}} = \left(\mathbf{H}^{\mathrm{H}}\mathbf{H} + \sigma_w^2\mathbf{I}_T\right)^{-1}\mathbf{H}^{\mathrm{H}}, \tag{2.22}$$

where $\mathbf{I}_T$ is a $T \times T$ identity matrix, and makes a trade-off between noise enhancement and IAI. The resulting filter output is given by

$$\widehat{\mathbf{x}}_{\mathrm{MMSE}} = \mathbf{G}_{\mathrm{MMSE}}\mathbf{y} = \left(\mathbf{H}^{\mathrm{H}}\mathbf{H} + \sigma_w^2\mathbf{I}_T\right)^{-1}\mathbf{H}^{\mathrm{H}}\mathbf{y}. \tag{2.23}$$

2.5.3.3 Nulling and cancelling methods

Nulling and cancelling methods combine the spatial nulling process with interference cancellation and tries to separate the individual substreams.

V-BLAST

The most popular nulling and cancelling method is V-BLAST [84]. In V-BLAST algorithm, signal detection is executed not in parallel, but iteratively. V-BLAST algorithm first detects the strongest substream and then subtracts the contribution of this substream from the received signals. This process is repeated until all the substreams have been detected. V-BLAST algorithm has two variants according to equalization matrix used for the nulling process. ZF V-BLAST uses $\mathbf{G}_{\mathrm{ZF}}$ and MMSE V-BLAST uses $\mathbf{G}_{\mathrm{MMSE}}$ for the nulling process.

2.5.3.4 Nulling and cancelling methods with QR decomposition

V-BLAST is a computationally-burdened algorithm due to the pseudoinverse calculation in each step of detection. To avoid this calculation, QR decomposition can be used.

ZF BLAST with QR Decomposition (ZF-QRD)

The QR-decomposition [86] of the channel matrix $\mathbf{H}$ is given as

$$\mathbf{H} = \mathbf{QR}, \tag{2.24}$$

where $\mathbf{Q}$ is an $R \times T$ unitary matrix, $\mathbf{R}$ is an $T \times T$ upper triangular matrix. By multiplying the received signal $\mathbf{y}$ from the left with $\mathbf{Q}^{\mathrm{H}}$, a $T \times 1$ modified received signal vector

$$\widetilde{\mathbf{y}} = \mathbf{Q}^{\mathrm{H}}\mathbf{y} = \mathbf{Rx} + \widetilde{\mathbf{w}} \tag{2.25}$$

is created. Since $\mathbf{Q}$ is unitary, the statistical properties of the noise term $\widetilde{\mathbf{w}} = \mathbf{Q}^{\mathrm{H}}\mathbf{w}$ remain unchanged. Then, with the help of the upper triangular structure of $\mathbf{R}$, the estimate of t-th element of $\mathbf{x}$ is obtained as

$$\hat{x}_t = r_{t,t}x_t + \sum_{j=t+1}^{T} r_{t,j}x_j + \widetilde{w}_t \quad t = 1,2,\ldots,T \tag{2.26}$$

Here, $\hat{x}_T$ does not contain any interference and it can be estimated using appropriate scaling with $\frac{1}{r_{T,T}}$. Assuming correct previous decisions, this process proceeds with $\hat{x}_{T-1},\ldots,\hat{x}_1$ and the interference can be perfectly cancelled in each step.

MMSE BLAST with QR Decomposition (MMSE-QRD)

There is a similarity between ZF and MMSE detectors. Considering $(T+R)\times T$ extended channel matrix $\breve{\mathbf{H}}$, and a $(T+R)\times 1$ extended receive vector $\breve{\mathbf{y}}$ through

$$\breve{\mathbf{H}} = \begin{bmatrix} \mathbf{H} \\ \sigma_w \mathbf{I}_T \end{bmatrix} \tag{2.27}$$

and

$$\breve{\mathbf{y}} = \begin{bmatrix} \mathbf{y} \\ \mathbf{0}_{T,1} \end{bmatrix} \tag{2.28}$$

the output of the MMSE filter given by equation 2.23 can be expressed as

$$\widehat{\mathbf{x}}_{\text{MMSE}} = \breve{\mathbf{H}}^{+}\breve{\mathbf{y}} = \left(\breve{\mathbf{H}}^{\text{H}}\breve{\mathbf{H}}\right)^{-1}\breve{\mathbf{H}}^{\text{H}}\breve{\mathbf{y}}. \tag{2.29}$$

It means that ZF filter matrix based on the extended channel matrix $\breve{\mathbf{H}}$ is equal to MMSE filter matrix based on the channel matrix $\mathbf{H}$. When this similarity is applied to QR decomposition, QR decompositon of the extended channel matrix becomes

$$\breve{\mathbf{H}} = \begin{bmatrix} \mathbf{H} \\ \sigma_w \mathbf{I}_T \end{bmatrix} = \breve{\mathbf{Q}}\breve{\mathbf{R}} = \begin{bmatrix} \mathbf{Q}_1 \\ \mathbf{Q}_2 \end{bmatrix}\breve{\mathbf{R}} = \begin{bmatrix} \mathbf{Q}_1\breve{\mathbf{R}} \\ \mathbf{Q}_2\breve{\mathbf{R}} \end{bmatrix}, \tag{2.30}$$

where the $(T+R)\times T$ matrix $\breve{\mathbf{Q}}$ was split into the $R\times T$ matrix $\mathbf{Q}_1$ and the $T\times T$ matrix $\mathbf{Q}_2$. As a result, filtered receive vector becomes

$$\widetilde{\mathbf{y}} = \breve{\mathbf{Q}}^{\text{H}}\mathbf{y} = \mathbf{Q}_1^{\text{H}}\mathbf{y} = \breve{\mathbf{R}}\mathbf{x} - \sigma_w\mathbf{Q}_2^{\text{H}}\mathbf{x} + \mathbf{Q}_1^{\text{H}}\mathbf{w}. \tag{2.31}$$

Here, the term including $\mathbf{Q}_2^{\text{H}}$ is the remaining interference that can not be removed by the SIC. In order to get the corresponding optimum MMSE solution, the matrices $\mathbf{R}$, and $\mathbf{Q}$ encountered in the ZF-QRD algorithm only have to be substituted by $\breve{\mathbf{R}}$ and $\mathbf{Q}_1$, respectively [85].

3. GENERALIZED FREQUENCY DIVISION MULTIPLEXING WITH INDEX MODULATION

3.1 System Model of GFDM-IM

For a GFDM symbol with M subsymbols each containing K subcarriers, the m-th subsymbol is divided into L_m IM subblocks, each consists of $u_m = K/L_m$ subcarriers. In an IM subblock, only v_m out of u_m available subcarriers are used to transmit QAM symbols and the active subcarrier positions are used to convey additional bits. Thus, each IM subblock can transmit a message of $\alpha_m = v_m \log_2(Q)$ bits carried by the QAM symbols and $\beta_m = \lfloor \log_2 (C(u_m, v_m)) \rfloor$ bits corresponding to active subcarrier indices, where $C(\mu, \nu)$ shows the binomial coefficient. Therefore, QAM-bits and IM-bits which can be mapped to one GFDM-IM subsymbol become $p_m = L_m \alpha_m$ and $g_m = L_m \beta_m$, respectively, and the total number of bits that can be transmitted within the GFDM-IM scheme is given by $P + G$ bits, where $P = \sum_{m=0}^{M-1} p_m$ and $G = \sum_{m=0}^{M-1} g_m$.

According to Fig. 3.1, P information bits enter the transmitter to be carried by the QAM symbols. First, these P bits are split into M groups with p_m bits and then each group of p_m-bits is divided into L_m groups each containing α_m bits. After that, α_m-bit sequences are mapped by Q-ary mappers to create the modulated symbols vector $\mathbf{s}_m^l = \left[s_m^l(1), s_m^l(2), \ldots, s_m^l(v_m) \right]^{\mathrm{T}}$, where $s_m^l(\gamma) \in \mathscr{S}$, for $l = 1, 2, \ldots, L_m$ and $\mathscr{S}$ denotes Q-ary signal constellation with Q elements. Meanwhile, G information bits enter the transmitter to be carried by the active subcarrier indices. These G bits are split into M groups with g_m bits first and then each group of g_m-bits is divided into L_m groups each containing β_m bits. These β_m-bit sequences are used by index selectors to select the active subcarrier indices $\mathbf{i}_m^l = \left[i_m^l(1), i_m^l(2), \ldots, i_m^l(v_m) \right]^{\mathrm{T}}$, where $i_m^l(\gamma) \in \{1, \ldots, u_m\}$, by a selection rule. Therefore, $\mathbf{i}_m^l$ has $c_m = 2^{\beta_m}$ possible realizations. Note that the proposed GFDM-IM scheme provides two transmission paths with IM and QAM. After that, $\mathbf{s}_m^l$ and $\mathbf{i}_m^l$ vectors are combined to create the GFDM-IM subblocks $\mathbf{d}_m^l = \left[d_m^l(1), d_m^l(2), \ldots, d_m^l(u_m) \right]^{\mathrm{T}}$, where $d_m^l(\gamma) \in \{0, \mathscr{S}\}$,

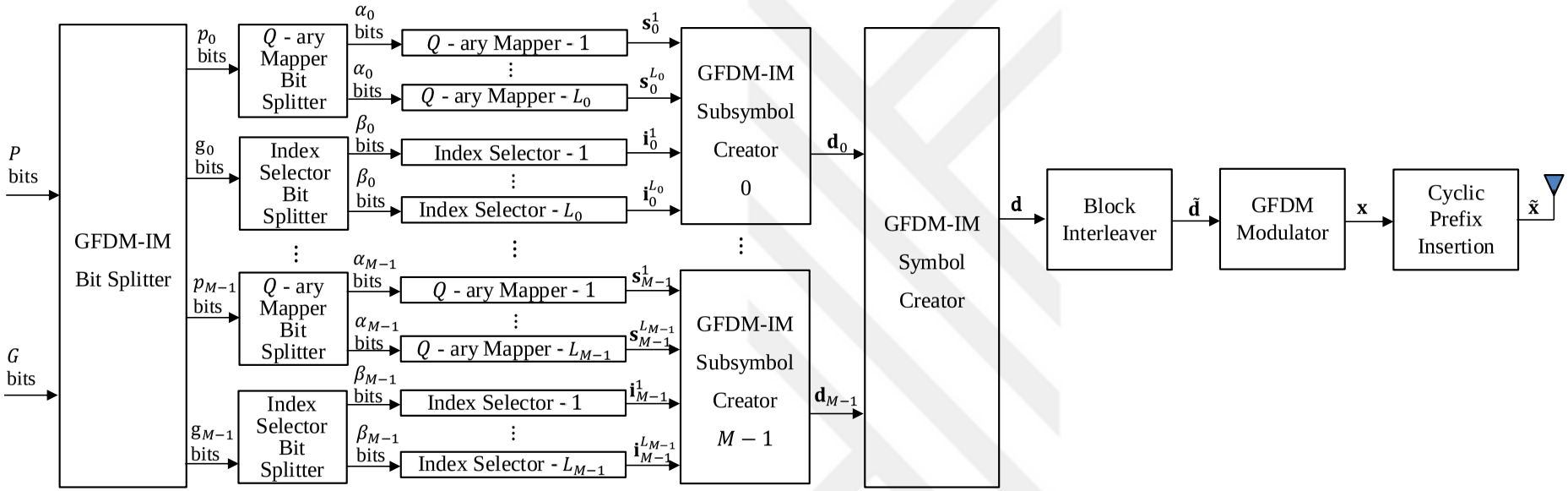

Figure 3.1 : Block diagram of the GFDM-IM transmitter.

and the resulting GFDM-IM subblocks are concatenated to obtain the GFDM-IM subsymbol $\mathbf{d}_m = [d_{0,m}, d_{1,m}, \ldots, d_{K-1,m}]$. Then, GFDM-IM symbol creator combines the GFDM-IM subsymbols and forms the GFDM-IM symbol

$$\mathbf{d} = [d_{0,0}, \ldots, d_{K-1,0}, d_{0,1}, \ldots, d_{K-1,1}, \ldots, d_{K-1,M-1}], \tag{3.1}$$

where $d_{k,m} \in \{0, \mathscr{S}\}$, for $k = 0, \ldots, K-1, m = 0, \ldots, M-1$, is the data symbol of k-th subcarrier on m-th subsymbol. At this point, in order to have uncorrelated channels, a block interleaver with size $L_m \times u_m$ is employed for inner subsymbols of $\mathbf{d}$ and the interleaved data vector $\widetilde{\mathbf{d}}$, where $\widetilde{d}_{k,m} = d_{(\mathrm{mod}(k,u_m)L_m + \lfloor k/u_m \rfloor), m}$, for $k = 0, \ldots, K-1, m = 1, \ldots, M-2$, is obtained. Here, $\mathrm{mod}(\mu, \nu)$ is the modulo of μ with respect to ν. Then, the resulting GFDM-IM symbol $\widetilde{\mathbf{d}}$ is modulated using a GFDM modulator and the GFDM transmit signal becomes $\mathbf{x} = \mathbf{A}\widetilde{\mathbf{d}}$, where $\mathbf{A}$ is an $N \times N$ GFDM modulation matrix [2]. Finally, a CP with length N_{CP} is appended to $\mathbf{x}$ and the resulting vector $\widetilde{\mathbf{x}} = \left[\mathbf{x}(KM - N_{\mathrm{CP}} + 1 : KM)^{\mathrm{T}}, \mathbf{x}^{\mathrm{T}}\right]^{\mathrm{T}}$ is sent over a frequency-selective Rayleigh fading channel.

At the receiver side, considering the block diagram in Fig. 3.2 and under the assumption that CP is longer than the channel delay spread (N_{Ch}), the received signal vector $\mathbf{y}$ can be expressed as

$$\mathbf{y} = \mathbf{H}\mathbf{x} + \mathbf{w} = \mathbf{H}\mathbf{A}\widetilde{\mathbf{d}} + \mathbf{w} = \widetilde{\mathbf{H}}\widetilde{\mathbf{d}} + \mathbf{w}, \tag{3.2}$$

after the removal of CP. Here, $\mathbf{y} = [y(0), y(1), \ldots, y(N-1)]^{\mathrm{T}}$ is the vector of received signals, $\mathbf{H}$ is the $N \times N$ circular convolution matrix constructed from the channel impulse response coefficients given by $\mathbf{h} = [h(1), h(2), \ldots, h(N_{\mathrm{Ch}})]^{\mathrm{T}}$, $\widetilde{\mathbf{H}} = \mathbf{H}\mathbf{A}$ is the equivalent channel of the MIMO system which combines GFDM modulation and the wireless channel, and $\mathbf{w}$ is an $N \times 1$ vector of AWGN samples. The elements of $\mathbf{h}$ and $\mathbf{w}$ follow $\mathscr{CN}(0,1)$ and $\mathscr{CN}(0, \sigma_w^2)$ distributions, respectively, where σ_w^2 is the variance of the noise samples.

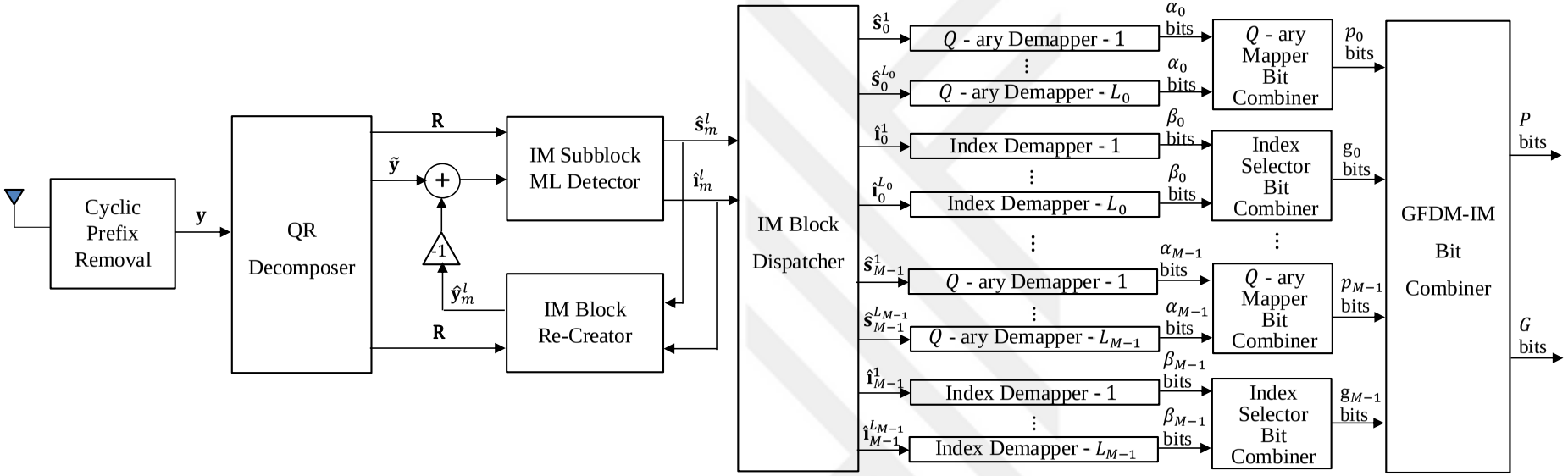

Figure 3.2 : Block diagram of the GFDM-IM receiver.

3.2 Near-ML Detection of GFDM-IM Scheme

At this stage, in order to realize joint detection and demodulation with reduced complexity, a near-optimum detection method is developed for SISO GFDM-IM system considering variable-sized IM subblocks. The QR-decomposition [86] of $\widetilde{\mathbf{H}}$ is given as $\widetilde{\mathbf{H}}\mathbf{P} = \mathbf{Q}\mathbf{R}$, where $\mathbf{Q}$ is an $N \times N$ unitary matrix, $\mathbf{R}$ is an $N \times N$ upper triangular matrix, $\mathbf{P}$ permutes the columns of $\widetilde{\mathbf{H}}$ prior to decomposition in order to realize deinterleaving. Then, multiplying the received signals with $\mathbf{Q}^{\mathrm{H}}$ yields

$$\widetilde{\mathbf{y}} = \mathbf{Q}^{\mathrm{H}}\mathbf{y} = \mathbf{R}\mathbf{d} + \widetilde{\mathbf{w}}, \tag{3.3}$$

where $\widetilde{\mathbf{w}} = \mathbf{Q}^{\mathrm{H}}\mathbf{w}$. After that, the ML solution of the last IM subblock is obtained using the upper triangular form of $\mathbf{R}$ and the interference caused by this subblock is removed. Then, the system size is decreased by u_m and the operation continues until the first IM subblock is detected. Algorithm 1 shows the proposed detection method. Here, the subscripts u_m, $\bar{u}_m$ and : denote the last u_m, all but the last u_m and all elements of the subscripted object, respectively. Finally, the original information bits are obtained by the subsequent blocks.

Algorithm 1 ML-SIC detection

1: **Input** $= \widetilde{\mathbf{y}}, \mathbf{R}$
2: **Output** $= \hat{\mathbf{s}}_m^l$, $\hat{\mathbf{i}}_m^l$, for $m = 0, \ldots, M-1, l = 1, \ldots, L_m$
3: **for** $m \leftarrow M-1$ to 0 **do**
4: **for** $l \leftarrow L_m$ to 1 **do**
5: $\hat{\mathbf{d}}_m^l = \underset{\mathbf{I},\mathscr{S}}{\operatorname{argmin}} \|\widetilde{\mathbf{y}}_{u_m} - \mathbf{R}_{u_m,u_m}\mathbf{d}_m^l\|^2$
6: $\hat{\mathbf{y}}_m^l = \mathbf{R}_{:,u_m}\hat{\mathbf{d}}_m^l, \widetilde{\mathbf{y}} \leftarrow \widetilde{\mathbf{y}} - \hat{\mathbf{y}}_m^l$
7: $\widetilde{\mathbf{y}} \leftarrow \widetilde{\mathbf{y}}_{\bar{u}_m}, \mathbf{R} \leftarrow \mathbf{R}_{\bar{u}_m,\bar{u}_m}$
8: **end for**
9: **end for**

3.3 Performance Analysis of GFDM-IM Scheme

In this section, the BLER performance of the GFDM-IM scheme is analytically evaluated using the near-optimum detector. When the channel state information is perfectly known at the receiver, the IM subblock ML detector computes an estimate of the transmitted IM subblock vector according to metric given in line 5 of Algorithm

1. At this point, the probability that the IM subblock ML detector detects the IM subblock vector $\mathbf{e}_m^l = [e_m^l(1), e_m^l(2), \ldots e_m^l(u_m)]$ instead of $\mathbf{d}_m^l$ is examined. In such cases, pairwise error probability (PEP) is used as a measure of error performance. For a given channel realization, taking account of equation 3.3, the conditional PEP (CPEP) at the l-th stage of the m-th subsymbol of ML-SIC receiver can be calculated as

$$P\left(\mathbf{d}_m^l \to \mathbf{e}_m^l | \mathbf{R}_m^l\right) = P\left(\left\|\widetilde{\mathbf{y}}_m^l - \mathbf{R}_m^l \mathbf{d}_m^l\right\|^2 > \left\|\widetilde{\mathbf{y}}_m^l - \mathbf{R}_m^l \mathbf{e}_m^l\right\|^2\right), \tag{3.4}$$

where $\widetilde{\mathbf{y}}_m^l$, $\mathbf{d}_m^l$ and $\mathbf{e}_m^l$ are $u_m \times 1$ vectors, $\mathbf{R}_m^l$ is an $u_m \times u_m$ upper triangular matrix. After some algebra, CPEP at the l-th stage of the m-th subsymbol of ML-SIC receiver is obtained as [43]

$$P\left(\mathbf{d}_m^l \to \mathbf{e}_m^l | \mathbf{R}_m^l\right) = Q\left(\sqrt{\frac{\left\|\mathbf{R}_m^l(\mathbf{d}_m^l - \mathbf{e}_m^l)\right\|^2}{2\sigma_w^2}}\right), \tag{3.5}$$

where $Q(x)$ is the Gaussian Q-function. Here, since the distribution of the entries of $\mathbf{R}_m^l$ are complicated, a semi-analytical approach can be used to obtain a tight unconditional PEP (UPEP) approximation. In order to perform averaging over $\mathbf{R}_m^l$, $J = 10^6$ samples of $\mathbf{R}_m^l$ are generated as $\mathbf{R}_m^l(j)$, $j = 1, 2, \ldots, J$, and the UPEP at the l-th stage of the m-th subsymbol of ML-SIC receiver can be obtained as

$$P\left(\mathbf{d}_m^l \to \mathbf{e}_m^l\right) \approx \frac{1}{J}\sum_{j=1}^{J} Q\left(\sqrt{\frac{\left\|\mathbf{R}_m^l(\mathbf{d}_m^l - \mathbf{e}_m^l)\right\|^2}{2\sigma_w^2}}\right) \tag{3.6}$$

for each SNR value. On the other hand, $P\left(\mathbf{d}_m^l \to \mathbf{e}_m^l\right)$ is also the probability of incorrect decision for the transmitted IM subblock vector $\mathbf{d}_m^l$ assuming no error at the previous stages. Therefore, the probability that all the IM subblock vectors are detected correctly can be shown as

$$P_{\mathscr{C}} = \prod_{m=0}^{M-1}\prod_{l=1}^{L_m}\left(1 - P\left(\mathbf{d}_m^l \to \mathbf{e}_m^l\right)\right). \tag{3.7}$$

As a result, the probability of having at least one error in the detected GFDM block can be expressed as

$$P_{\mathscr{E}} = 1 - P_{\mathscr{C}} = 1 - \prod_{m=0}^{M-1}\prod_{l=1}^{L_m}\left(1 - P\left(\mathbf{d}_m^l \to \mathbf{e}_m^l\right)\right). \tag{3.8}$$

Equation 3.8 is referred as BLER and can be upper bounded by [87]

$$P_{\mathscr{E}} \leq \sum_{m=0}^{M-1}\sum_{l=1}^{L_m} P\left(\mathbf{d}_m^l \to \mathbf{e}_m^l\right). \tag{3.9}$$

3.4 Complexity and OOB Emission Analysis

Computational complexities of classical MMSE based joint detection and demodulation (JDD), ML-SIC and ML detectors are analyzed with respect to the number of complex multiplications (CMs) and presented in Table 3.1. From Table 3.1, it is observed that the detector with the proposed ML-SIC technique has the lowest complexity.

In GFDM, each subcarrier is filtered individually using a prototype filter. While filtering results non-orthogonality and inter-carrier interference (ICI), it reduces OOB emission. Since abrupt signal changes between subsequent GFDM blocks cause high OOB emission, in [88], a guard GFDM subsymbol insertion into each block is proposed to achieve more smooth transitions. In this case, OOB emission can be reduced further with a reduced spectral efficiency of $(M-1)/M$. Decrease in the spectral efficiency can be compensated by increasing subsymbol count, which leads to increased latency. As it will be shown in Section 3.5, by applying sparse IM numerology to the edge GFDM subsymbols, transitions between GFDM blocks can be smoothed without using guard subsymbol. From Fig. 3.3, it is observed that using sparse IM numerology at the edge GFDM subsymbols can reduce OOB emission with a moderate loss in spectral efficiency, hence preventing an increased latency.

3.5 Numerical Analysis

In this section, theoretical and Monte Carlo simulation results for the proposed GFDM-IM scheme are presented for Rayleigh multi-path fading channels with Extended Pedestrian A (EPA) channel model [89]. Raised cosine (RC) filter with a roll-off factor (a) of 0.1 is used as a GFDM prototype filter. In order to obtain same spectral efficiency, the following system parameters are considered: GFDM and plain GFDM-IM schemes have $M = 13$ subsymbols and their first and last subsymbols are deactivated. The proposed GFDM-IM scheme has $M = 11$ subsymbols and its first and last subsymbols have sparse IM numerology with $u_m = 32, v_m = 1$. For inner GFDM subsymbols for both plain GFDM-IM and the proposed GFDM-IM schemes, u_m is chosen as 4, and v_m is chosen as 2 and 3 for binary phase shift keying (BPSK) and 4-QAM transmissions, respectively, and the active subcarrier positions are determined using the look-up table in Table 3.2. A GFDM block includes 1 GFDM symbol and an

Table 3.1 : Computational complexity of three different receivers.

Receiver	Process	Complexity (CMs)
MMSE	Forming $\widetilde{\mathbf{H}}$, JDD	$N_{\mathrm{Ch}}N^2 + 3N^3 + N^2$
	IM Demod.	$\sum_{m=0}^{M-1} L_m v_m c_m Q^{v_m}$
	Total	$\sim \mathcal{O}\left(3N^3\right)$
ML-SIC	Forming $\widetilde{\mathbf{H}}$, QRD	$N_{\mathrm{Ch}}N^2 + 2N^3 + N^2$
	ML Detection.	$\sum_{m=0}^{M-1} L_m c_m Q^{v_m}\left(u_m v_m + u_m\right)$
	SIC	$N\sum_{m=0}^{M-1} L_m v_m$
	Total	$\sim \mathcal{O}\left(2N^3\right)$
ML	Forming $\widetilde{\mathbf{H}}$	$N_{\mathrm{Ch}}N^2$
	ML Detection.	$\left(N\sum_{m=0}^{M-1} L_m v_m\right)\prod_{m=0}^{M-1}\left(c_m Q^{v_m}\right)^{L_m}$
	Total	$\sim \mathcal{O}\left(\left(N\sum_{m=0}^{M-1} L_m v_m\right)\prod_{m=0}^{M-1}\left(c_m Q^{v_m}\right)^{L_m}\right)$

Table 3.2 : A look-up table example for $u_m = 4$.

Bits	Indices for $v_m = 2$	Indices for $v_m = 3$
[0 0]	$\{1,2\}$	$\{1,2,3\}$
[0 1]	$\{2,3\}$	$\{1,2,4\}$
[1 0]	$\{3,4\}$	$\{1,3,4\}$
[1 1]	$\{1,4\}$	$\{2,3,4\}$

OFDM block includes 11 OFDM symbols with $K = 128$, $N_{\text{CP}} = 32$. Plain GFDM-IM scheme uses classical MMSE detector, and both the proposed GFDM-IM and the GFDM schemes use ML-SIC detector. E_b is the average transmitted energy per bit and N_0 is the noise power spectral density.

Fig. 3.3 shows the OOB emission of classical and IM-based GFDM and OFDM schemes for BPSK transmission for the given system parameters. From Fig. 3.3, it is observed that smooth transitions provided by sparse IM numerology yields 6 dB additional OOB emission suppression with respect to GFDM scheme at the expense of reduced spectral efficiency. On the other hand, while the proposed GFDM-IM scheme reduces OOB emission suppression of GFDM and plain GFDM-IM schemes by approximately 20 dB at the same spectral efficiency, it provides 15% shortening of the symbol length and still provides 13 dB OOB emission suppression with respect to OFDM. The OOB emission suppression of the proposed GFDM-IM scheme can be increased with more sparse subcarrier usage at the expense of reduced spectral efficiency or increased latency. Consequently, the proposed flexible IM numerology can provide an attractive trade-off among OOB emission, spectral efficiency and latency, and has significant advantages for fragmented spectrum usage.

Fig. 3.4 compares the uncoded BLER performance of the proposed GFDM-IM scheme with plain GFDM-IM scheme, OFDM-IM scheme [31] as well as classical GFDM and OFDM schemes for BPSK transmission. Here, IM-only curves belong to the bits conveyed by the indices of the active subcarriers and the spectral efficiency of the GFDM-IM schemes are given by $(P+G)/(N+N_{\text{CP}})$ [bits/s/Hz]. From Fig. 3.4, for a target BLER value of 10^{-3}, it is observed that the proposed GFDM-IM scheme achieves 0.8 and 5 dB better BLER performance than the plain GFDM-IM scheme considering overall and IM-only performances, respectively, at the same spectral efficiency. Note that ML-SIC detector provides a significant improvement for IM-only transmission in terms of BLER and this improvement can be exploited to provide

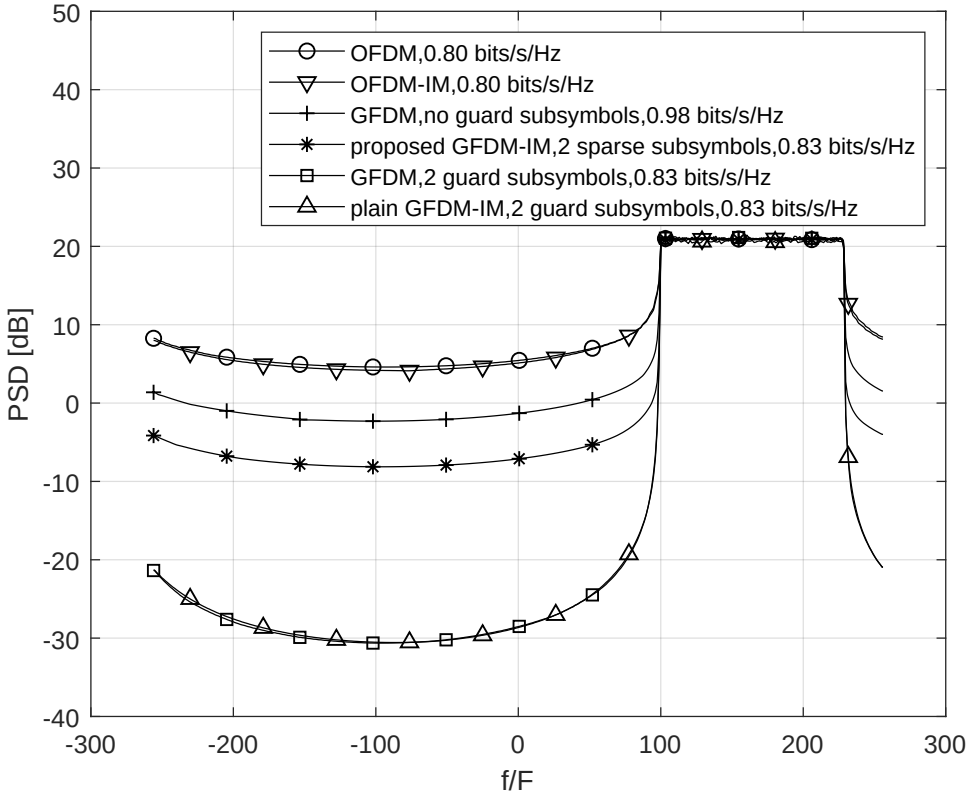

Figure 3.3 : OOB emission for BPSK transmission.

different quality of service classes. On the other hand, BLER performance gains of the proposed GFDM-IM scheme with respect to OFDM-IM, GFDM and OFDM schemes are risen to 6, 8 and 14 dB, respectively. According to Table 3.1, the computational complexity of the ML-SIC and the classical MMSE detectors required to implement the receiver block of the proposed GFDM-IM scheme are on the order of $\sim \mathscr{O}(5.6 \times 10^9)$ and $\sim \mathscr{O}(8.4 \times 10^9)$, respectively. As a result, ML-SIC technique provides 34% less complexity with respect to classical MMSE detector.

Fig. 3.5 shows the BLER performance for 4-QAM transmission. From Fig. 3.5, it is found that the proposed GFDM-IM scheme provides the similar BLER gains as in BPSK transmissions with respect to other methods. The performance improvements provided by the ML-SIC detector with respect to classical MMSE detector are the result of joint detection and GFDM-IM demodulation. Besides, performance improvement of GFDM-IM with respect to GFDM is the result of coding gain due to enhanced distance spectrum of IM. For comparison, the theoretical upper bounds obtained from equation 3.9 are also depicted in Figs. 3.4 and 3.5. As seen from Figs. 3.4 and 3.5, the theoretical upper bounds become relatively tight with the simulation results as the SNR increases.

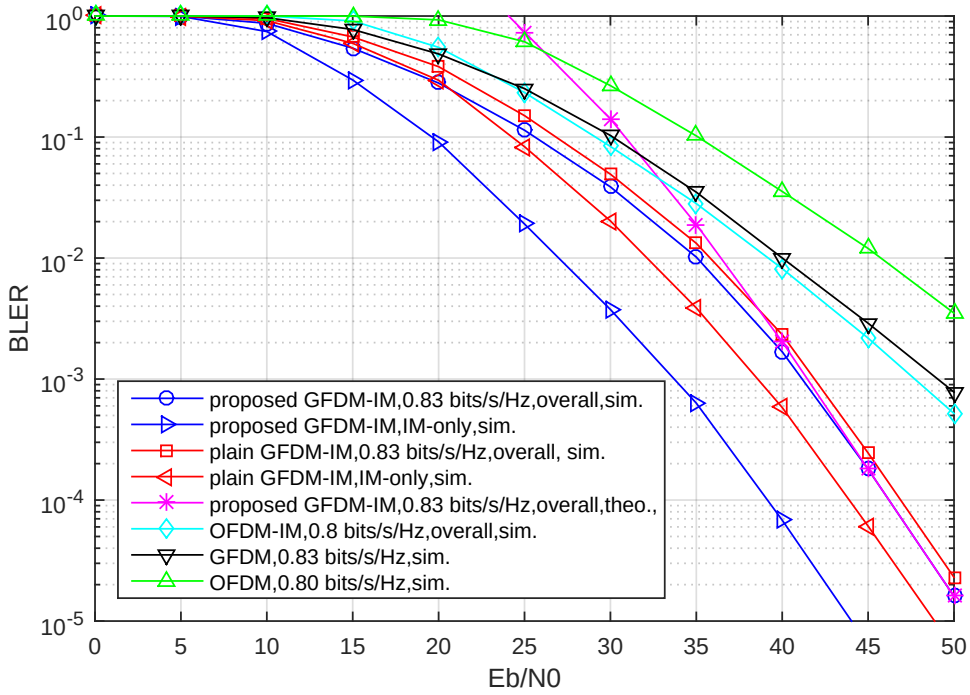

Figure 3.4 : Uncoded BLER performance for BPSK transmission.

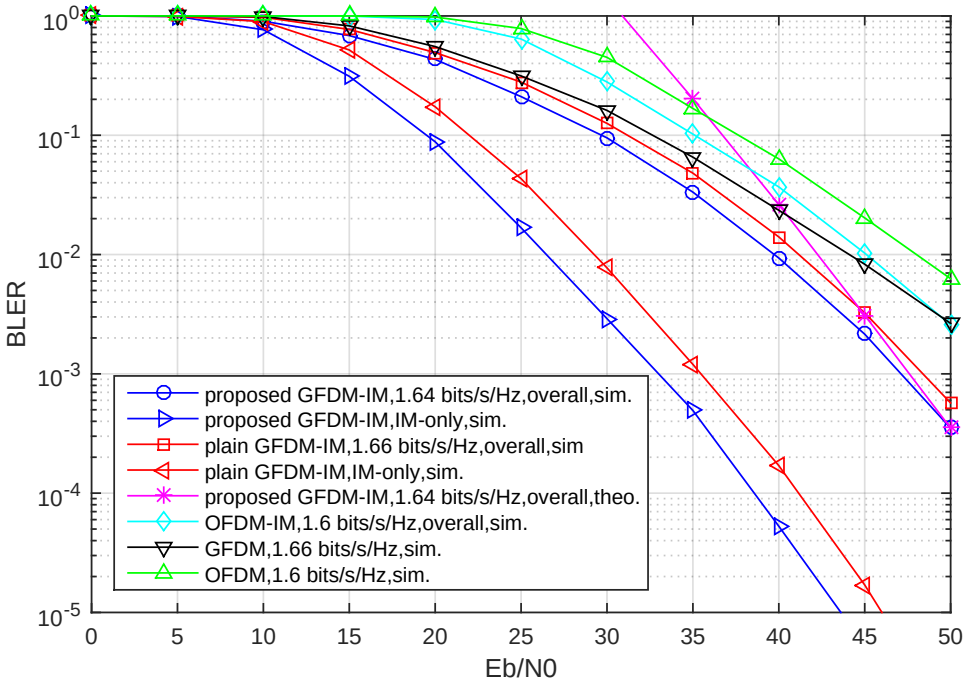

Figure 3.5 : Uncoded BLER performance for 4-QAM transmission.

4. GENERALIZED FREQUENCY DIVISION MULTIPLEXING WITH FLEXIBLE SPACE AND FREQUENCY INDEX MODULATION

4.1 GFDM-FIM Transmitter

As mentioned earlier, GFDM has a block structure consisting of $N = KM$ samples, where K subcarriers constitute a GFDM subsymbol and M GFDM subsymbols constitute a GFDM symbol. In this study, a MIMO-GFDM system with T transmit and R receive antennas is considered. The system has four control signals named as EN_{SM}, EN_{QM}, EN_{IM}, and EN_{DM}, which control SM, QSM, IM, and dual mode IM (DMIM) operation modes, respectively, in an on/off fashion, where EN_{SM}, EN_{QM}, EN_{IM}, $EN_{DM} \in \{0,1\}$. The overall system parameters are given in Table 4.1. Specific implementations of SM and IM schemes with respect to control signals are given in Table 4.2. Thanks to these control signals, existing schemes, such as, GFDM-based IM, DMIM, SM, and SFIM and new SM and IM schemes, such as, GFDM based QSM, space and frequency DMIM (SFDMIM), quadrature SFIM (QSFIM) and quadrature SFDMIM (QSFDMIM) can be implemented by using a single transmitter structure.

The block diagram of the proposed GFDM-FIM transmitter is given in Fig. 4.1. Primary bit splitter block accepts P data bits from the input bit stream along with the control signals and splits these P bits into L groups with p bits, i.e., $p = P/L$. Then, each group of p bits is mapped to a subcarrier group with u elements in three stages. In this mapping operation, antenna and subcarrier indices as well as Q-ary QAM (Q-QAM) constellations can be used. Besides, constellation symbols can be expanded to in-phase and quadrature components. In order to apply this mapping, secondary bit splitter partitions these p bits into four groups, which contain p_T, p_{IM}, p_A, and p_B bits according to status of the control signals.

Table 4.1 : System parameters used by GFDM-FIM transmitter and receiver.

Description	Parameter
Number of transmit antennas	T
Number of receive antennas	R
Number of subcarriers in a GFDM subsymbol	K
Number of GFDM subsymbols	M
Total number of subcarriers in a GFDM symbol	N
SM control signal	EN_{SM}
QSM control signal	EN_{QM}
IM control signal	EN_{IM}
Dual Mode IM control signal	EN_{DM}
Number of subcarriers in a subcarrier IM group	u
Number of subcarriers in a primary IM subgroup	v
Number of subcarriers in a secondary IM subgroup	$u-v$
Number of IM subcarrier groups	L
Number of symbols in primary symbol constellation	Q_A
Number of symbols in secondary symbol constellation	Q_B

Table 4.2 : Flexible IM control table for GFDM-FIM transmitter and receiver.

Scheme	EN_{SM}	EN_{QM}	EN_{IM}	EN_{DM}
GFDM	0	0	0	0
GFDM-IM	0	0	1	0
GFDM-DMIM	0	0	1	1
SM-GFDM	1	0	0	0
QSM-GFDM	1	1	0	0
SFIM-GFDM	1	0	1	0
QSFIM-GFDM	1	1	1	0
SFDMIM-GFDM	1	0	1	1
QSFDMIM-GFDM	1	1	1	1

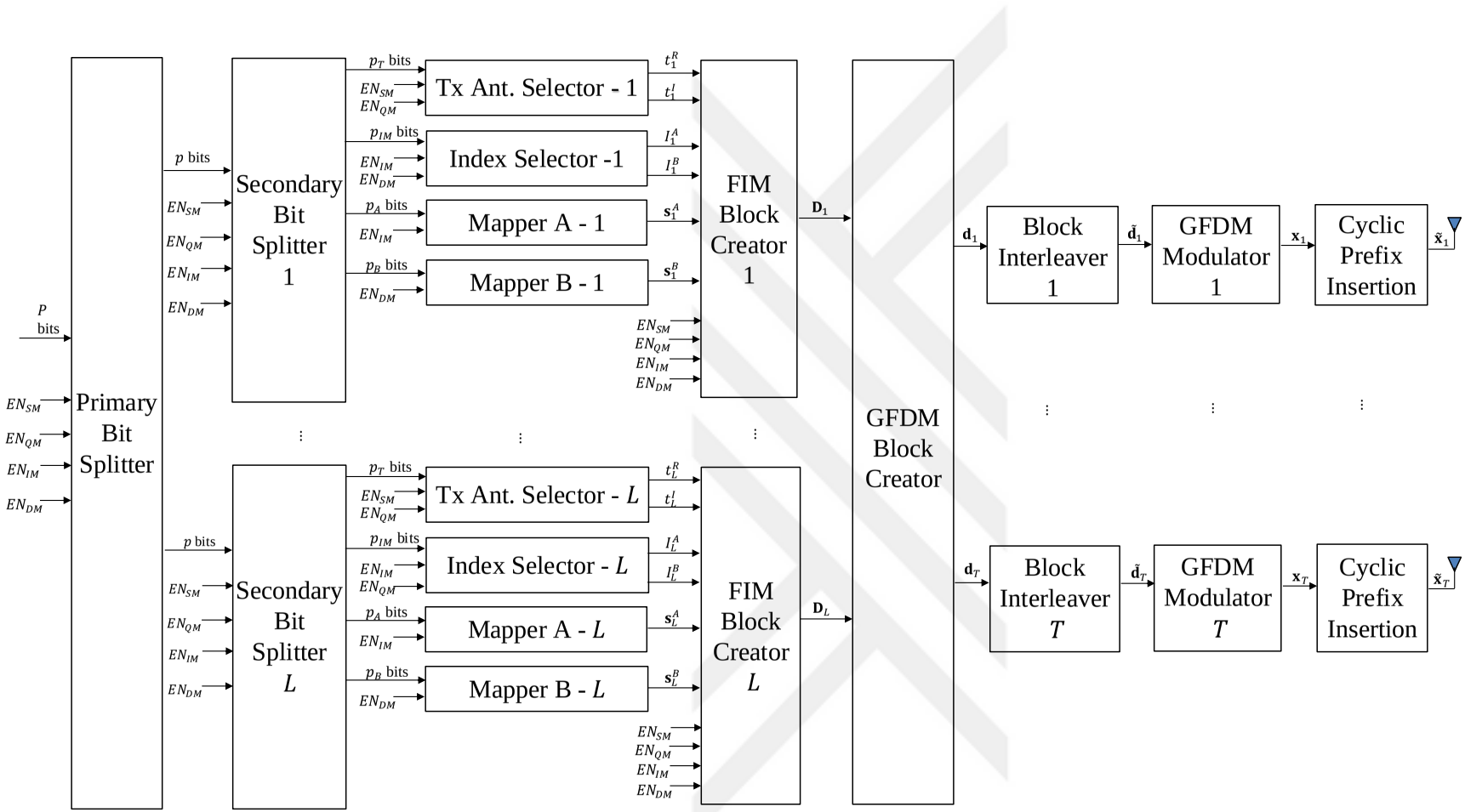

Figure 4.1 : Block diagram of the GFDM-FIM transmitter.

The first stage of the mapping is transmit antenna selection. At this stage, transmit antenna selector block gets

$$p_T = EN_{SM}(1 + EN_{QM})\log_2(T) \tag{4.1}$$

bits and selects the indices of the transmit antennas. When both SM and QSM modes are enabled, i.e., $EN_{SM} = 1$, $EN_{QM} = 1$, the first and second $\log_2(T)$-bits parts of the p_T-bit sequence are used to determine the transmit antennas corresponding to the real and the imaginary parts of the vector of the modulated symbols for the subcarrier IM group as t_l^R and t_l^I, respectively, where $t_l^R, t_l^I \in \{1,\ldots,T\}$. When the QSM mode is disabled, i.e., $EN_{QM} = 0$, only t_l^R is determined and it is used as the transmit antenna for both the real and the imaginary parts of the vector of the modulated symbols. Note that when the SM mode is disabled, i.e., $EN_{SM} = 0$, Tx antenna selector block remains inactive and transmission is always realized through a pre-determined transmit antenna.

The second stage of the mapping is index selection. At this stage, when IM mode is enabled, i.e., $EN_{IM} = 1$, index selector blocks gets p_{IM} bits to select the indices of the subcarriers in the primary IM subgroup, denoted as

$$I_l^A = \left\{ i_{l,1}^A, i_{l,2}^A, \ldots, i_{l,v}^A \right\}, \tag{4.2}$$

where $i_{l,\gamma}^A \in \{1,\ldots,u\}$, for $\gamma = 1,\ldots,v$, and $l \in \{1,\ldots,L\}$. Here, I_l^A is determined to modulate v subcarriers by a selection rule, besides when the DMIM mode is enabled along with the IM mode, i.e., $EN_{DM} = 1$, the remaining $u - v$ subcarriers constitute the indices of the subcarriers in the secondary IM subgroup, denoted as,

$$I_l^B = \left\{ i_{l,1}^B, i_{l,2}^B, \ldots, i_{l,u-v}^B \right\}, \tag{4.3}$$

where $i_{l,\gamma}^B \in \{1,\ldots,u\}$, for $\gamma = 1,\ldots,u-v$ and $l \in \{1,\ldots,L\}$. Since I_l^A has $c = 2^{p_{IM}}$ possible realizations, only c out of $C(u,v)$ possible combinations are used. Therefore, p_{IM} can be defined as

$$p_{IM} = EN_{IM}\lfloor \log_2 (C(u,v)) \rfloor. \tag{4.4}$$

Note that when the IM mode is disabled, i.e., $EN_{IM} = 0$, index selector block remains inactive and all subcarriers are used without any selection.

The third stage of the mapping is QAM modulation. At this stage, mapper A gets p_A bits to modulate the subcarriers selected by I_l^A and uses constellation set of $\mathscr{S}^A$, which

has Q_A elements, to modulate v subcarriers. Therefore, p_A can be defined as

$$p_A = v \log_2(Q_A). \tag{4.5}$$

When the DMIM mode is enabled along with the IM mode, i.e., $EN_{DM} = 1$, mapper B gets p_B bits to modulate the subcarriers selected by I_l^B and uses constellation set of $\mathscr{S}^B$, which has Q_B elements, to modulate $u - v$ subcarriers. Therefore, p_B can be defined as

$$p_B = EN_{IM} EN_{DM} (u - v) \log_2(Q_B). \tag{4.6}$$

At this point, in order to reliably detect the subcarrier index subgroups at the receiver, the constellations used by the mappers A and B have to be disjoint sets, i.e., $\mathscr{S}^A \cap \mathscr{S}^B = \varnothing$, where $\cap$ shows intersection operation and $\varnothing$ is the empty set. As a result, the vector of the modulated symbols mapped by mapper A for the index subgroup I_l^A, which carries p_A bits, and the vector of the modulated symbols mapped by mapper B for the index subgroup I_l^B, which carries p_B bits, can be expressed by

$$\mathbf{s}_l^A = \left[s_l^A(1), s_l^A(2), \ldots, s_l^A(v) \right]^{\mathrm{T}}, \tag{4.7}$$

$$\mathbf{s}_l^B = \left[s_l^B(1), s_l^B(2), \ldots, s_l^B(u-v) \right]^{\mathrm{T}}, \tag{4.8}$$

where $s_l^A(\gamma) \in \mathscr{S}^A$, for $\gamma = 1, \ldots, v$, $s_l^B(\gamma) \in \mathscr{S}^B$, for $\gamma = 1, \ldots, u - v$, respectively. Note that, when the IM mode is disabled, i.e., $EN_{IM} = 0$, both u and v are equal to 1 and $\mathbf{s}_l^A$ contains one Q-ary symbol and $\mathbf{s}_l^B$ is a null vector. Then, FIM block creator combines $\mathbf{s}_l^A$ and $\mathbf{s}_l^B$ and creates the vector of the modulated symbols for the subcarrier group l as

$$\mathbf{s}_l = \left[s_l(1), s_l(2), \ldots, s_l(u) \right]^{\mathrm{T}}, \tag{4.9}$$

where $\mathbf{s}_l(\gamma) \in \left\{ \mathscr{S}^A, \mathscr{S}^B, 0 \right\}$, for $\gamma = 1, \ldots, u$. After that, transmit antenna assignment procedure is executed according to status of the control signal EN_{QM}. When the QSM mode is enabled, i.e., $EN_{QM} = 1$, the in-phase parts of $\mathbf{s}_l$ are assigned to antenna t_l^R and the quadrature parts of the $\mathbf{s}_l$ are assigned to antenna t_l^I as

$$\mathbf{s}_{t_l^R,l} = \left[s_{t_l^R,l}(1), s_{t_l^R,l}(2), \ldots, s_{t_l^R,l}(u) \right]^{\mathrm{T}}, \tag{4.10}$$

$$\mathbf{s}_{t_l^I,l} = \left[s_{t_l^I,l}(1), s_{t_l^I,l}(2), \ldots, s_{t_l^I,l}(u) \right]^{\mathrm{T}}, \tag{4.11}$$

where $s_{t_l^R,l}(\gamma) \in \left\{ \Re\{\mathscr{S}^A\}, \Re\{\mathscr{S}^B\}, 0 \right\}$, for $t_l^R \in \{1, \ldots, T\}$, $s_{t_l^I,l}(\gamma) \in \left\{ \Im\{\mathscr{S}^A\}, \Im\{\mathscr{S}^B\}, 0 \right\}$, for $t_l^I \in \{1, \ldots, T\}$, $\gamma = 1, \ldots, u$, $\Re\{\Gamma\}$ is the real part of

a complex variable Γ and $\Im\{\Gamma\}$ is the imaginary part of a complex variable Γ. On the other hand, when the QSM mode is disabled, i.e., $EN_{QM} = 0$, both the in-phase and quadrature parts of $\mathbf{s}_l$ are assigned to transmit antenna t_l^R, i.e., $s_{t_l^R,l}(\gamma) \in \{\mathscr{S}^A, \mathscr{S}^B, 0\}$ and $\mathbf{s}_{t_l^I,l}$ is a null vector. Afterwards, FIM block creator sets the subcarriers of the inactive antennas to zero and arranges the transmit symbols for block l in a $T \times u$ matrix $\mathbf{D}_l$, where t_l^R-th row of $\mathbf{D}_l$ is $\mathbf{s}_{t_l^R,l}$ and t_l^I-th row of $\mathbf{D}_l$ is $\mathbf{s}_{t_l^I,l}$. Then, GFDM block creator combines the FIM blocks and the GFDM transmit signal block is obtained as

$$\mathbf{D} = [\mathbf{D}_1, \mathbf{D}_2, \ldots, \mathbf{D}_L], \tag{4.12}$$

where $\mathbf{D}$ is a $T \times N$ matrix. As a result, the GFDM symbol for the transmit antenna t, which is t-th row vector of $\mathbf{D}$, can be expressed by

$$\mathbf{d}_t = [d_{t,0,0}, \ldots, d_{t,K-1,0}, d_{t,0,1}, \ldots, d_{t,K-1,1}, \ldots, d_{t,K-1,M-1}], \tag{4.13}$$

where $d_{t,k,m}$ is the data symbol of m-th timeslot on k-th subcarrier belonging to t-th antenna. In [43] and [49], a block interleaver is used to render the channel memoryless; therefore, when the IM mode is active, i.e., $EN_{IM} = 1$, $L \times u$ block interleaving is applied to $\mathbf{d}_t$ and the interleaved data vector $\widetilde{\mathbf{d}}_t$ is obtained. After block interleaving, $\widetilde{\mathbf{d}}_t$ is modulated using a GFDM modulator and the overall GFDM transmit signal $x_t(n)$ of t-th transmit antenna is given by

$$x_t(n) = \sum_{k=0}^{K-1} \sum_{m=0}^{M-1} \widetilde{d}_{t,k,m} g_{k,m}(n), \tag{4.14}$$

where $n \in \{0, \ldots, N-1\}$ denotes the sampling index and

$$g_{k,m}(n) = g\left((n - mK)_{\mathrm{mod}N}\right) \exp\left(j2\pi \frac{kn}{K}\right) \tag{4.15}$$

is the transmit filter circularly shifted to the m-th timeslot and modulated to the k-th subcarrier. After collecting the filter samples in a vector $\mathbf{g}_{k,m} = \left[g_{k,m}(0), \ldots, g_{k,m}(N-1)\right]^{\mathrm{T}}$, equation 4.14 can be rewritten as

$$\mathbf{x}_t = \mathbf{A}\widetilde{\mathbf{d}}_t, \tag{4.16}$$

where $\mathbf{A}$ is a $KM \times KM$ transmitter matrix [2] with the following structure:

$$\mathbf{A} = [\mathbf{g}_{0,0}, \ldots, \mathbf{g}_{K-1,0}, \mathbf{g}_{0,1}, \ldots, \mathbf{g}_{K-1,1}, \ldots, \mathbf{g}_{K-1,M-1}]. \tag{4.17}$$

The last step at the transmitter side is the addition of a CP with length N_{CP} in order to make the convolution with the channel circular and the resulting vector

$$\widetilde{\mathbf{x}}_t = \left[\mathbf{x}_t\left(KM - N_{\mathrm{CP}} + 1 : KM\right)^{\mathrm{T}}, \mathbf{x}_t^{\mathrm{T}}\right]^{\mathrm{T}} \tag{4.18}$$

is obtained. Finally, $\widetilde{\mathbf{x}}_t$ is transmitted over a frequency-selective Rayleigh fading channel.

4.2 GFDM-FIM Receiver

The block diagram of the proposed GFDM-FIM receiver is given in Fig. 4.2. After the removal of CP, assuming that the wireless channel remains constant during the transmission of a GFDM block, CP is longer than the tap length of the channel (N_{Ch}) and perfect synchronization is ensured, the overall received signal can be expressed as

$$\begin{bmatrix}\mathbf{y}_1\\ \vdots\\ \mathbf{y}_R\end{bmatrix} = \begin{bmatrix}\mathbf{H}_{1,1} & \cdots & \mathbf{H}_{1,T}\\ \vdots & \ddots & \vdots\\ \mathbf{H}_{R,1} & \cdots & \mathbf{H}_{R,T}\end{bmatrix}\begin{bmatrix}\mathbf{x}_1\\ \vdots\\ \mathbf{x}_T\end{bmatrix} + \begin{bmatrix}\mathbf{w}_1\\ \vdots\\ \mathbf{w}_R\end{bmatrix}, \tag{4.19}$$

where $\mathbf{y}_r = [y_r(0), y_r(1), \ldots, y_r(N-1)]^{\mathrm{T}}$ is the vector of received signals at the r-th receive antenna, $\mathbf{H}_{r,t}$, for $t = 1, \ldots, T$, $r = 1, \ldots, R$, is the $N \times N$ circular convolution matrix constructed from the channel impulse response coefficients between the t-th transmit antenna and the r-th receive antenna given by $\mathbf{h}_{r,t} = [h_{r,t}(0), h_{r,t}(1), \ldots, h_{r,t}(N_{\mathrm{Ch}}-1)]^{\mathrm{T}}$, where $h_{r,t}(n)$ follows $\mathscr{CN}(0,1)$ distribution, $\mathbf{w}_r$ is an $N \times 1$ vector of AWGN samples with elements distributed as $\mathscr{CN}(0, \sigma_w^2)$. After substituting equation 4.16 in equation 4.19, an equivalent MIMO channel model is obtained as

$$\begin{bmatrix}\mathbf{y}_1\\ \vdots\\ \mathbf{y}_R\end{bmatrix} = \begin{bmatrix}\mathbf{H}_{1,1}\mathbf{A} & \cdots & \mathbf{H}_{1,T}\mathbf{A}\\ \vdots & \ddots & \vdots\\ \mathbf{H}_{R,1}\mathbf{A} & \cdots & \mathbf{H}_{R,T}\mathbf{A}\end{bmatrix}\begin{bmatrix}\widetilde{\mathbf{d}}_1\\ \vdots\\ \widetilde{\mathbf{d}}_T\end{bmatrix} + \begin{bmatrix}\mathbf{w}_1\\ \vdots\\ \mathbf{w}_R\end{bmatrix}. \tag{4.20}$$

Equation 4.20 can be rewritten in a more compact form as

$$\mathbf{y} = \widetilde{\mathbf{H}}\widetilde{\mathbf{d}} + \mathbf{w}, \tag{4.21}$$

where the dimensions of $\mathbf{y}$, $\widetilde{\mathbf{H}}$, $\widetilde{\mathbf{d}}$ and $\mathbf{w}$ are $NR \times 1$, $NR \times NT$, $NT \times 1$ and $NR \times 1$, respectively. The most critical part of the GFDM-FIM receiver is the block of MIMO detection, GFDM and SFIM demodulation. For MIMO-OFDM, MIMO detection and

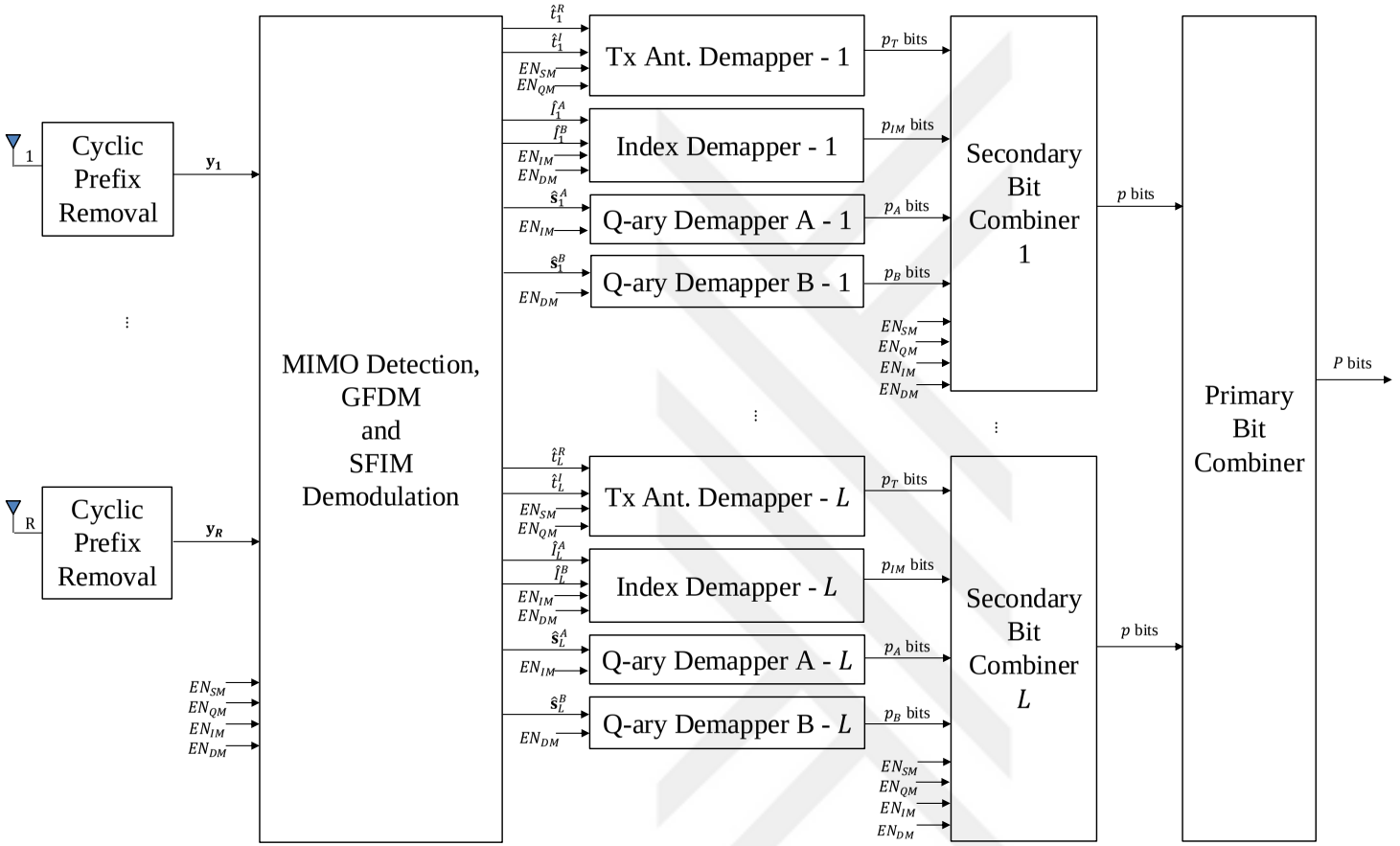

Figure 4.2 : Block diagram of the GFDM-FIM receiver.

SFIM demodulation can be performed at the subcarrier level due to orthogonality in the frequency domain. In GFDM, the inherent ICI prevents the frequency domain decoupling of GFDM subcarriers for both SISO and MIMO transmission schemes. In [48], MIMO detection, GFDM demodulation and spatial demodulation are treated independently, where a poor error performance has been obtained. In [49], GFDM demodulation and index demodulation are handled as two distinct tasks. In [50], while joint MIMO detection and GFDM demodulation has been proposed, SFIM demodulation has been treated in an independent way. As will be shown later, these methods are also applicable for the GFDM-FIM receiver. Besides, in this study, a new method is proposed by treating MIMO detection, GFDM and SFIM demodulation jointly. These methods will be presented as three alternatives for MIMO detection, GFDM and SFIM demodulation block of the GFDM-FIM receiver in the subsequent subsections.

After MIMO detection, GFDM and SFIM demodulation, the information bits are recovered by applying the inverse mapping process for both modulated symbols and indices of the active transmit antennas and subcarriers. Then, the secondary bit combiner combines the outputs of the demappers and forms the p-bit sequence, which is the estimate of the input of the secondary bit splitter. Finally, the primary bit combiner combines all p-bit groups and forms the original P-bit data sequence.

4.2.1 ZF-SDD based separate MIMO detection, GFDM and SFIM demodulation

The block diagram of the proposed ZF-SDD Based Separate MIMO Detection, GFDM and SFIM Demodulation method is given in Fig. 4.3. Based on the system model in equation 4.19, after performing FFT operations in each antenna branch of the receiver, the input-output relationship of the GFDM-FIM scheme in the frequency domain is obtained as

$$\mathbf{y}_r^F = \sum_{t=1}^{T} \mathrm{diag}(\mathbf{x}_t^F)\mathbf{h}_{r,t}^F + \mathbf{w}_r^F, \tag{4.22}$$

where $\mathbf{y}_r^F = [y_r^F(0), y_r^F(1), \ldots, y_r^F(N-1)]^{\mathrm{T}}$ is the vector of received signals at the r-th receive antenna, for $r = 1, \ldots, R$, and $\mathbf{h}_{r,t}^F = \left[h_{r,t}^F(0), h_{r,t}^F(1), \ldots, h_{r,t}^F(N-1)\right]^{\mathrm{T}}$ is the frequency response of the wireless channel between the transmit antenna t and the

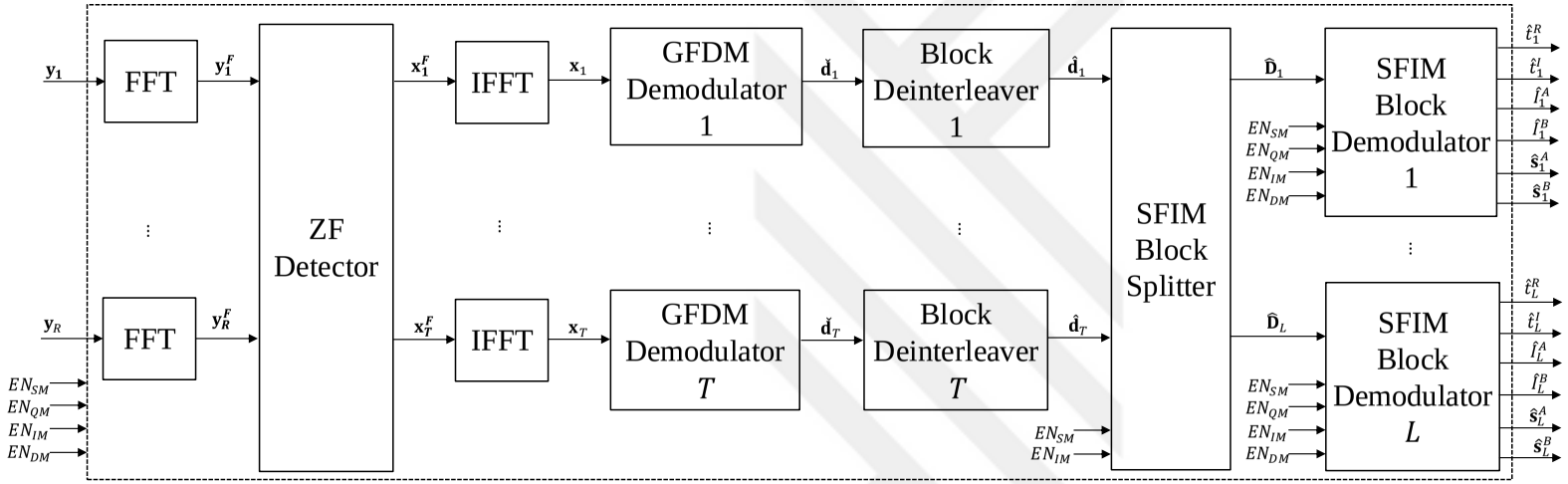

Figure 4.3 : Block diagram of the ZF-SDD based separate MIMO detection, GFDM and SFIM demodulation.

receive antenna r, where $h_{r,t}^F(\gamma)$ follows $\mathscr{CN}(0,1)$ distribution, $\mathbf{w}_r^F$ is an $N \times 1$ vector of noise samples distributed as $\mathscr{CN}(0,\sigma_w^2)$. Since GFDM block is made up of KM subcarriers, the following signal model is obtained from equation 4.22 for k-th subcarrier of m-th subsymbol:

$$\begin{bmatrix} y_1^F(k,m) \\ y_2^F(k,m) \\ \vdots \\ y_R^F(k,m) \end{bmatrix} = \begin{bmatrix} h_{1,1}^F(k,m) & \cdots & h_{1,T}^F(k,m) \\ h_{2,1}^F(k,m) & \cdots & h_{2,T}^F(k,m) \\ \vdots & \ddots & \vdots \\ h_{R,1}^F(k,m) & \cdots & h_{R,T}^F(k,m) \end{bmatrix} \begin{bmatrix} x_1^F(k,m) \\ x_2^F(k,m) \\ \vdots \\ x_T^F(k,m) \end{bmatrix} + \begin{bmatrix} w_1^F(k,m) \\ w_2^F(k,m) \\ \vdots \\ w_R^F(k,m) \end{bmatrix}. \tag{4.23}$$

Equation 4.23 can be rewritten in a more compact form as

$$\mathbf{y}_{k,m}^F = \mathbf{H}_{k,m}^F \mathbf{x}_{k,m}^F + \mathbf{w}_{k,m}^F, \tag{4.24}$$

where $\mathbf{y}_{k,m}^F$ is the received signal vector, $\mathbf{H}_{k,m}^F$, for $k = 0,\ldots,K-1, m = 0,\ldots,M-1$, is the $R \times T$ corresponding channel matrix that contains the channel coefficients between transmit and receive antennas and assumed to be perfectly known at the receiver, $\mathbf{x}_{k,m}^F$ is the data vector, which contains the simultaneously transmitted symbols from all transmit antennas and $\mathbf{w}_{k,m}^F$ is the noise vector. Here, an estimate of $\mathbf{x}_{k,m}^F$ can be obtained by using ZF detection approach as follows:

$$\widehat{\mathbf{x}}_{k,m}^F = \left(\mathbf{H}_{k,m}^F\right)^{-1} \mathbf{y}_{k,m}^F. \tag{4.25}$$

Rearranging of vectors $\widehat{\mathbf{x}}_{k,m}^F$ as column vectors of a matrix gives

$$\widehat{\mathbf{X}}^F = \left[(\widehat{\mathbf{x}}_{0,0}^F)^{\mathrm{T}}, \ldots, (\widehat{\mathbf{x}}_{K-1,0}^F)^{\mathrm{T}}, (\widehat{\mathbf{x}}_{0,1}^F)^{\mathrm{T}}, \ldots, (\widehat{\mathbf{x}}_{K-1,M-1}^F)^{\mathrm{T}}\right], \tag{4.26}$$

where each row contains an estimate of the frequency domain representation of the transmit vector for the corresponding antenna, that is:

$$\widehat{\mathbf{X}}^F = \begin{bmatrix} \widehat{\mathbf{x}}_1^F \\ \widehat{\mathbf{x}}_2^F \\ \vdots \\ \widehat{\mathbf{x}}_T^F \end{bmatrix}. \tag{4.27}$$

Then, IFFT of size N is applied to $\widehat{\mathbf{x}}_t^F$ and $\widehat{\mathbf{x}}_t$ is obtained. Afterwards, linear GFDM demodulation of the $\widehat{\mathbf{x}}_t$ is obtained by using ZF approach:

$$\breve{\mathbf{d}}_t = \mathbf{A}^{-1} \widehat{\mathbf{x}}_t \tag{4.28}$$

After this point, if block interleaving was applied at the transmitter, $L \times u$ block deinterleaving is applied to $\breve{\mathbf{d}}_t$ and $\widehat{\mathbf{d}}_t$ is obtained. SFIM block splitter partitions $\widehat{\mathbf{d}}_t$ into L groups with length u and arranges these groups in a $T \times u$ matrix given by

$$\widehat{\mathbf{D}}_l = \begin{bmatrix} \widehat{\mathbf{s}}_{1,l} \\ \vdots \\ \widehat{\mathbf{s}}_{T,l} \end{bmatrix} = \begin{bmatrix} \widehat{\mathbf{d}}_1((l-1)u+1:lu) \\ \vdots \\ \widehat{\mathbf{d}}_T((l-1)u+1:lu) \end{bmatrix}. \tag{4.29}$$

Note that when the IM mode is disabled, i.e., $EN_{IM} = 0$, u is equal to 1 and $\widehat{\mathbf{s}}_{t,l}$, for $t = 1,\ldots,T$, has only one element. Then, SFIM block demodulator makes a joint decision on the indices of transmit antennas corresponding to the in-phase and the quadrature parts of the vector of the modulated symbols, subcarrier index subgroups as well as constellation symbols considering all possible realizations of $\mathbf{D}_l$ by minimizing the following metric:

$$\left\{\hat{t}_l^R, \hat{t}_l^I, \hat{I}_l^A, \hat{\mathbf{s}}_l^A, \hat{\mathbf{s}}_l^B\right\} = \underset{t, I^A, \mathscr{S}^A, \mathscr{S}^B}{\arg\min} \|\widehat{\mathbf{D}}_l - \mathbf{D}_l\|_F^2. \tag{4.30}$$

Here, $\|\cdot\|_F$ is the Frobenius norm.

4.2.2 MMSE based joint MIMO detection and GFDM demodulation, separate SFIM demodulation

The block diagram of the proposed MMSE Based Joint MIMO Detection and GFDM Demodulation, Separate SFIM Demodulation method is given in Fig. 4.4. Thanks to system model in equation 4.21, unlike ZF-SDD based MIMO detection, GFDM and SFIM demodulation, which uses ZF detector in the frequency domain, thus, handles MIMO detection and GFDM demodulation separately, GFDM modulation and MIMO channel can be linearly modeled. As a result, JDD through MMSE filtering can be performed by

$$\breve{\mathbf{D}} = \left(\widetilde{\mathbf{H}}^{\mathrm{H}}\widetilde{\mathbf{H}} + \sigma_w^2\mathbf{I}\right)^{-1}\widetilde{\mathbf{H}}^{\mathrm{H}}\mathbf{y}, \tag{4.31}$$

where t-th row of $\breve{\mathbf{D}}$ is $\breve{\mathbf{d}}_t$, which is the estimation of the output of the t-th block interleaver. Then, block deinterleaving, SFIM block splitting and SFIM block demodulation are performed as explained in Section 4.2.1.

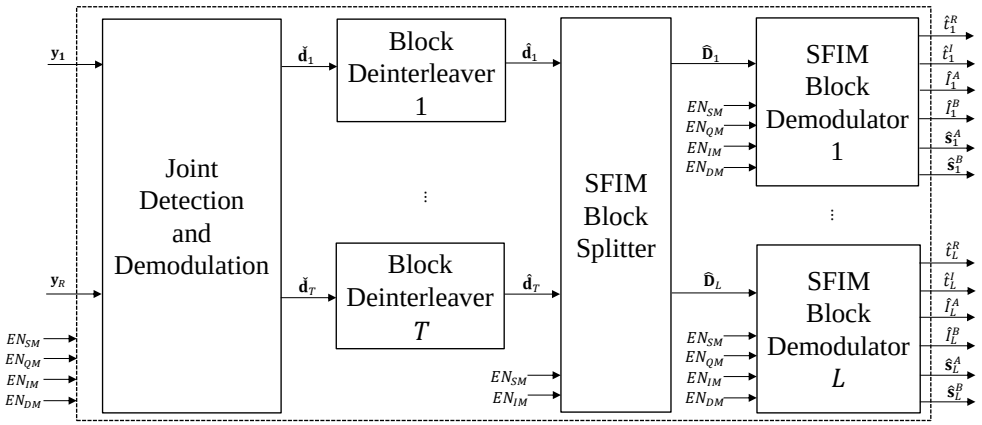

Figure 4.4 : Block diagram of the MMSE-JDD based joint MIMO detection and GFDM demodulation, separate SFIM demodulation.

4.2.3 ML-SIC based joint MIMO detection, GFDM and SFIM demodulation

The block diagram of the proposed ML-SIC Based Joint MIMO Detection, GFDM and SFIM Demodulation method is given in Fig. 4.5. In GFDM, as mentioned earlier, the inherent ICI prevents the frequency domain decoupling of GFDM subcarriers for both SISO and MIMO transmission schemes; therefore, simultaneous detection of all subcarriers is required for optimum decision. Since this process is computationally infeasible, low complexity solutions are required for the optimum detection problem of MIMO-GFDM. In [24], an algorithm including SD of subcarrier groups with SIC is proposed for SMX. By properly organizing the columns of $\widetilde{\mathbf{H}}$ in equation 4.21, the algorithm in [24] can be modified to jointly detect the antenna and subcarrier indices as well as the transmitted symbols for GFDM-FIM schemes. The QR decomposition [86] of the channel matrix $\widetilde{\mathbf{H}}$ is given as

$$\widetilde{\mathbf{H}} = \mathbf{QRP}^{\mathrm{T}}, \tag{4.32}$$

where $\mathbf{Q}$ is an $NR \times NT$ unitary matrix, $\mathbf{R}$ is an $NT \times NT$ upper triangular matrix, and $\mathbf{P}$ sorts the columns of $\widetilde{\mathbf{H}}$ prior to decomposition to detect the transmitted symbols at the SFIM block level. Note that if block interleaving was applied at the transmitter, block deinterleaving must be applied to the columns of $\widetilde{\mathbf{H}}$ prior to sorting. The QR decomposer combines the received signals, i.e., $\mathbf{y} = \left[\mathbf{y}_1{}^{\mathrm{T}}, \mathbf{y}_2{}^{\mathrm{T}}, \ldots, \mathbf{y}_R{}^{\mathrm{T}}\right]^{\mathrm{T}}$, multiplies with $\mathbf{Q}^{\mathrm{H}}$ from the left and obtains the modified received signal vector

$$\widetilde{\mathbf{y}} = \mathbf{Q}^{\mathrm{H}}\mathbf{y} = \mathbf{R}\widetilde{\mathbf{d}} + \widetilde{\mathbf{w}}, \tag{4.33}$$

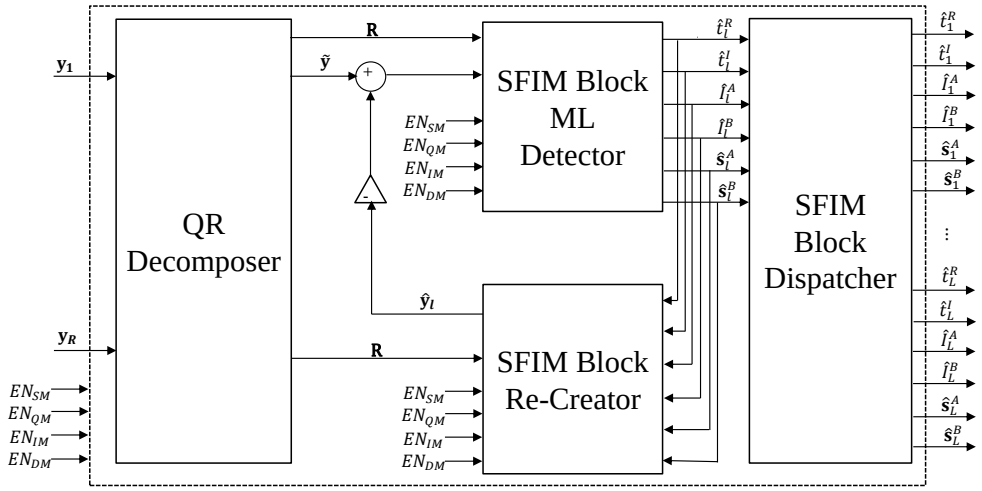

Figure 4.5 : Block diagram of the ML-SIC based joint MIMO detection, GFDM and SFIM demodulation.

where $\widetilde{\mathbf{w}} = \mathbf{Q}^{\mathrm{H}}\mathbf{w}$ and

$$\widetilde{\mathbf{d}} = \mathbf{P}^{\mathrm{T}}\mathbf{d} = \left[\mathbf{z}_1{}^{\mathrm{T}}, \mathbf{z}_2{}^{\mathrm{T}}, \ldots, \mathbf{z}_L{}^{\mathrm{T}}\right]^{\mathrm{T}}. \tag{4.34}$$

Here, $\mathbf{z}_l$, for $l = 1, \ldots, L$, is an $uT \times 1$ vector given by

$$\mathbf{z}_l = \left[\mathbf{s}_{1,l}, \mathbf{s}_{2,l}, \ldots, \mathbf{s}_{T,l}\right], \tag{4.35}$$

where $\mathbf{s}_{t,l}$, for $t = 1, \ldots, T$ and $l \in \{1, \ldots, L\}$, is an $u \times 1$ vector denoted by

$$\mathbf{s}_{t,l} = \left[s_{t,l}(1), s_{t,l}(2), \ldots, s_{t,l}(u)\right] = \left[\mathbf{d}_t((l-1)u+1 : lu)\right]. \tag{4.36}$$

As stated earlier, when the IM mode is disabled, i.e., $EN_{IM} = 0$, u is equal to 1 and $\widehat{\mathbf{s}}_{t,l}$, for $t = 1, \ldots, T$, has only one element. Then, with the help of the upper triangular structure of $\mathbf{R}$, the SFIM block ML detector finds the ML solution for the last SFIM block, cancels the interference originated from it, reduces the system size by uT and continues to the next SFIM block until all SFIM blocks are detected. The proposed detection algorithm is shown in Algorithm 2. Here, the subscripts uT, $u\bar{T}$ and : denote the last uT, all but the last uT and all elements (column/rows) of the subscripted object, respectively. After this point, for each SFIM block, transmit antennas corresponding to the in-phase and the quadrature parts of the vector of the modulated symbols, subcarrier index subgroups as well as constellation symbols, are estimated as $\hat{t}_l^R$, $\hat{t}_l^I$, $\hat{I}_l^A$, $\hat{I}_l^B$, $\hat{\mathbf{s}}_l^A$, $\hat{\mathbf{s}}_l^B$, respectively.

Algorithm 2 ML-SIC detection

1: **Input** $= \widetilde{\mathbf{y}}, \mathbf{R}$
2: **Output** $= \hat{t}_l^R, \hat{t}_l^I, \hat{I}_l^A, \hat{I}_l^B, \hat{\mathbf{s}}_l^A, \hat{\mathbf{s}}_l^B$ for $l = 1, \ldots, L$
3: **for** $l \leftarrow L$ to 1 **do**
4: $\quad \hat{\mathbf{z}}_l = \underset{t, I^A, \mathscr{S}^A, \mathscr{S}^B}{\operatorname{argmin}} \left\| \widetilde{\mathbf{y}}_{uT} - \mathbf{R}_{uT,uT}\mathbf{z}_l \right\|^2$
5: $\quad \hat{\mathbf{y}}_l = \mathbf{R}_{:,uT}\hat{\mathbf{z}}_l, \widetilde{\mathbf{y}} \leftarrow \widetilde{\mathbf{y}} - \hat{\mathbf{y}}_l$
6: $\quad \widetilde{\mathbf{y}} \leftarrow \widetilde{\mathbf{y}}_{\bar{uT}}, \mathbf{R} \leftarrow \mathbf{R}_{\bar{uT},\bar{uT}}$
7: **end for**

4.3 Complexity Analysis

Computational complexity of four different GFDM-FIM receivers is analyzed in terms of number of CMs performed in total and presented in Tables 4.3, 4.4, 4.5 and 4.6. Here, $\Phi_{J\times I}$ and $\Psi_{J\times I}$ stand for $J \times I$ matrices, $\phi_{J\times 1}$ and $\psi_{J\times 1}$ are used for $J \times 1$ vectors, $QR(\cdot)$ and $(\cdot)^+$ perform QR decomposition and pseudo-inversion, respectively. The results are summarized in Tables 4.7 and 4.8. According to Tables 4.7 and 4.8, it is observed that whereas the receivers with ML and ZF-SDD detection techniques have the highest and the lowest complexity, respectively, the receivers with ML-SIC and MMSE-JDD techniques provide an intermediate solution in terms of detection complexity.

4.4 Spectral Efficiency Analysis

As mentioned earlier, GFDM uses a single CP for the entire symbol block composed of K subcarriers with M timeslots. Thus, spectral efficiency gain of GFDM schemes over OFDM schemes with the same system parameters becomes

$$\rho_{GFDM} = 100\frac{N_{\mathrm{CP}}(M-1)}{KM + N_{\mathrm{CP}}}\%. \tag{4.37}$$

As it will be shown in Section 4.5, significant gains can be obtained over OFDM schemes in spectral efficiency according to equation 4.37. On the other hand, the activation of the QSM operation, i.e., $EN_{QM} = 1$, provides a spectral efficiency gain with a negligible increase in detection complexity and slightly decreased BER performance. For instance, spectral efficiency gain of the QSM-GFDM system over

SM-OFDM with the same system parameters is given by

$$\rho_{QSM} = 100\frac{\log_2(T)}{\log_2(TQ_A)}\%. \tag{4.38}$$

The spectral efficiency gain provided by the QSM operation is also viable for SFIM and SFDMIM schemes in a decreased manner. Whereas spectral efficiency gain of the QSFIM-GFDM system over SFIM-GFDM with the same system parameters is given by

$$\rho_{QSFIM} = 100\frac{\log_2(T)}{\log_2(TcQ_A^v)}\%, \tag{4.39}$$

spectral efficiency gain of the QSFDMIM-GFDM system over SFDMIM-GFDM becomes

$$\rho_{QSFDMIM} = 100\frac{\log_2(T)}{\log_2(TcQ_A^vQ_B^{u-v})}\%. \tag{4.40}$$

Furthermore, enabling DMIM operation, i.e., $EN_{DM} = 1$, also provides spectral efficiency gain with a moderately increased detection complexity and slightly decreased BER performance. For instance, spectral efficiency gain of the SFDMIM-GFDM system over SFIM-GFDM with the same system parameters is given by

$$\rho_{SFDMIM} = 100\frac{\log_2(Q_B^{u-v})}{\log_2(TcQ_A^v)}\%. \tag{4.41}$$

Spectral efficiency gains provided by QSM and DMIM operations will be discussed along with the computational complexity and BER performance through numerical results in Section 4.5.

Table 4.3 : Computational complexity of ZF-SDD based GFDM-FIM receiver.

Process	Scheme	Operation	Execution Count	Complexity (CMs)
DFT block	all	$\mathrm{DFT}\left(\phi_{N\times 1}\right)^{*}$	R	N^2R
ZF detection	all	$\left(\Phi_{R\times T}\right)^{+}\phi_{R\times 1}$	N	$2NT^2R+NT^3+NTR$
IDFT block	all	$\mathrm{IDFT}\left(\phi_{N\times 1}\right)^{*}$	T	N^2T
GFDM demod.	all	$\Phi_{N\times N}\phi_{N\times 1}$	T	N^2T
Block Deinter.	all	No CM	R	0
SFIM Demod.	SM	$\min(\|\phi_{T\times 1}-\psi_{T\times 1})\|^2)$	NTQ_A	NT^2Q_A
	QSM	$\min(\|\phi_{T\times 1}-\psi_{T\times 1})\|^2)$	NT^2Q_A	NT^3Q_A
	SFIM	$\min(\|\phi_{T\times u}-\psi_{T\times u})\|^2)$	$(N/u)cQ_A^vT$	$NcQ_A^vT^2$
	QSFIM	$\min(\|\phi_{T\times u}-\psi_{T\times u})\|^2)$	$(N/u)cQ_A^vT^2$	$NcQ_A^vT^3$
	SFDMIM	$\min(\|\phi_{T\times u}-\psi_{T\times u})\|^2)$	$(N/u)cQ_A^vQ_B^{u-v}T$	$NcQ_A^vQ_B^{u-v}T^2$
	QSFDMIM	$\min(\|\phi_{T\times u}-\psi_{T\times u})\|^2)$	$(N/u)cQ_A^vQ_B^{u-v}T^2$	$NcQ_A^vQ_B^{u-v}T^3$

* We consider direct calculation of N-point DFT and IDFT operations, which involve N^2 CMs, since M is odd.

Table 4.4 : Computational complexity of MMSE-JDD based GFDM-FIM receiver.

Process	Scheme	Operation	Execution Count	Complexity (CMs)
Forming $\widetilde{\mathbf{H}}$	all	$\Phi_{N\times N}\Psi_{N\times N}$ **	RT	$N_{\mathrm{Ch}}N^2RT$
JDD	all	$\left(\Phi_{NR\times NT}{}^{\mathrm{H}}\Phi_{NR\times NT}+\Psi_{NT\times NT}\right)^{-1}\Phi_{NR\times NT}{}^{\mathrm{H}}\phi_{NR\times 1}$	1	$2N^3T^2R+N^3T^3+N^2RT$
Block Deinter.	all	No CM	R	0
SFIM Demod.	SM	$\min(\|\phi_{T\times 1}-\psi_{T\times 1})\|^2)$	NTQ_A	NT^2Q_A
	QSM	$\min(\|\phi_{T\times 1}-\psi_{T\times 1})\|^2)$	NT^2Q_A	NT^3Q_A
	SFIM	$\min(\|\phi_{T\times u}-\psi_{T\times u})\|^2)$	$(N/u)cQ_A^vT$	$NcQ_A^vT^2$
	QSFIM	$\min(\|\phi_{T\times u}-\psi_{T\times u})\|^2)$	$(N/u)cQ_A^vT^2$	$NcQ_A^vT^3$
	SFDMIM	$\min(\|\phi_{T\times u}-\psi_{T\times u})\|^2)$	$(N/u)cQ_A^vQ_B^{u-v}T$	$NcQ_A^vQ_B^{u-v}T^2$
	QSFDMIM	$\min(\|\phi_{T\times u}-\psi_{T\times u})\|^2)$	$(N/u)cQ_A^vQ_B^{u-v}T^2$	$NcQ_A^vQ_B^{u-v}T^3$

** In every row of $\mathbf{H}_{r,t}$, which is Φ in this case, only N_{Ch} out of N elements are non-zero.

Table 4.5 : Computational complexity of ML-SIC based GFDM-FIM receiver.

Process	Scheme	Operation	Execution Count	Complexity (CMs)
Forming $\widetilde{\mathbf{H}}$	all	$\Phi_{N\times N}{\Psi_{N\times N}}^{\dagger}$	RT	$N_{\mathrm{Ch}}N^2RT$
Block Deinter.	all	No CM	R	0
Permutation	all	No CM	1	0
QRD	all	$QR\left(\Phi_{NR\times NT}\right)^{\dagger\dagger}$	1	$2N^3T^2R$
Modified recv. vector	all	${\Phi_{NR\times NT}}^{\mathrm{H}}\phi_{NR\times 1}$	1	N^2RT
ML Detection	SM	$\min(\|\phi_{T\times 1}-(\Phi_{T\times T}\psi_{T\times 1})\|^2)^{\dagger\dagger\dagger}$	NTQ_A	$N2T^2Q_A$
	QSM	$\min(\|\phi_{T\times 1}-(\Phi_{T\times T}\psi_{T\times 1})\|^2)^{\dagger\dagger\dagger}$	NT^2Q_A	$N2T^3Q_A$
	SFIM	$\min(\|\phi_{uT\times 1}-(\Phi_{uT\times uT}\psi_{uT\times 1})\|^2)^{\dagger\dagger\dagger\dagger}$	$(N/u)cQ_A^vT$	$(N/u)(cQ_A^vT(uvT+uT))$
	QSFIM	$\min(\|\phi_{uT\times 1}-(\Phi_{uT\times uT}\psi_{uT\times 1})\|^2)^{\dagger\dagger\dagger\dagger}$	$(N/u)cQ_A^vT^2$	$(N/u)(cQ_A^vT^2(uvT+uT))$
	SFDMIM	$\min(\|\phi_{uT\times 1}-(\Phi_{uT\times uT}\psi_{uT\times 1})\|^2)$	$(N/u)cQ_A^vQ_B^{u-v}T$	$(N/u)(cQ_A^vQ_B^{u-v}T(u^2T+uT))$
	QSFDMIM	$\min(\|\phi_{uT\times 1}-(\Phi_{uT\times uT}\psi_{uT\times 1})\|^2)$	$(N/u)cQ_A^vQ_B^{u-v}T^2$	$(N/u)(cQ_A^vQ_B^{u-v}T^2(u^2T+uT))$
SIC	SM	$\phi_{NT\times 1}-\Phi_{NT\times T}{\psi_{T\times 1}}^{\dagger\dagger\dagger}$	N	N^2T
	QSM	$\phi_{NT\times 1}-\Phi_{NT\times T}{\psi_{T\times 1}}^{\dagger\dagger\dagger}$	N	N^2T
	SFIM	$\phi_{NT\times 1}-\Phi_{NT\times uT}{\psi_{uT\times 1}}^{\dagger\dagger\dagger\dagger}$	(N/u)	N^2vT/u
	QSFIM	$\phi_{NT\times 1}-\Phi_{NT\times uT}{\psi_{uT\times 1}}^{\dagger\dagger\dagger\dagger}$	(N/u)	N^2vT/u
	SFDMIM	$\phi_{NT\times 1}-\Phi_{NT\times uT}\psi_{uT\times 1}$	(N/u)	N^2T
	QSFDMIM	$\phi_{NT\times 1}-\Phi_{NT\times uT}\psi_{uT\times 1}$	(N/u)	N^2T

† In every row of $\mathbf{H}_{r,t}$, which is Φ in this case, only N_{Ch} out of N elements are non-zero.
†† The modified Gram-Schmidt orthogonalization algorithm requires $2mn^2$ complex multiplication to compute the QR-factorization of an $m\times n$ matrix.
††† In ψ, only one complex element is nonzero.
†††† In ψ, only v complex elements are nonzero.

Table 4.6 : Computational complexity of ML based GFDM-FIM receiver.

Process	Scheme	Operation	Execution Count	Complexity (CMs)
Forming $\widetilde{\mathbf{H}}$	all	$\Phi_{N\times N}\Psi_{N\times N}{}^{\ddagger}$	RT	$N_{\text{Ch}}N^2RT$
Block Deinter.	all	No CM	R	0
ML Detection	SM	$\min(\|\phi_{NT\times 1}-(\Phi_{NR\times NT}\psi_{NT\times 1})\|^2)^{\ddagger\ddagger}$	$(Q_AT)^N$	$(Q_AT)^N(N^2R+NT)$
	QSM	$\min(\|\phi_{NT\times 1}-(\Phi_{NR\times NT}\psi_{NT\times 1})\|^2)^{\ddagger\ddagger}$	$(Q_AT^2)^N$	$(Q_AT^2)^N(N^2R+NT)$
	SFIM	$\min(\|\phi_{NT\times 1}-(\Phi_{NR\times NT}\psi_{NT\times 1})\|^2)^{\ddagger\ddagger\ddagger}$	$(cQ_A^vT)^{(N/u)}$	$(cQ_A^vT)^{(N/u)}((N^2Rv/u)+NT)$
	QSFIM	$\min(\|\phi_{NT\times 1}-(\Phi_{NR\times NT}\psi_{NT\times 1})\|^2)^{\ddagger\ddagger\ddagger}$	$(cQ_A^vT^2)^{(N/u)}$	$(cQ_A^vT^2)^{(N/u)}((N^2Rv/u)+NT)$
	SFDMIM	$\min(\|\phi_{NT\times 1}-(\Phi_{NR\times NT}\psi_{NT\times 1})\|^2)$	$(cQ_A^vQ_B^{u-v}T)^{(N/u)}$	$(cQ_A^vQ_B^{u-v}T)^{(N/u)}(N^2R+NT)$
	QSFDMIM	$\min(\|\phi_{NT\times 1}-(\Phi_{NR\times NT}\psi_{NT\times 1})\|^2)$	$(cQ_A^vQ_B^{u-v}T^2)^{(N/u)}$	$(cQ_A^vQ_B^{u-v}T^2)^{(N/u)}(N^2R+NT)$

‡ In every row of $\mathbf{H}_{r,t}$, which is Φ in this case, only N_{Ch} out of N elements are non-zero.
‡‡ In ψ, only N complex elements are nonzero.
‡‡‡ In ψ, only Nv/u complex elements are nonzero.

Table 4.7 : Summary of the computational complexity of SM, QSM and SFIM receivers.

Scheme	Receiver	Complexity (CMs)
Common Part (CmP)	ZF-SDD	$N^2(2T+R)+N(T^3+2T^2R+TR)$
	MMSE-JDD	$N^3(2T^2R+T^3)+N^2(N_{Ch}RT+RT)$
	ML-SIC	$N^3(2T^2R)+N^2(N_{Ch}RT+RT)$
	ML	$N^2N_{Ch}RT$
SM	ZF-SDD	$\text{CmP}+NT^2Q_A$
	MMSE-JDD	$\text{CmP}+NT^2Q_A$
	ML-SIC	$\text{CmP}+N(2T^2Q_A+NT)$
	ML	$\text{CmP}+(Q_AT)^N(N^2R+NT)$
QSM	ZF-SDD	$\text{CmP}+NT^3Q_A$
	MMSE-JDD	$\text{CmP}+NT^3Q_A$
	ML-SIC	$\text{CmP}+N(2T^3Q_A+NT)$
	ML	$\text{CmP}+(Q_AT^2)^N(N^2R+NT)$
SFIM	ZF-SDD	$\text{CmP}+NcQ_A^vT^2$
	MMSE-JDD	$\text{CmP}+NcQ_A^vT^2$
	ML-SIC	$\text{CmP}+(N/u)(cQ_A^vT(uvT+uT)+vNT)$
	ML	$\text{CmP}+(cQ_A^vT)^{N/u}((N^2Rv/u)+NT)$

Table 4.8 : Summary of the computational complexity of QSFIM, SFDMIM, QSFDMIM receivers.

Scheme	Receiver	Complexity (CMs)
Common Part (CmP)	ZF-SDD	$N^2(2T+R)+N(T^3+2T^2R+TR)$
	MMSE-JDD	$N^3(2T^2R+T^3)+N^2(N_{Ch}RT+RT)$
	ML-SIC	$N^3(2T^2R)+N^2(N_{Ch}RT+RT)$
	ML	$N^2N_{Ch}RT$
QSFIM	ZF-SDD	$\text{CmP}+NcQ_A^vT^3$
	MMSE-JDD	$\text{CmP}+NcQ_A^vT^3$
	ML-SIC	$\text{CmP}+(N/u)((cQ_A^vT^2(uvT+uT)+vNT))$
	ML	$\text{CmP}+(cQ_A^vT^2)^{N/u}((N^2Rv/u)+NT)$
SFDMIM	ZF-SDD	$\text{CmP}+NcQ_A^vQ_B^{u-v}T^2$
	MMSE-JDD	$\text{CmP}+NcQ_A^vQ_B^{u-v}T^2$
	ML-SIC	$\text{CmP}+(N/u)(cQ_A^vQ_B^{u-v}T(u^2T+uT)+uNT)$
	ML	$\text{CmP}+(cQ_A^vQ_B^{u-v}T)^{N/u}(N^2R+NT)$
QSFDMIM	ZF-SDD	$\text{CmP}+NcQ_A^vQ_B^{u-v}T^3$
	MMSE-JDD	$\text{CmP}+NcQ_A^vQ_B^{u-v}T^3$
	ML-SIC	$\text{CmP}+(N/u)(cQ_A^vQ_B^{u-v}T^2(u^2T+uT)+uNT)$
	ML	$\text{CmP}+(cQ_A^vQ_B^{u-v}T^2)^{N/u}(N^2R+NT)$

Table 4.9 : System parameters use for numerical analysis.

Description	Parameter	Value
Number of subcarriers	K	128
Number of subsymbols	M	5
Pulse shaping filter	g	RC
Length of cyclic prefix	N_{CP}	32
Number of channel taps for EPA channel	N_{Ch}	7

4.5 Numerical Analysis

In this section, uncoded and coded BER performances of the proposed GFDM-FIM schemes are evaluated by computer simulations for Rayleigh fading with EPA channel model [89] using the parameters given in Table 4.9. The chosen pulse shape for the GFDM prototype filter is the RC filter. The SNR is defined as $SNR = E_s/N_0$, where E_s is the average transmitted energy per symbol.

4.5.1 BER performance of SM and QSM schemes

Figs. 4.6 and 4.7 show the uncoded BER performance of the proposed detection methods for SM-GFDM and QSM-GFDM schemes, respectively, using 4-QAM and a roll-off factor of 0.1. From Fig. 4.6(a), for a 2×2 MIMO configuration and at a BER value of 10^{-4}, it is observed that the proposed ML-SIC scheme achieves 18.1 and 13.7 dB better BER performance than the ZF-SDD and MMSE-JDD detection methods, respectively. In Fig. 4.6(b), BER performance gains of the ML-SIC scheme with respect to ZF-SDD and MMSE-JDD detection methods for a 4×4 MIMO configuration are increased to 28.7 and 21 dB, respectively. Besides, from Figs. 4.6 and 4.7, for 2×2 and 4×4 QSM-GFDM systems using 4-QAM, it is observed that BER performance gains of the ML-SIC scheme with respect to other methods are approximately the same with SM-GFDM counterparts. This significant performance improvement of the ML-SIC detection method arises from the joint detection and demodulation of the transmit antenna indices and the data symbols in a near-optimal manner. In addition, it is observed that increasing the number of antennas enhances the BER performance of the ML-SIC detector. The reason behind this improvement is the increased diversity order of the ML-SIC detector with the number of receive antennas.

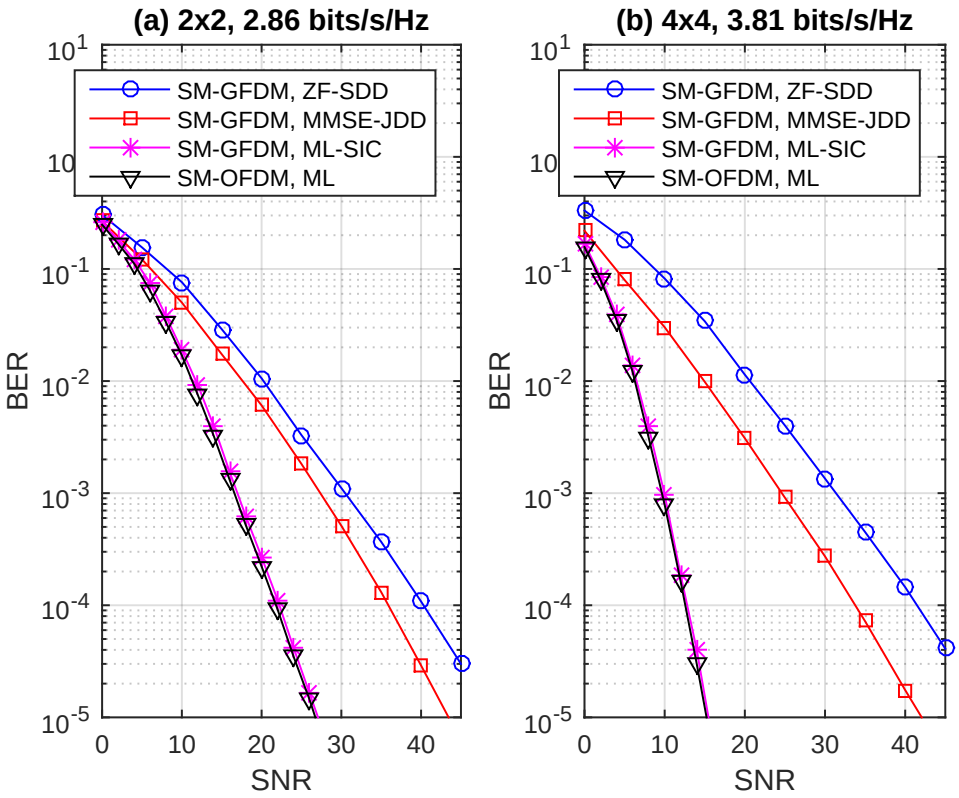

Figure 4.6 : Uncoded BER performance of ZF-SDD, MMSE-JDD, ML-SIC and ML detection methods for (a) 2×2 (b) 4×4 SM schemes using 4-QAM and a roll-off factor of 0.1.

Table 4.10 : The total number of CMs for SM-GFDM receivers using 4-QAM.

Ant. Config.	ZF-SDD	MMSE-JDD	ML-SIC	ML
2×2	2.49×10^{6}	6.31×10^{9}	4.21×10^{9}	1×10^{581}
4×4	5.09×10^{6}	5.04×10^{10}	3.36×10^{10}	1×10^{783}

On the other hand, the number of CMs required to implement the configurations given in Figs. 4.6 and 4.7 are given in Tables 4.10 and 4.11, respectively. From Tables 4.10 and 4.11, as mentioned earlier, it is observed that whereas the receivers with ML and ZF-SDD detection techniques have the highest and the lowest complexity, respectively, the receivers with ML-SIC and MMSE-JDD techniques provide an intermediate solution in terms of detection complexity. Therefore, ML-SIC detection technique can provide an interesting trade-off between complexity and BER performance for SM-GFDM and QSM-GFDM systems.

Figs. 4.6 and 4.7 include BER performances of OFDM applications with ML detection in addition to GFDM schemes. From Figs. 4.6 and 4.7, it is observed that BER performances of the SM-GFDM and QSM-GFDM systems with ML-SIC detection are

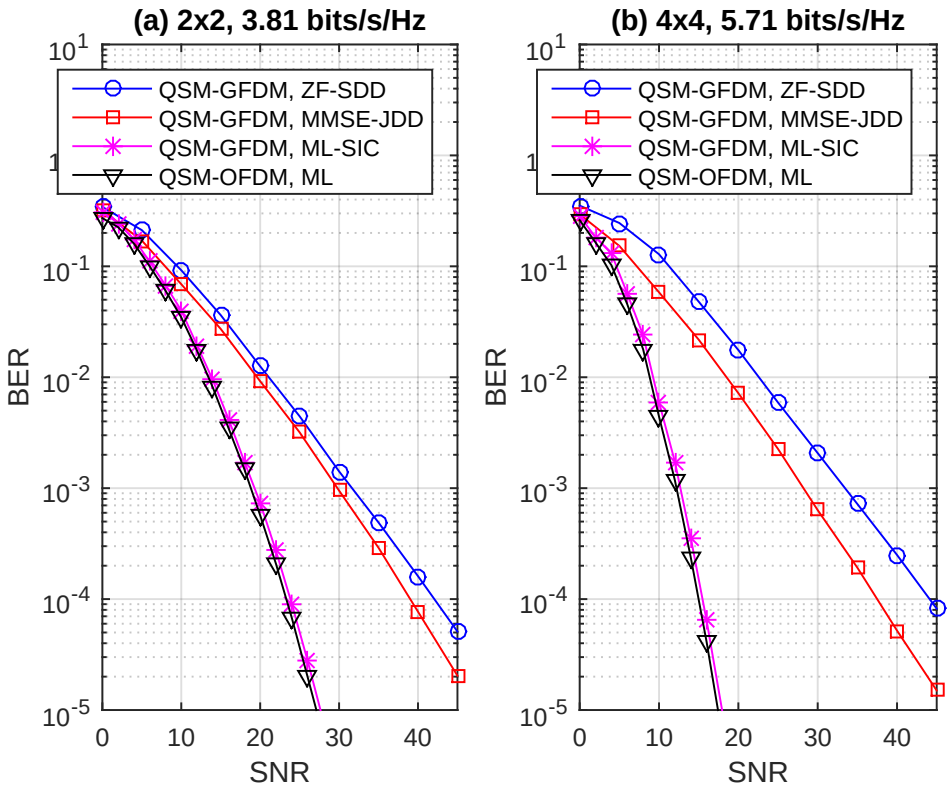

Figure 4.7 : Uncoded BER performance of ZF-SDD, MMSE-JDD, ML-SIC and ML detection methods for (a) 2×2 (b) 4×4 QSM schemes using 4-QAM and a roll-off factor of 0.1.

Table 4.11 : The total number of CMs for QSM-GFDM receivers using 4-QAM.

Ant. Config.	ZF-SDD	MMSE-JDD	ML-SIC	ML
2×2	2.50×10^{6}	6.31×10^{9}	4.21×10^{9}	1×10^{783}
4×4	5.21×10^{6}	5.04×10^{10}	3.36×10^{10}	1×10^{1157}

slightly worse than their OFDM counterparts with ML detection. The performance loss of the GFDM schemes with ML-SIC detection is due to nonorthogonal subcarriers and the error propagation of the QR decomposition used in ML-SIC detection. However, according to equation 4.37 and Table 4.9, the GFDM schemes provide 19% spectral efficiency gain over the OFDM schemes. Furthermore, from equation 4.38 and Table 4.9, it is observed that spectral efficiency gains of QSM-GFDM scheme over SM-GFDM schemes using 4-QAM become 33% and 50% for 2×2 and 4×4 MIMO configurations, respectively, with a negligible increase in detection complexity and slightly decreased BER performance.

Fig. 4.8(a) compares the uncoded BER performances of the 2×2 SM-GFDM system using 8-QAM and the 2×2 QSM-GFDM system using 4-QAM with the ML-SIC detection method considering roll-off factors of 0.1 and 0.5 in order to achieve the same spectral efficiency. The results in Fig. 4.8(a) demonstrate that the QSM-GFDM scheme provides approximately 1.8 dB BER gain with respect to SM-GFDM scheme for the 2×2 MIMO configuration at a BER value of 10^{-4}. Besides, from Fig. 4.8(b), it is observed that 4×4 QSM-GFDM system using 4-QAM provides approximately 2.8 dB BER gain with respect to 4×4 SM-GFDM system using 16-QAM. On the other hand, according to Tables 4.7, 4.8 and 4.9, the computational complexity of the ML-SIC based 2×2 SM-GFDM receiver for 8-QAM and 4×4 SM-GFDM receiver for 16-QAM are on the order of 4.21×10^9 and 3.36×10^{10}, respectively. By comparing these results with the computational complexity of 2×2 QSM-GFDM receiver for 4-QAM and 4×4 QSM-GFDM receiver for 4-QAM in Table 4.11, it is observed that these improvements are provided at no additional complexity. Furthermore, from Figs. 4.8(a) and 4.8(b), it is observed that increasing the roll-off factor slightly degrades the performance.

4.5.2 BER performance of SFIM and QSFIM schemes

Figs. 4.9 and 4.10 show the uncoded BER performance of the proposed detection methods for SFIM and QSFIM schemes, respectively, using 4-QAM and a roll-off factor of 0.1. Here, the look-up table given in Table 4.12 is used to determine the IM subgroups. From Fig. 4.9(a), for a 2×2 MIMO configuration and at a BER value of 10^{-4}, it is observed that the proposed ML-SIC scheme achieves 25.7 and 13.4

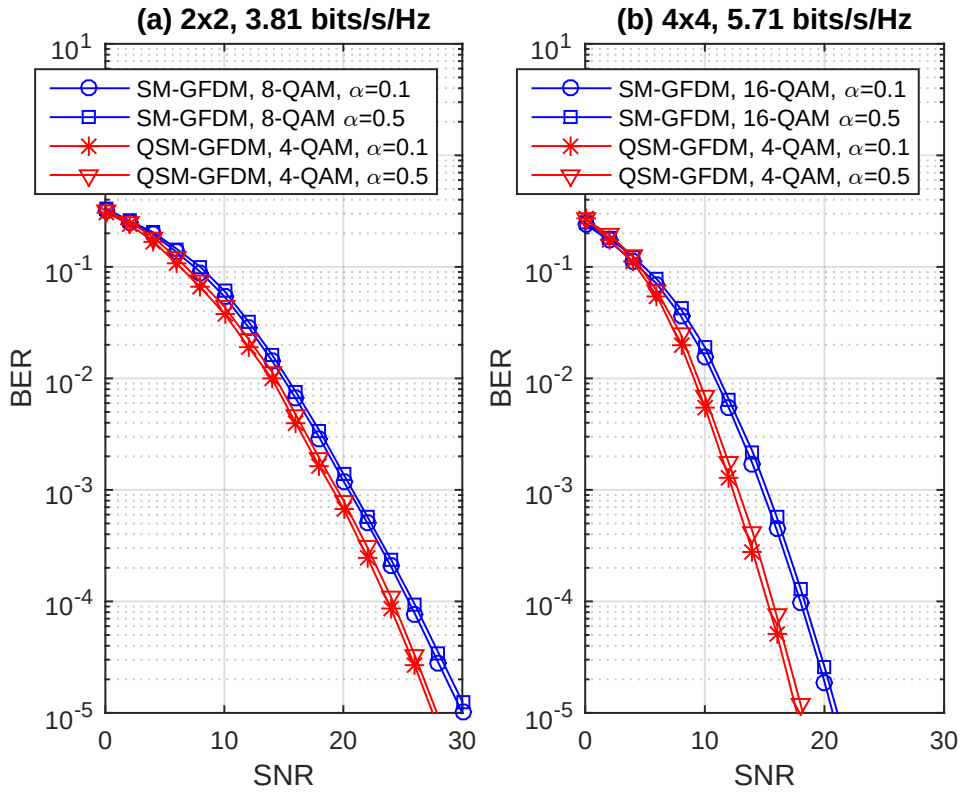

Figure 4.8 : Uncoded BER performance of SM-GFDM and QSM-GFDM schemes using ML-SIC detection method for (a) 2×2 (b) 4×4 with 4-QAM and roll-off factors (α) of 0.1 and 0.5.

dB better BER performance than the ZF-SDD and MMSE-JDD detection methods, respectively. In Fig. 4.9(b), for a 4×4 MIMO configuration, BER performance gains of the ML-SIC scheme with respect to ZF-SDD and MMSE-JDD detection methods are increased to 32.8 and 15.8 dB, respectively. From Figs. 4.9 and 4.10, for QSFIM scheme, it is observed that BER performance gains of the ML-SIC scheme with respect to other methods are approximately the same with the gains in SFIM systems as in the cases of SM and QSM. The significant performance improvements observed in Figs. 4.9 and 4.10 are due to joint detection and demodulation of the transmit antenna indices and the active subcarrier indices as well as QAM data symbols and the increased diversity order of ML-SIC. On the other hand, the number of CMs required to implement the configurations given in Figs. 4.9 and 4.10 are given in Tables 4.13 and 4.14, respectively. From Tables 4.13 and 4.14, it is observed that an interesting trade-off between complexity and BER performance is also valid for SFIM-GFDM and QSFIM-GFDM systems when ML-SIC detection is used. Besides, according to equation 4.39 and Table 4.9, QSFIM-GFDM schemes provide 14% and 25% spectral efficiency gains over SFIM-GFDM schemes for 2×2 and 4×4 MIMO configurations,

Table 4.12 : A look-up table example for IM subgroups with $u = 4$ and $v = 2$.

Bits	Indices	subblocks
[0 0]	{1,2}	$[s_\chi \;\; s_\zeta \;\; 0 \;\; 0]^{\mathrm{T}}$
[0 1]	{2,3}	$[0 \;\; s_\chi \;\; s_\zeta \;\; 0]^{\mathrm{T}}$
[1 0]	{3,4}	$[0 \;\; 0 \;\; s_\chi \;\; s_\zeta]^{\mathrm{T}}$
[1 1]	{1,4}	$[s_\chi \;\; 0 \;\; 0 \;\; s_\zeta]^{\mathrm{T}}$

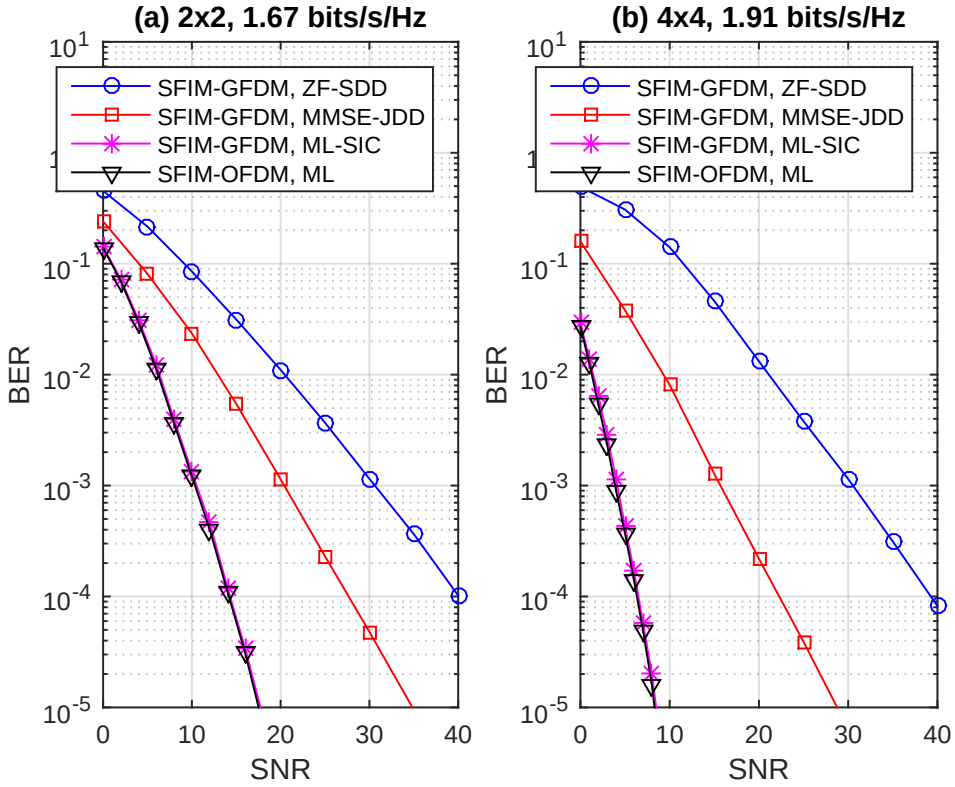

Figure 4.9 : Uncoded BER performance of ZF-SDD, MMSE-JDD, ML-SIC and ML detection methods for (a) 2×2 (b) 4×4 SFIM schemes using 4-QAM and a roll-off factor of 0.1.

respectively, with a negligible increase in detection complexity and slightly decreased BER performance. Additionally, the performance loss of the GFDM systems using ML-SIC detection with respect to OFDM systems is also observed for SFIM and QSFIM schemes.

Fig. 4.11(a) investigates the effects of combination of SM and IM schemes in terms of uncoded BER performance and spectral efficiency for ML-SIC detection method using a roll-off factor of 0.1. From Fig. 4.11(a), at a BER value of 10^{-4}, it is observed that 4×4 SFIM-GFDM system for BPSK provides approximately 6.4 dB BER gain with respect to 4×4 SM-GFDM system for BPSK at the same computational complexity. Note that, for this configuration, spectral efficiency of the SFIM-GFDM scheme is the

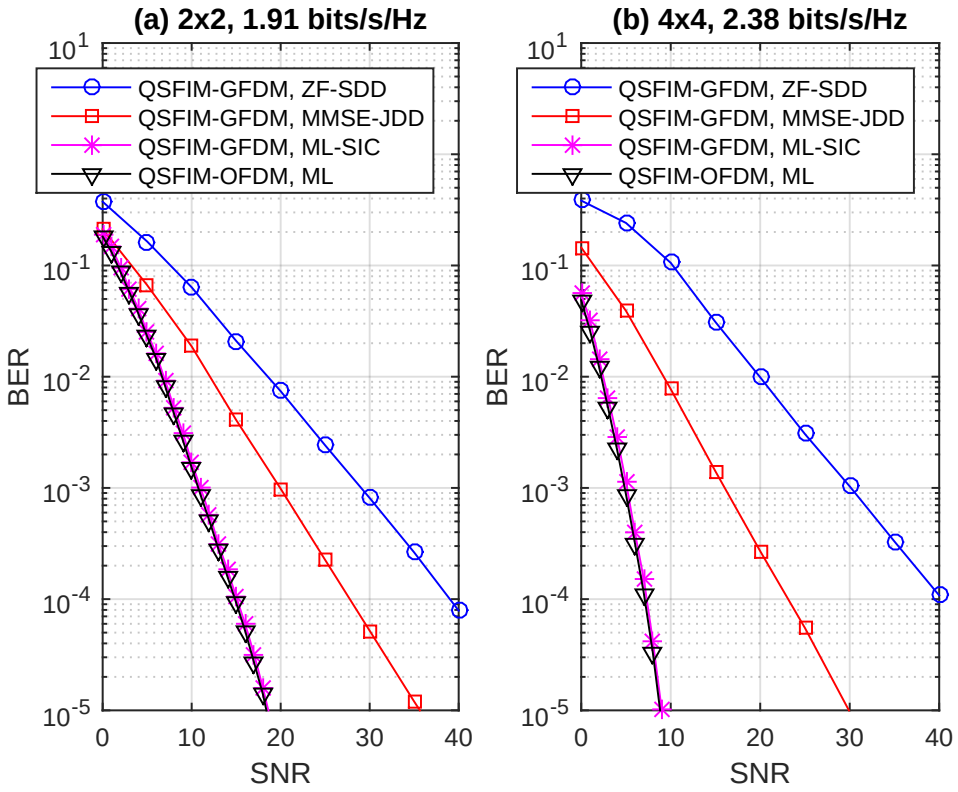

Figure 4.10 : Uncoded BER performance of ZF-SDD, MMSE-JDD, ML-SIC and ML detection methods for (a) 2×2 (b) 4×4 QSFIM schemes using 4-QAM and a roll-off factor of 0.1.

Table 4.13 : The total number of CMs for SFIM-GFDM receivers using 4-QAM.

Ant. Config.	ZF-SDD	MMSE-JDD	ML-SIC	ML
2×2	2.64×10^6	6.30×10^9	4.21×10^9	1×10^{341}
4×4	5.70×10^6	5.04×10^{10}	3.36×10^{10}	1×10^{389}

Table 4.14 : The total number of CMs for QSFIM-GFDM receivers using 4-QAM.

Ant. Config.	ZF-SDD	MMSE-JDD	ML-SIC	ML
2×2	2.80×10^6	6.31×10^9	4.21×10^9	1×10^{389}
4×4	7.67×10^6	5.04×10^{10}	3.36×10^{10}	1×10^{485}

half as that of the SM-GFDM scheme. On the other hand, 4×4 SM-GFDM system for BPSK achieves 2 dB better BER performance than 4×4 SFIM-GFDM system for 16-QAM at the same spectral efficiency. The BER performance gain of the SFIM scheme is due to the improved Euclidean distance spectrum of IM. As a result, it is observed that SFIM scheme can provide an interesting trade-off between spectral efficiency and BER performance.

Fig. 4.11(b) shows the uncoded BER performances of the 4×4 SFIM-GFDM system for 8-QAM and the 4×4 QSFIM-GFDM system for 4-QAM considering a roll-off factor of 0.1 and 0.5 in order to achieve the same spectral efficiency. The results in Fig. 4.11 demonstrate that the QSFIM-GFDM scheme provides approximately 3.9 dB BER gain with respect to SFIM-GFDM scheme for the 4×4 MIMO configuration and at a BER value of 10^{-4}. On the other hand, according to Tables 4.7, 4.8 and 4.9, the computational complexity of the ML-SIC based 4×4 SFIM-GFDM receiver for 8-QAM is on the order of 3.36×10^{10}. By comparing this result with the computational complexity of 4×4 QSFIM-GFDM receiver for 4-QAM in Table 4.14, it is observed that this improvement is provided at no additional complexity. Besides, the results show that slight degradation of BER performance due to increased roll-off factor is also valid for SFIM-GFDM and QSFIM-GFDM schemes.

Fig. 4.12 compares the uncoded BER performances of SM, IM and QAM parts of the SFIM scheme for a 4×4 MIMO configuration with ML-SIC detection method using 4-QAM and a roll-off factor of 0.1. From Fig. 4.12, it is observed that SM part has 2 dB better BER performance with respect to overall SFIM BER. As a result, by proper mapping at the primary and the secondary bit splitter parts of the transmitter, information bits, which need high reliability, can be transmitted through antenna indices and thus, SFIM scheme provides an extra level of flexibility.

4.5.3 BER performance of SFDMIM and QSFDMIM schemes

Figs. 4.13 and 4.14 show the uncoded BER performance of the proposed detection methods for SFDMIM and QSFDMIM schemes, respectively, using 4-QAM and a roll-off factor of 0.1. In order to determine the primary and secondary IM subgroups, the look-up table given in Table 4.15 is used. For DMIM operation, an 8-level QAM constellation, illustrated in Fig. 4.15 is employed. The DMIM constellations are

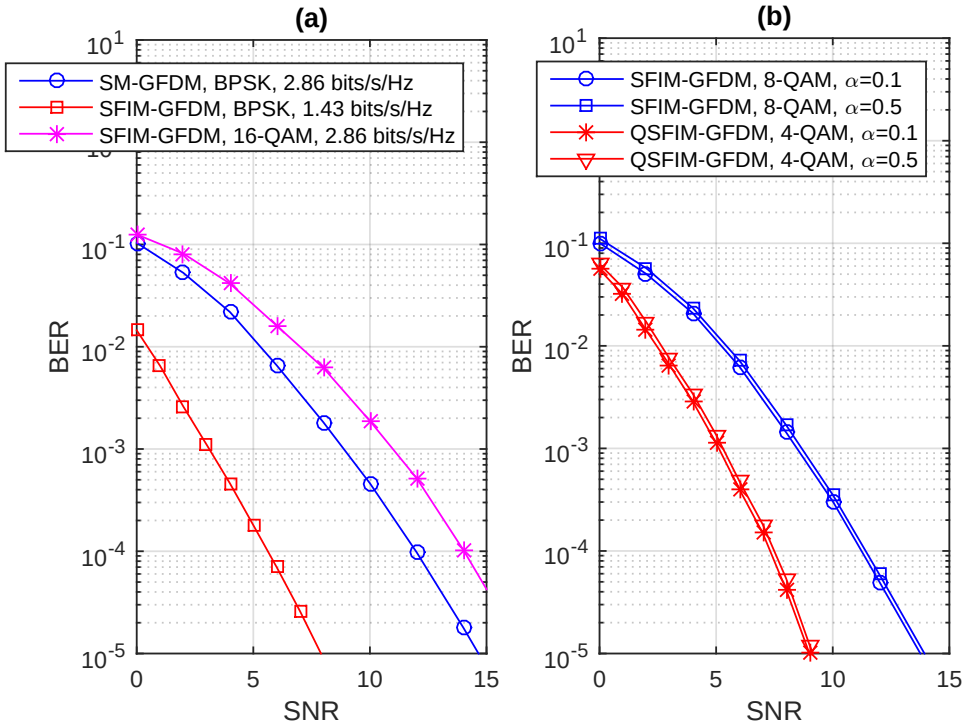

Figure 4.11 : Uncoded BER performance comparisons of SFIM-GFDM with (a) SM-GFDM with a roll-off factor of 0.1 (b) QSFIM-GFDM with roll-off factors (α) of 0.1 and 0.5, for a 4×4 MIMO configuration with ML-SIC detection method.

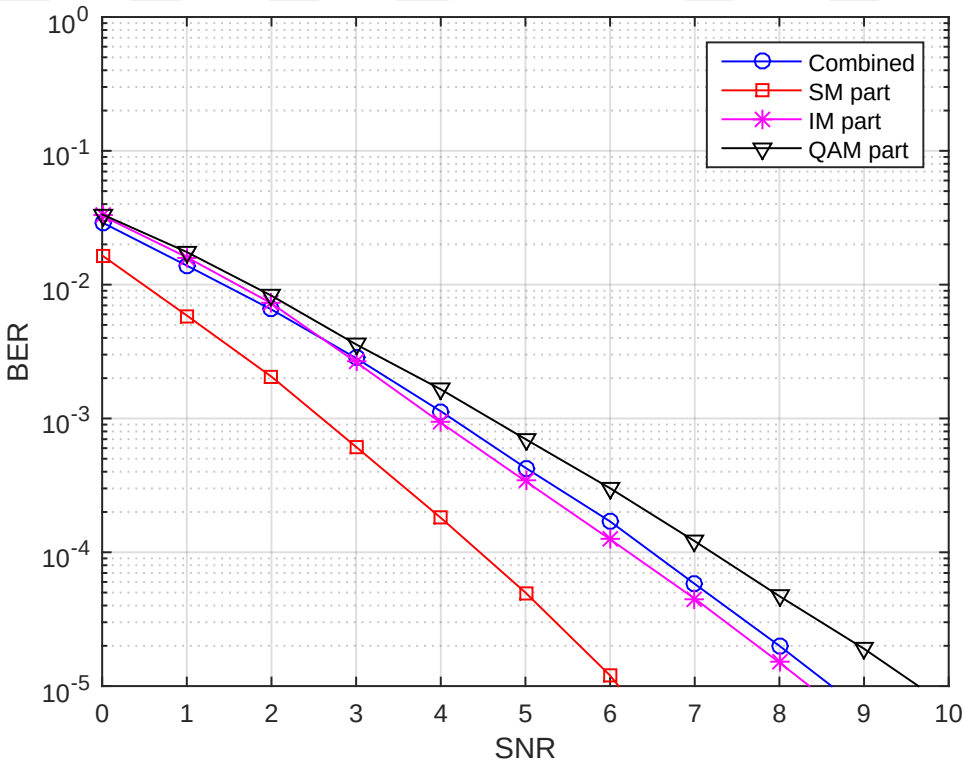

Figure 4.12 : Uncoded BER performance comparisons of SM, IM and QAM parts of SFIM-GFDM scheme for a 4×4 MIMO configuration with ML-SIC detection method using 4-QAM and a roll-off factor of 0.1.

Table 4.15 : A look-up table example for DMIM subgroups with $u = 4, v = 2$.

Bits	Indices	subgroups
[0 0]	$\{1,2\}$	$\left[s_l^A(1) \quad s_l^A(2) \quad s_l^B(1) \quad s_l^B(2)\right]^{\mathrm{T}}$
[0 1]	$\{2,3\}$	$\left[s_l^B(1) \quad s_l^A(1) \quad s_l^A(2) \quad s_l^B(2)\right]^{\mathrm{T}}$
[1 0]	$\{3,4\}$	$\left[s_l^B(1) \quad s_l^B(2) \quad s_l^A(1) \quad s_l^A(2)\right]^{\mathrm{T}}$
[1 1]	$\{1,4\}$	$\left[s_l^A(1) \quad s_l^B(1) \quad s_l^B(2) \quad s_l^A(2)\right]^{\mathrm{T}}$

defined as $\mathscr{S}^A = \left\{(1+j)/\sqrt{6}, (-1+j)/\sqrt{6}, (1-j)/\sqrt{6}, (-1-j)/\sqrt{6}\right\}$ and $\mathscr{S}^B = \left\{(3+j)/\sqrt{6}, (-3+j)/\sqrt{6}, (3-j)/\sqrt{6}, (-3-j)/\sqrt{6}\right\}$ for Mapper A and Mapper B, respectively. From Fig. 4.13(a), for a 2×2 MIMO configuration and at a BER value of 10^{-4}, it is observed that the proposed ML-SIC scheme achieves 21.2 and 15.9 dB better BER performance than the ZF-SDD and MMSE-JDD detection methods, respectively. In Fig. 4.13(b), for 4×4 MIMO configuration, BER performance gains of the ML-SIC scheme with respect to ZF-SDD and MMSE-JDD detection methods were increased to 29.2 and 20.4 dB, respectively. From Fig. 4.14, for QSFDMIM scheme, it is observed that BER performance gains of the ML-SIC scheme are approximately the same with the SFDMIM system. On the other hand, the number of CMs required to implement the configurations given in Figs. 4.13 and 4.14 are given in Tables 4.16 and 4.17, respectively. From Tables 4.16 and 4.17, it is observed that the interesting trade-off between complexity and BER performance is also valid for SFDMIM-GFDM and QSFDMIM-GFDM systems when ML-SIC detection is used. Furthermore, from equation 4.41 and Table 4.9, it is observed that spectral efficiency gains of SFDMIM-GFDM scheme over SFIM-GFDM schemes using 4-QAM become 57% and 50% for 2×2 and 4×4 MIMO configurations, respectively. On the other hand, from equation 4.40 and Table 4.9, it is observed that spectral efficiency gains of QSFDMIM-GFDM scheme over SFDMIM-GFDM schemes using 4-QAM become 9% and 16% for 2×2 and 4×4 MIMO configurations, respectively. For both cases, a negligible increase in detection complexity and a slightly decreased BER performance are noticed. Additionally, the performance loss of the GFDM systems using ML-SIC detection with respect to OFDM systems is also observed for SFDMIM and QSFDMIM schemes.

Fig. 4.16 investigates the effect of DMIM operation in terms of uncoded BER performances for a 4×4 MIMO configuration with ML-SIC detection method and

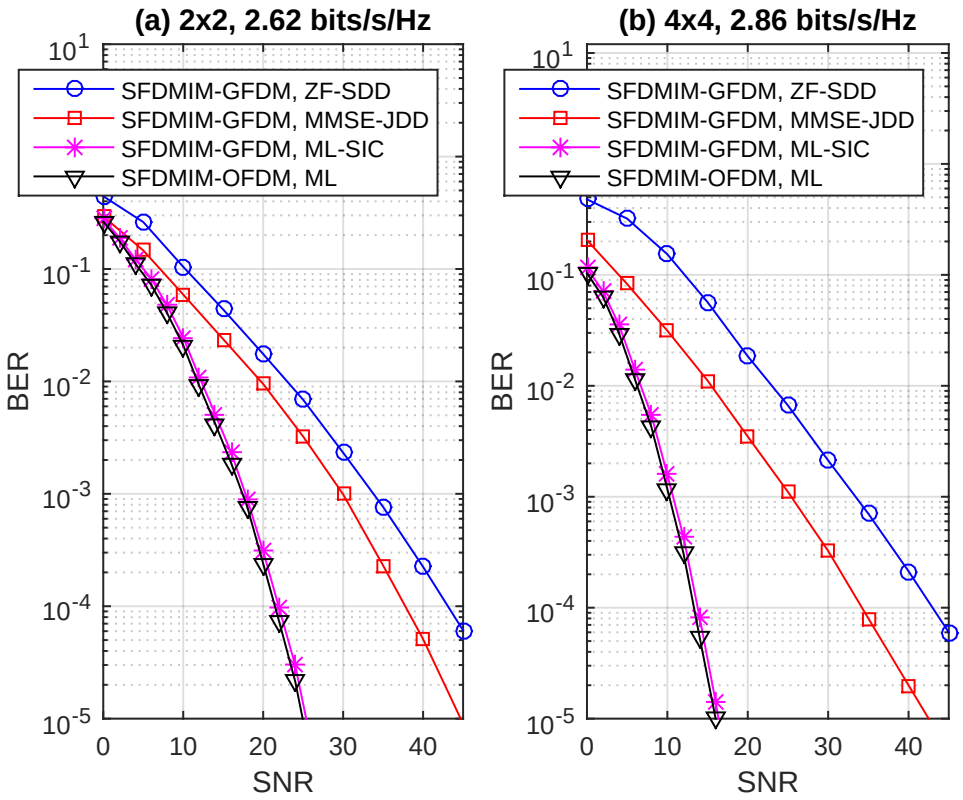

Figure 4.13 : Uncoded BER performance of ZF-SDD, MMSE-JDD, ML-SIC and ML detection methods for (a) 2×2 (b) 4×4 SFDMIM schemes using 4-QAM and a roll-off factor of 0.1.

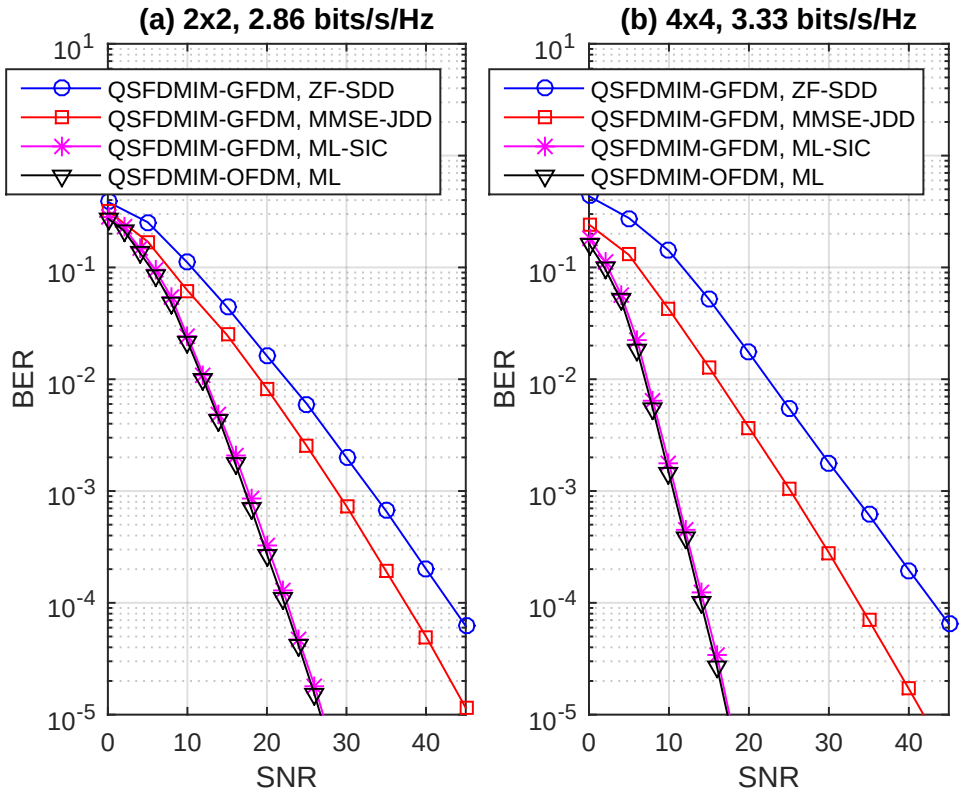

Figure 4.14 : Uncoded BER performance of ZF-SDD, MMSE-JDD, ML-SIC and ML detection methods for (a) 2×2 (b) 4×4 QSFDMIM schemes using 4-QAM and a roll-off factor of 0.1.

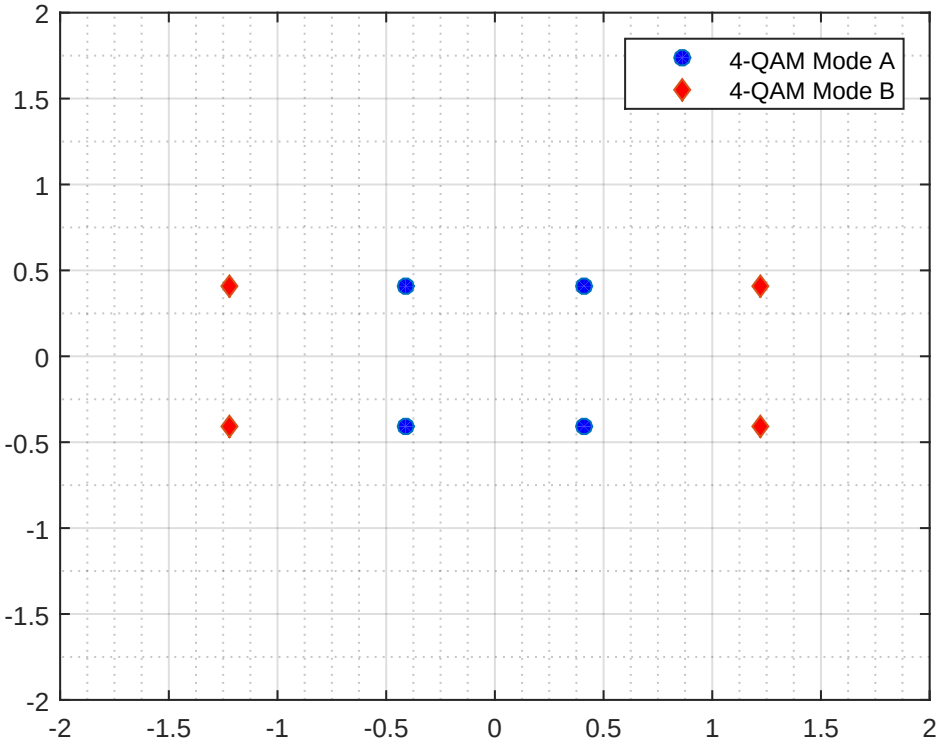

Figure 4.15 : An example of DMIM constellation design for Q_A and Q_B with $Q_A = Q_B = 4$.

Table 4.16 : The total number of CMs for SFDMIM-GFDM receivers using 4-QAM.

Ant. Config.	ZF-SDD	MMSE-JDD	ML-SIC	ML
2×2	5.10×10^{6}	6.31×10^{9}	4.22×10^{9}	1×10^{533}
4×4	1.55×10^{7}	5.04×10^{10}	3.37×10^{10}	1×10^{581}

Table 4.17 : The total number of CMs for QSFDMIM-GFDM receivers using 4-QAM.

Ant. Config.	ZF-SDD	MMSE-JDD	ML-SIC	ML
2×2	7.72×10^{6}	6.31×10^{9}	4.23×10^{9}	1×10^{581}
4×4	4.70×10^{7}	5.04×10^{10}	3.38×10^{10}	1×10^{677}

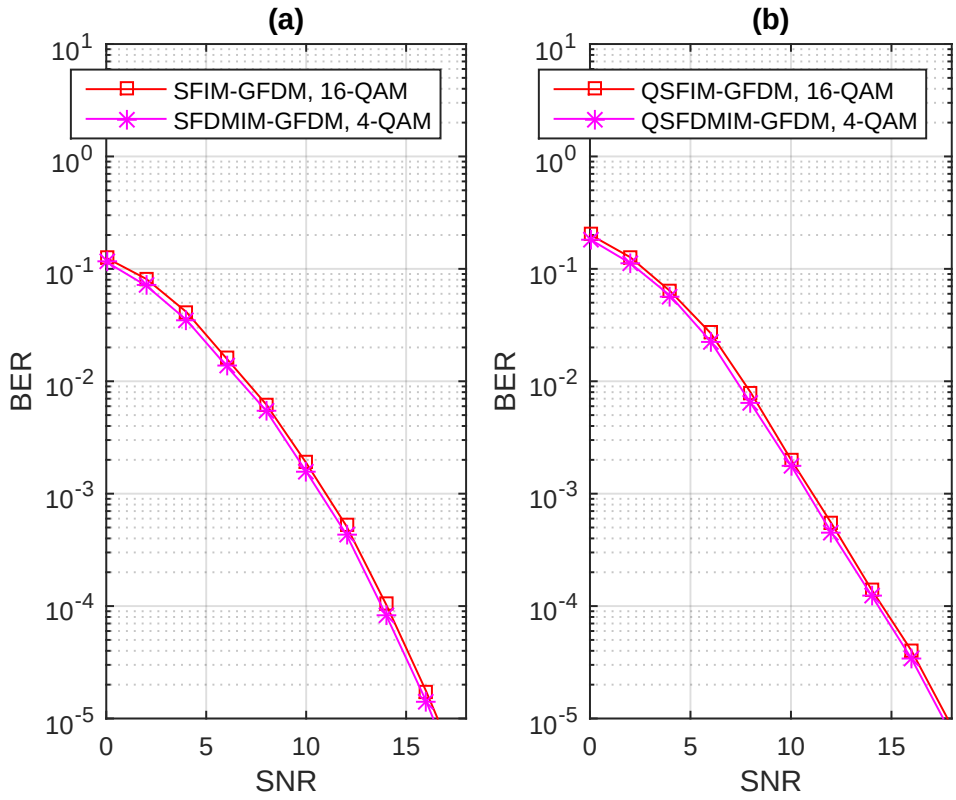

Figure 4.16 : Uncoded BER performance comparisons of IM and DMIM schemes using ML-SIC detection method for a 4×4 MIMO configuration and a roll-off factor of 0.1. (a) SFIM vs SFDMIM (b) QSFIM vs QSFDMIM.

a roll-off factor of 0.1. From Fig. 4.16, at a BER value of 10^{-4}, it is observed that using DMIM scheme instead of IM provides 0.2 dB BER gain for both SFIM and QSFIM schemes at the same spectral efficiency. On the other hand, according to Tables 4.7, 4.8 and 4.9, the computational complexity of the ML-SIC based 4×4 SFIM-GFDM receiver for 16-QAM and 4×4 QSFIM-GFDM receiver for 16-QAM are on the order of 3.36×10^{10} and 3.37×10^{10}, respectively. By comparing these results with the computational complexity of 4×4 SFDMIM-GFDM receiver for 4-QAM and 4×4 QSFDMIM-GFDM receiver for 4-QAM in Tables 4.16 and 4.17, respectively, it is observed that these improvements are provided with increased computational complexity.

4.5.4 Coded BER performance analysis

Fig. 4.17 shows the coded BER performances of the GFDM-FIM schemes for a 4×4 MIMO configuration with ML-SIC detection method using 4-QAM and a roll-off factor of 0.1. For the channel code, the rate 1/3 convolutional code with generator sequence $q = [133, 171, 165]$ was chosen [90]. From Fig. 4.17, it is observed that

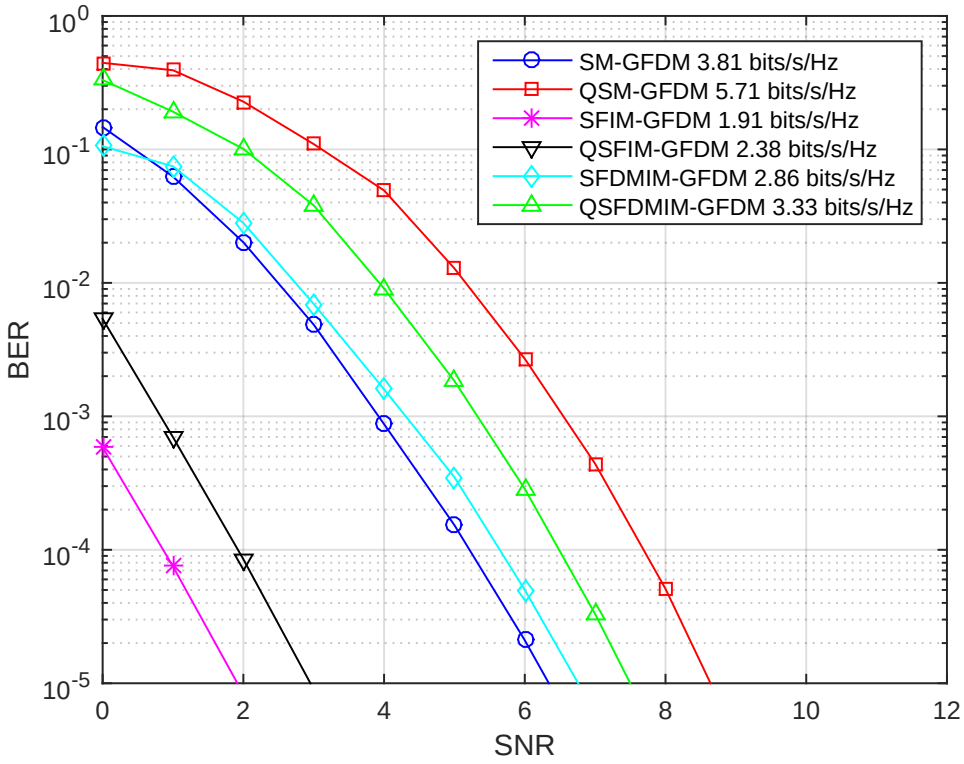

Figure 4.17 : Coded BER performance of the convolutional coded GFDM-FIM schemes using ML-SIC detection method for a 4×4 MIMO configuration with 4-QAM and a roll-off factor of 0.1.

channel coding provides significant BER gains between 5.4 and 8.1 dB with respect to uncoded schemes. Note that coded BER performances get worse with the increasing spectral efficiency.

Fig. 4.18 compares the coded BER performances of the GFDM-FIM schemes using ML-SIC detection method and a roll-off factor of 0.1 for 3.81 bits/s/Hz spectral efficiency. Here, a 16-level QAM constellation, illustrated in Fig. 4.19 is employed for 8-QAM DMIM operation. The DMIM constellations are defined as $\mathscr{S}^A = \{(-3+j)/\sqrt{10},\ (-3-j)/\sqrt{10},\ (-1+j)/\sqrt{10},\ (-1-j)/\sqrt{10},\ (3+j)/\sqrt{10},\ (3-j)/\sqrt{10},\ (1+j)/\sqrt{10},(1-j)/\sqrt{10}\}$ and $\mathscr{S}^B = \{(-3+3j)/\sqrt{10},\ (-3-3j)/\sqrt{10},\ (-1+3j)/\sqrt{10},\ (-1-3j)/\sqrt{10},\ (3+3j)/\sqrt{10},\ (3-3j)/\sqrt{10},\ (1+3j)/\sqrt{10},\ (1-3j)/\sqrt{10}\}$ for mapper A and mapper B, respectively. From Fig. 4.18, it is observed that the BER performances of the GFDM-FIM schemes for a 4×4 MIMO configuration are significantly better than that of the GFDM-FIM schemes for a 2×2 MIMO configuration independent of the modulation order. Therefore, it can be stated that the coded BER performances of the GFDM-FIM schemes using ML-SIC detection method are mainly determined by the number of receive antennas. Besides, it is

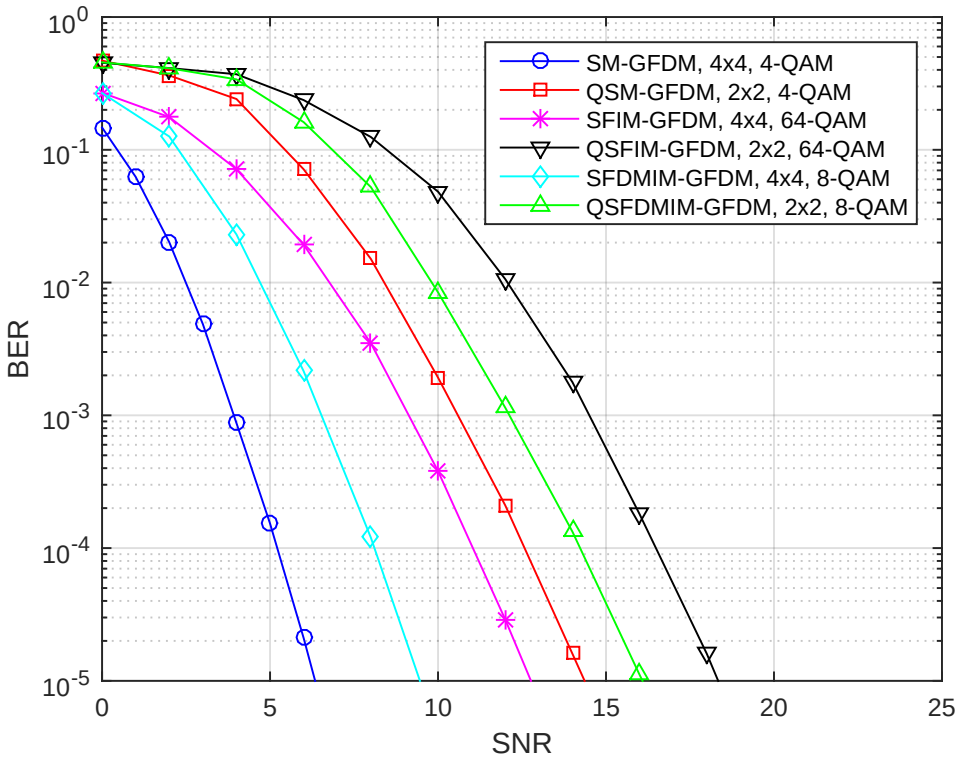

Figure 4.18 : Coded BER performance of the convolutional coded GFDM-FIM schemes using ML-SIC detection method and a roll-off factor of 0.1 for 3.81 bits/s/Hz spectral efficiency.

observed that the coded BER performances of the GFDM-FIM schemes become worse with the increasing modulation order for the same number of receive antennas. Thus, it can be stated that the modulation order is a secondary factor on the coded BER performances of the GFDM-FIM schemes using the ML-SIC detection method.

4.6 Discussion

In this section, the obtained numerical results for BER performance, computational complexity and spectral efficiency are discussed. Then, based on these results, a recommendation table for selecting the proper GFDM-FIM scheme considering performance criterion is given. The obtained numerical results are summarized below:

1. SM, IM, and SFIM schemes along with the QSM and DMIM variants are all applicable with GFDM.

2. Suboptimal ZF-SDD and MMSE-JDD detection methods and near-optimum ML-SIC detection method can be used with all proposed MIMO-GFDM applications.

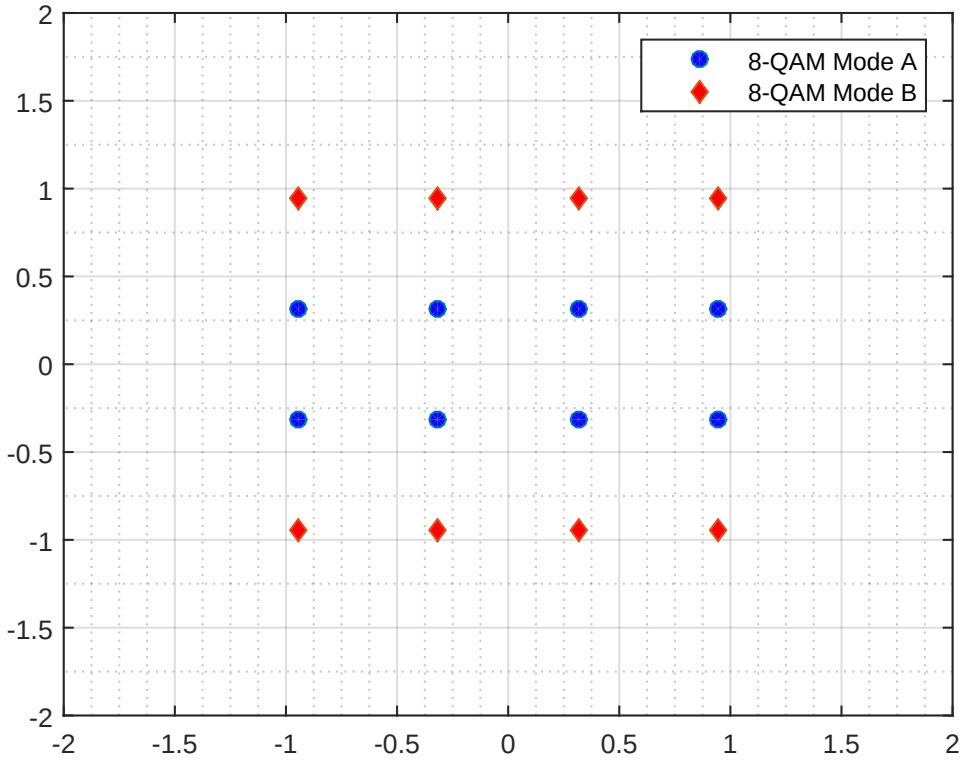

Figure 4.19 : An example of DMIM constellation design for Q_A and Q_B with $Q_A = Q_B = 8$.

3. ML-SIC detection method provides significant BER performance gains with respect to ZF-SDD and MMSE-JDD detection methods at the cost of increased computational complexity. This significant performance improvements arise from the joint detection and demodulation of spatial and frequency indices as well as QAM data symbols in a near-optimal manner. Therefore, ML-SIC detection technique can provide an interesting trade-off between complexity and BER performance.

4. BER performance of the ML-SIC detection method increases with increasing number of receive antennas. The reason behind this improvement is the increased diversity order of the ML-SIC detector with the number of receive antennas.

5. BER performance of the ML-SIC detection methods are slightly worse than their OFDM counterparts with ML detection. This performance loss is due to nonorthogonal subcarriers and the error propagation of the QR decomposition. Note that for this case, GFDM provides significant spectral efficiency gains with respect to OFDM.

6. Enabling QSM operation provides significant spectral efficiency gains with a negligible increase in detection complexity and slightly decreased BER performance.

On the other hand, QSM operation provides BER performance gains at the same spectral efficiency with no additional complexity.

7. Increasing the roll-off factor of the pulse shaping filter slightly degrades the performance of the GFDM-FIM schemes.

8. SFIM schemes provides BER performance gain at the cost of decreased spectral efficiency. This BER performance gain is due to the improved Euclidean distance spectrum of IM. Therefore SFIM scheme can provide an interesting trade-off between spectral efficiency and BER performance.

9. Enabling DMIM operation provides significant spectral efficiency gains with an increased detection complexity and slightly decreased BER performance. On the other hand, DMIM operation improves the BER performance slightly at the same spectral efficiency with additional complexity.

10. Thanks to using space and frequency indices together, proposed SFIM scheme provides a multi-layer scheme, which reveals different BER performances and spectral efficiencies. In this context, information bits transmitted through antenna indices has an extra 2 dB BER performance gain in addition to SFIM BER gain. As a result, SFIM scheme has a strong potential to support different use cases by using common space, frequency and time resources at the same time.

11. Channel coding improves the BER performance of the GFDM-FIM scheme as expected.

12. The coded BER performances of the GFDM-FIM schemes using ML-SIC detection method are mainly determined by the number of receive antennas. Besides, the modulation order is the secondary factor on the coded BER performances of the GFDM-FIM schemes using ML-SIC detection method.

In Table 4.18, the proposed MIMO-GFDM applications are sorted from the lowest to the highest in terms of the computational complexity for a 4×4 MIMO configuration with 4-QAM transmission. As stated earlier, ZF-SDD detection method has the lowest complexity among the proposed detection methods, since QSM, IM, and DMIM operations increase the computational complexity. Table 4.19 lists the proposed MIMO-GFDM applications from the lowest transmit power to the highest transmit power for a 4×4 MIMO configuration with 4-QAM transmission at a BER value of

Table 4.18 : Computational complexities sorted from the lowest to the highest for a 4×4 MIMO configuration with 4-QAM.

Order	Scheme & Detection Method
1	SM, ZF-SDD
2	QSM, ZF-SDD
3	SFIM, ZF-SDD
4	QSFIM, ZF-SDD
5	SFDMIM, ZF-SDD
6	QSFDMIM, ZF-SDD
7	SM, ML-SIC
8	QSM, ML-SIC
9	SFIM, ML-SIC
10	QSFIM, ML-SIC
11	SFDMIM, ML-SIC
12	QSFDMIM, ML-SIC
13	SM, MMSE-JDD
14	QSM, MMSE-JDD
15	SFIM, MMSE-JDD
16	QSFIM, MMSE-JDD
17	SFDMIM, MMSE-JDD
18	QSFDMIM, MMSE-JDD

10^{-4}. It is observed that, SFIM scheme needs the lowest transmit power to reach the desired BER value. In Table 4.20, the proposed MIMO-GFDM applications are ranked from the highest to the lowest in terms of spectral efficiency for a 4×4 MIMO configuration with 4-QAM transmission. According to these results, QSM-GFDM has the highest spectral efficiency among the proposed schemes. According to Tables 4.18, 4.19 and 4.20, it is obvious that there is not any scheme, which has best performance for all performance criterion at the same time. Therefore, performance criterion have to be prioritized and the proper scheme must be selected considering the related criterion among the proposed MIMO-GFDM schemes. In Table 4.21, based on the results in Tables 4.18, 4.19 and 4.20, a recommendation table to select the proper MIMO-GFDM scheme is given considering various emphasis of complexity, spectral efficiency and transmit power criterion. Table 4.21 shows that GFDM-FIM has a strong potential to engineer the space-frequency structure according to channel conditions and use cases and provides a great flexibility, which can be easily tuned to address the required performance criterion.

Table 4.19 : Required transmit power sorted from the lowest to the highest to achieve a BER value of 10^{-4} for a 4×4 MIMO configuration with 4-QAM.

Order	Scheme & Detection Method
1	SFIM, ML-SIC
2	QSFIM, ML-SIC
3	SM, ML-SIC
4	SFDMIM, ML-SIC
5	QSFDMIM, ML-SIC
6	QSM, ML-SIC
7	SFIM, MMSE-JDD
8	QSFIM, MMSE-JDD
9	SM, MMSE-JDD
10	SFDMIM, MMSE-JDD
11	QSFDMIM, MMSE-JDD
12	QSM, MMSE-JDD
13	SFIM, ZF-SDD
14	QSFIM, ZF-SDD
15	SM, ZF-SDD
16	SFDMIM, ZF-SDD
17	QSFDMIM, ZF-SDD
18	QSM, ZF-SDD

Table 4.20 : Spectral efficiencies sorted from the highest to the lowest for a 4×4 MIMO configuration with 4-QAM.

Order	Scheme
1	QSM
2	SM
3	QSFDMIM
4	SFDMIM
5	QSFIM
6	SFIM

Table 4.21 : Recommendations about selecting the proper GFDM-FIM scheme.

Complexity	Transmit Power	Spectral Efficiency	Scheme	Receiver
Lowest	Low	Do not care	SM	ZF-SDD
Lowest	Do not care	High	QSM	ZF-SDD
Low	Lowest	Do not care	SFIM	ML-SIC
Do not care	Lowest	High	QSFIM	ML-SIC
Low	Do not care	Highest	SM	ZF-SDD
Do not care	Low	Highest	QSM	ZF-SDD
Moderate	Moderate	Do not care	SFDMIM	ML-SIC
Moderate	Do not care	Moderate	QSFDMIM	ML-SIC
Do not care	Moderate	Moderate	SFDMIM	MMSE-JDD

5. SPATIAL MULTIPLEXING GENERALIZED FREQUENCY DIVISION MULTIPLEXING WITH INDEX MODULATION

5.1 SMX-GFDM-IM Transmitter

In this study, a GFDM-based SMX system with T transmit and R receive antennas is considered. The block diagram of the SMX-GFDM-IM transmitter is given in Fig. 5.1. A GFDM block consists of K subcarriers each carrying M timeslots on it, where $N = KM$ is the total number of samples in a GFDM block. According to Fig. 5.1, a total of pT information bits are taken from the input and divided into T groups with p bits. These p bits are mapped by GFDM-IM mappers in each branch of the transmitter as shown in Fig. 5.2. In this mapping operation, information bits are used to determine the active subcarriers positions as well as Q-ary modulation symbols and GFDM-IM block $\mathbf{d}_t = [d_{t,0,0}, \ldots, d_{t,K-1,0}, d_{t,0,1}, \ldots, d_{t,K-1,1}, \ldots, d_{t,K-1,M-1}]$, where $d_{t,k,m}(n) \in \{0, \mathscr{S}\}$, for $k = 0,1,\ldots,K-1$, $m = 0,1,\ldots,M-1$, $t = 1,2,\ldots,T$ and $\mathscr{S}$ denotes Q-ary signal constellation with Q elements, is obtained.

According to Fig. 5.2, in each branch of the transmitter, IM bit splitter takes p bits from the input and splits these p bits into L groups each containing p_i bits and L groups each containing p_q bits to be mapped into GFDM-IM subblocks $\mathbf{d}_t^l = \left[d_t^l(1), d_t^l(2), \ldots, d_t^l(u)\right]^{\mathrm{T}}$, where $d_t^l(\gamma) \in \{0, \mathscr{S}\}$, for $\gamma = 1,2,\ldots,u$, $l = 1,2,\ldots,L$ and $u = N/L$. First, p_i-bit sequences are processed by the index selectors to determine the active subcarrier positions by a selection rule. For each GFDM-IM subblock l of t-th transmit antenna, only v out of u available subcarriers are chosen as active, where the chosen subcarrier indices are denoted by $\mathbf{i}_t^l = \left[i_t^l(1), i_t^l(2), \ldots, i_t^l(v)\right]^{\mathrm{T}}$, $i_t^l(\gamma) \in \{1,2,\ldots,u\}$, for $\gamma = 1,2,\ldots,v$, and the remaining $u - v$ subcarriers are set to zero. Therefore, $\mathbf{i}_t^l$ has $c = 2^{p_i}$ possible realizations and p_i can be defined as $\lfloor \log_2(C(u,v)) \rfloor$. Meanwhile, p_q-bit sequences are mapped by Q-ary mappers to create the modulated symbols vector $\mathbf{s}_t^l = \left[s_t^l(1), s_t^l(2), \ldots, s_t^l(v)\right]^{\mathrm{T}}$, where $s_t^l(\gamma) \in \mathscr{S}$, for $\gamma = 1,2,\ldots,v$, $l = 1,2,\ldots,L$. For each GFDM-IM subblock $\mathbf{d}_t^l$, $p_q = v\log_2(Q)$ bits are conveyed by v elements of s_t^l whose corresponding subcarrier indices given by $\mathbf{i}_t^l$.

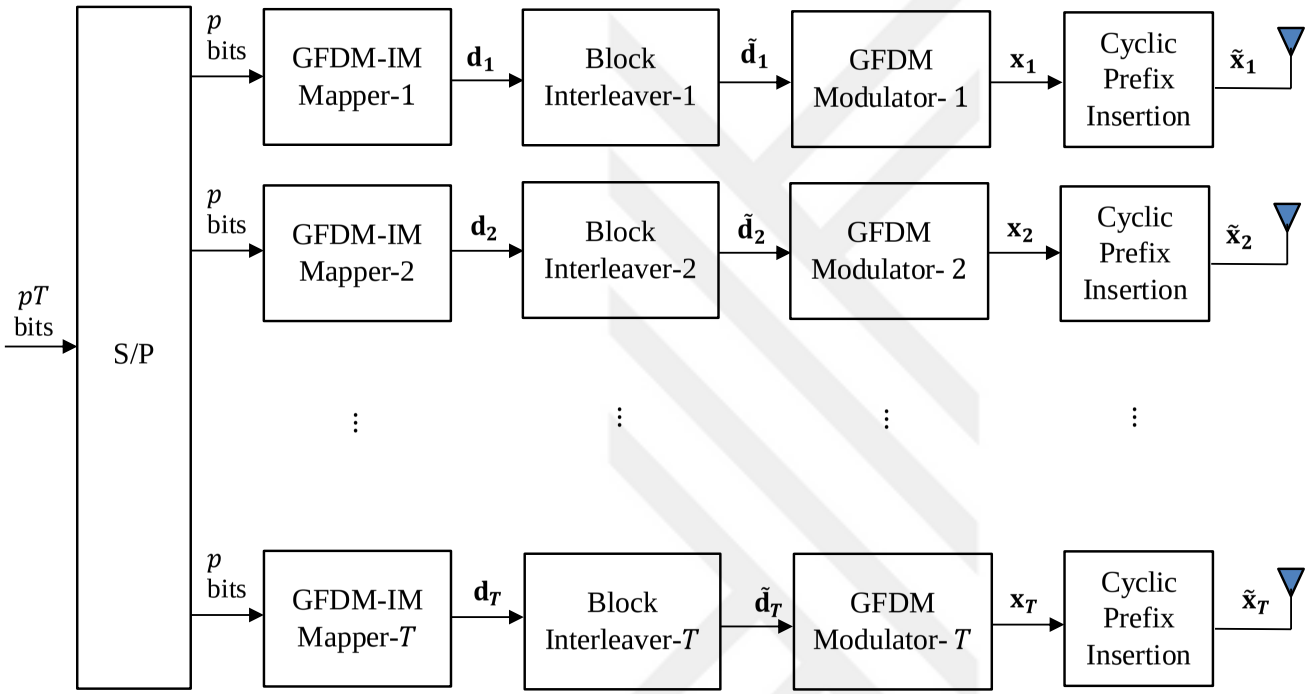

Figure 5.1 : Block diagram of the SMX-GFDM-IM transmitter.

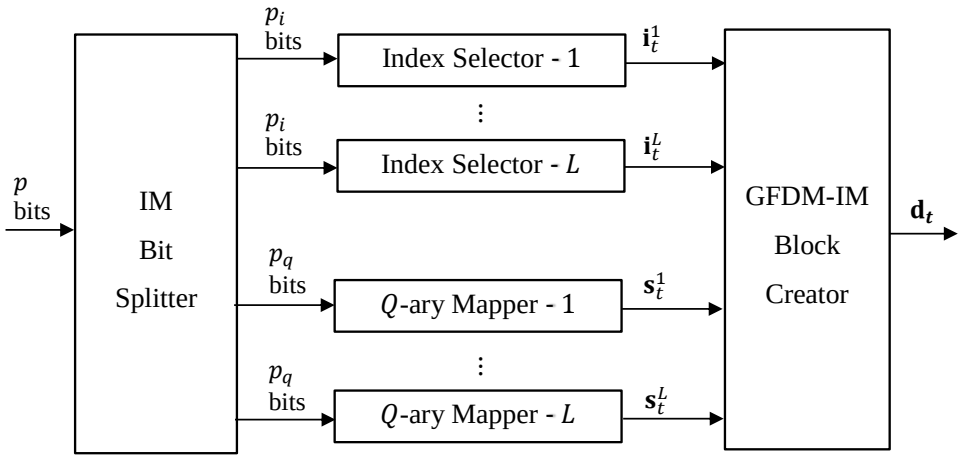

Figure 5.2 : GFDM-IM mappers at each branch of the transmitter.

After that, in each branch of the transmitter, GFDM-IM block creator constructs the GFDM-IM subblocks $\mathbf{d}_t^l$ by using $\mathbf{s}_t^l$ and $\mathbf{i}_t^l$ for all l first and then concatenates these L IM subblocks to obtain the GFDM-IM block $\mathbf{d}_t$. At this point, a block interleaver with size $L \times u$ is employed for $\mathbf{d}_t$ to obtain uncorrelated channels and the interleaved data vector $\widetilde{\mathbf{d}}_t$ is obtained. Then, $\widetilde{\mathbf{d}}_t$ is modulated using a GFDM modulator and the resulting GFDM transmit signal of t-th transmit antenna is given by

$$x_t(n) = \sum_{k=0}^{K-1} \sum_{m=0}^{M-1} \widetilde{d}_{t,k,m} g_{k,m}(n), \tag{5.1}$$

where $n \in \{0,\ldots,N-1\}$ is the sampling index and

$$g_{k,m}(n) = g\left((n-mK)_{\mathrm{mod}N}\right) \exp\left(j2\pi \frac{kn}{K}\right) \tag{5.2}$$

is the pulse shaping filter circularly shifted to the m-th timeslot and modulated to the k-th subcarrier. Equation 5.1 can be reformulated as $\mathbf{x}_t = \mathbf{A}\widetilde{\mathbf{d}}_t$ [2]. Here, $\mathbf{A}$ is an $N \times N$ GFDM modulation matrix given by

$$\mathbf{A} = \left[\mathbf{g}_{0,0},\ldots,\mathbf{g}_{K-1,0},\mathbf{g}_{0,1},\ldots,\mathbf{g}_{K-1,1},\ldots,\mathbf{g}_{K-1,M-1}\right], \tag{5.3}$$

where $\mathbf{g}_{k,m} = \left[g_{k,m}(0),\ldots,g_{k,m}(N-1)\right]^{\mathrm{T}}$ is a vector constructed with pulse shaping filter samples. Finally, in order to make the convolution with the channel circular, a CP with length N_{CP} is added to $\mathbf{x}_t$ and the resulting vector $\widetilde{\mathbf{x}}_t = \left[\mathbf{x}_t(N-N_{\mathrm{CP}}+1:N)^{\mathrm{T}}, \mathbf{x}_t^{\mathrm{T}}\right]^{\mathrm{T}}$ is sent over a frequency-selective Rayleigh fading channel.

5.2 SMX-GFDM-IM Receiver

The block diagram of the SMX-GFDM-IM receiver is given in Fig. 5.3. After the removal of CP, based on the assumption that perfect synchronization is ensured, CP is longer than the channel delay spread (N_{Ch}) and the wireless channel remains constant within one GFDM-IM block, the overall received signal is given by

$$\begin{bmatrix} \mathbf{y}_1 \\ \vdots \\ \mathbf{y}_R \end{bmatrix} = \begin{bmatrix} \mathbf{H}_{1,1}\mathbf{A} & \cdots & \mathbf{H}_{1,T}\mathbf{A} \\ \vdots & \ddots & \vdots \\ \mathbf{H}_{R,1}\mathbf{A} & \cdots & \mathbf{H}_{R,T}\mathbf{A} \end{bmatrix} \begin{bmatrix} \widetilde{\mathbf{d}}_1 \\ \vdots \\ \widetilde{\mathbf{d}}_T \end{bmatrix} + \begin{bmatrix} \mathbf{w}_1 \\ \vdots \\ \mathbf{w}_R \end{bmatrix}, \tag{5.4}$$

where $\mathbf{y}_r = [y_r(0), y_r(1), \ldots, y_r(N-1)]^{\text{T}}$ is the vector of the received signals at the r-th receive antenna, $\mathbf{H}_{r,t}$, for $r = 1, \ldots, R$, $t = 1, \ldots, T$, is the $N \times N$ circular convolution matrix constructed from the channel impulse response coefficients between the t-th transmit antenna and the r-th receive antenna given by $\mathbf{h}_{r,t} = [h_{r,t}(0), h_{r,t}(1), \ldots, h_{r,t}(N_{\text{Ch}}-1)]^{\text{T}}$, where $h_{r,t}(n)$ follows $\mathscr{CN}(0,1)$ distribution, $\mathbf{w}_r$ is an $N \times 1$ vector of additive white Gaussian noise (AWGN) samples with elements distributed as $\mathscr{CN}(0, \sigma_w^2)$. Equation 5.4 can be rewritten in a more compact form as

$$\mathbf{y} = \widetilde{\mathbf{H}}\widetilde{\mathbf{d}} + \mathbf{w}, \tag{5.5}$$

where the dimensions of $\mathbf{y}$, $\widetilde{\mathbf{H}}$, $\widetilde{\mathbf{d}}$ and $\mathbf{w}$ are $NR \times 1$, $NR \times NT$, $NT \times 1$ and $NR \times 1$, respectively.

5.2.1 Maximum Likelihood (ML) detection of SMX-GFDM-IM

In GFDM, each subcarrier is filtered individually using a prototype filter. While this filtering operation reduces OOB emission, it causes non-orthogonality and ICI. Therefore, frequency domain decoupling of GFDM subcarriers cannot be possible and the ML solution $\hat{\mathbf{d}}$ can be expressed as

$$\hat{\mathbf{d}} = \underset{\mathbf{d} \in \{0, \mathscr{S}\}}{\operatorname{argmin}} \left\| \mathbf{y} - \widetilde{\mathbf{H}}\widetilde{\mathbf{d}} \right\|^2. \tag{5.6}$$

From equation 5.6, it is obvious that a straightforward solution to ML detection of SMX-GFDM-IM scheme is extremely complex. Therefore, low complexity solutions are needed.

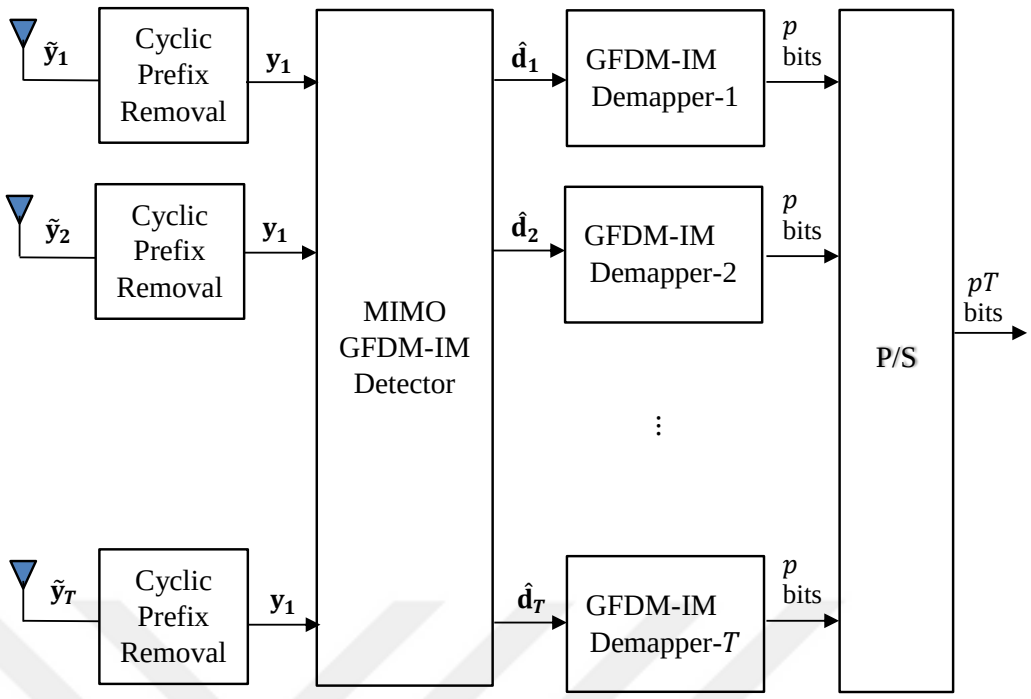

Figure 5.3 : Block diagram of the SMX-GFDM-IM receiver.

5.2.2 MMSE detection of SMX-GFDM-IM

As a suboptimal but less complex alternative to extremely complex brute-force ML detection of SMX-GFDM-IM, MMSE-based detection can be considered. Based on the system model in equation 5.5, MMSE detection can be performed by

$$\begin{bmatrix} \mathbf{z}_1 \\ \mathbf{z}_2 \\ \vdots \\ \mathbf{z}_T \end{bmatrix} = \left(\widetilde{\mathbf{H}}^{\mathrm{H}}\widetilde{\mathbf{H}} + \sigma_w^2\mathbf{I}\right)^{-1}\widetilde{\mathbf{H}}^{\mathrm{H}}\mathbf{y}, \tag{5.7}$$

where $\mathbf{z}_t = \left[\mathbf{z}_t^{1\mathrm{T}}, \mathbf{z}_t^{2\mathrm{T}}, \ldots, \mathbf{z}_t^{L\mathrm{T}}\right]^{\mathrm{T}}$, for $t = 1,2,\ldots,T$ and $\mathbf{z}_t^l$, for $l = 1,2,\ldots,L$, is a $u \times 1$ vector. Then, the MMSE solution $\hat{\mathbf{d}}_t^l$ for l-th GFDM-IM subblock of t-th transmit antenna is given by

$$\hat{\mathbf{d}}_t^l = \underset{\mathbf{d}_t^l \in \{0,\mathscr{S}\}}{\operatorname{argmin}} \left\|\mathbf{z}_t^l - \mathbf{d}_t^l\right\|^2. \tag{5.8}$$

After this point, detected GFDM-IM subblocks are concatenated to construct the estimated GFDM-IM blocks $\hat{\mathbf{d}}_t$ for each transmit antenna and GFDM-IM demappers retrieve the original information bits in each branch of the receiver.

5.2.3 Near-ML detection of SMX-GFDM-IM

In [24], a combination of SD and SIC has been proposed for SMX-GFDM system utilizing QR decomposition and it has been reported that the proposed method achieves near-ML performance in the high SNR regimes. In Chapter 4, this method has been adapted for GFDM-based space and frequency IM schemes. QR decomposition-based near-ML detection is also applicable for SMX-GFDM-IM system. The MMSE-QRD [85] of $\widetilde{\mathbf{H}}$ is given as

$$\begin{bmatrix} \widetilde{\mathbf{H}}\mathbf{P} \\ \sigma_w \mathbf{I}_{NT} \end{bmatrix} = \mathbf{QR} = \begin{bmatrix} \mathbf{Q}_1 \\ \mathbf{Q}_2 \end{bmatrix} \mathbf{R}, \tag{5.9}$$

where $\mathbf{Q}$ is an $(NT+NR)\times NT$ unitary matrix which is partitioned into $NR\times NT$ matrix $\mathbf{Q}_1$ and $NT\times NT$ matrix $\mathbf{Q}_2$, $\mathbf{R}$ is an $NT\times NT$ upper triangular matrix, $\mathbf{P}$ permutes the columns of $\widetilde{\mathbf{H}}$ prior to decomposition in order to realize deinterleaving. Then, multiplying the received signals with $\mathbf{Q}_1^{\mathrm{H}}$ yields

$$\widetilde{\mathbf{y}} = \mathbf{Q}_1^{\mathrm{H}}\mathbf{y} = \mathbf{Rd} - \sigma_w \mathbf{Q}_2^{\mathrm{H}}\mathbf{d} + \mathbf{Q}_1^{\mathrm{H}}\mathbf{w}. \tag{5.10}$$

Here, first term is the useful signal, second and third terms are the remaining interference that can not be removed by the SIC and channel noise, respectively. Ignoring the interference yields

$$\widetilde{\mathbf{y}} = \mathbf{Q}_1^{\mathrm{H}}\mathbf{y} = \mathbf{Rd} + \widetilde{\mathbf{w}}, \tag{5.11}$$

where $\widetilde{\mathbf{w}} = {\mathbf{Q}_1}^{\mathrm{H}}\mathbf{w}$. At this point, with the help of the upper triangular structure of $\mathbf{R}$, starting from the last GFDM-IM subblock of last transmit antenna, the near-ML solution $\hat{\mathbf{d}}_t^l$ for l-th GFDM-IM subblock of t-th transmit antenna is given by

$$\hat{\mathbf{d}}_t^l = \underset{\mathbf{d}_t^l \in \{0,\mathscr{S}\}}{\operatorname{argmin}} \left\| \widetilde{\mathbf{y}}_t^l - \mathbf{R}_t^l \mathbf{d}_t^l \right\|^2, \tag{5.12}$$

where $\widetilde{\mathbf{y}}_t^l$ is a $u\times 1$ vector constructed from the last u elements of $\widetilde{\mathbf{y}}$, $\mathbf{R}_t^l$ is a $u\times u$ upper triangular matrix constructed from the last u rows and columns of $\mathbf{R}$ and $\mathbf{d}_t^l$ is a $u\times 1$ vector. After that, the interference originated from $\mathbf{d}_t^l$ is obtained as

$$\hat{\mathbf{y}}_t^l = \mathbf{R}_{:,u}\hat{\mathbf{d}}_t^l, \tag{5.13}$$

where the subscripts u and : denote the last u and all elements (column/rows) of the subscripted object, respectively, and canceled:

$$\widetilde{\mathbf{y}} \leftarrow \widetilde{\mathbf{y}} - \hat{\mathbf{y}}_t^l. \tag{5.14}$$

Then, the system size is reduced by u which is shown as

$$\widetilde{\mathbf{y}} \leftarrow \widetilde{\mathbf{y}}_{\bar{u}}, \quad \mathbf{R} \leftarrow \mathbf{R}_{\bar{u},\bar{u}}, \tag{5.15}$$

where the subscript $\bar{u}$ denote the all but the last u elements of the subscripted object, and detection operation continues to the next GFDM-IM subblock until all subblocks are detected. After this point, original information bits are retrieved as explained in Section 5.2.2.

5.3 Complexity Analysis

Computational complexities of SMX-GFDM-IM receivers with MMSE, MMSE-QRD and ML detectors are analyzed in terms of number of complex multiplications (CMs) performed in total and presented in Tables 5.1, 5.2 and 5.3, respectively. Here, $\Phi_{J\times I}$ and $\Psi_{J\times I}$ are used for $J \times I$ matrices, $\phi_{J\times 1}$ and $\psi_{J\times 1}$ stand for $J \times 1$ vectors. The complexity orders in terms of total number of CMs are presented in Table 5.4. From Table 5.4, it is observed that SMX-GFDM-IM receiver with ML detector has the highest computational complexity and the computational complexity of MMSE and MMSE-QRD detection-based receivers are approximately the same.

5.4 Numerical Analysis and Discussion

In this section, uncoded and coded BER performances of the SMX-GFDM-IM schemes are evaluated by Monte Carlo simulations for Rayleigh multi-path fading channels with EPA channel model [89]. RC with a roll-off factor (a) of 0.5 is chosen as a pulse shape for the GFDM prototype filter. The SNR is defined as $SNR = E_s/N_0$. System parameters are shown in Table 5.5.

Figs. 5.4 and 5.5 compare the uncoded BER performances of the SMX-GFDM-IM schemes with SMX-OFDM and SMX-GFDM schemes for 2×2 and 4×4 MIMO configurations, respectively, using BPSK transmission. In order to select the active subcarrier indices, the look-up table in Table 5.6 is used. From Fig. 5.4, for a 2×2 MIMO configuration and at a BER value of 10^{-4}, it is observed that the

Table 5.1 : Computational Complexity of MMSE Detection-Based SMX-GFDM-IM Receiver.

Process	Operation	Execution Count	Complexity (CMs)
Forming $\widetilde{\mathbf{H}}$	$\Phi_{N\times N}\Psi_{N\times N}{}^{*}$	RT	$N_{\mathrm{Ch}}N^2RT$
MMSE detect.	$\left(\Phi_{NR\times NT}{}^{\mathrm{H}}\Phi_{NR\times NT}+\Psi_{NT\times NT}\right)^{-1}\Phi_{NR\times NT}{}^{\mathrm{H}}\phi_{NR\times 1}$	1	$2N^3T^2R+N^3T^3+N^2RT$
Block deintlv.	No CM	R	0
SMX-IM demod.	$\min(\|\phi_{u\times 1}-\psi_{u\times 1})\|^2)$	$(N/u)cQ^vT$	NcQ^vT

* In every row of $\mathbf{H}_{r,t}$, only N_{Ch} out of N elements are non-zero.

Table 5.2 : Computational Complexity of MMSE-QRD Detection-Based SMX-GFDM-IM Receiver.

Process	Operation	Execution Count	Complexity (CMs)
Forming $\widetilde{\mathbf{H}}$	$\Phi_{N\times N}{\Psi_{N\times N}}^{\dagger}$	RT	$N_{\mathrm{Ch}}N^2RT$
MMSE-QRD	$QR\left(\Phi_{(NR+NT)\times NT}\right)^{\dagger\dagger}$	1	$2N^3T^2(T+R)$
Modified recv. vector	${\Phi_{NR\times NT}}^{\mathrm{H}}\phi_{NR\times 1}$	1	N^2RT
ML detect.	$\min(\lVert\phi_{u\times 1}-(\Phi_{u\times u}\psi_{u\times 1})\rVert^2)^{\dagger\dagger\dagger}$	$(N/u)cQ^vT$	$(N/u)(cQ^vT(uv+u))$
SIC	${\phi_{NT\times 1}-\Phi_{NT\times u}\psi_{u\times 1}}^{\dagger\dagger\dagger}$	$(N/u)T$	N^2T^2v/u

† In every row of $\mathbf{H}_{r,t}$, only N_{Ch} out of N elements are non-zero.
†† The modified Gram-Schmidt orthogonalization algorithm requires $2mn^2$ complex multiplication to compute the QR-factorization of an $m\times n$ matrix.
††† In ψ, only v complex elements are nonzero.

Table 5.3 : Computational Complexity of ML Detection-Based SMX-GFDM-IM Receiver.

Process	Operation	Execution Count	Complexity (CMs)
Forming $\widetilde{\mathbf{H}}$	$\Phi_{N\times N}\Psi_{N\times N}{}^{\ddagger}$	RT	$N_{\mathrm{Ch}}N^2RT$
ML Detection.	$\min(\lVert\phi_{NT\times 1}-(\Phi_{NR\times NT}\psi_{NT\times 1})\rVert^2)^{\ddagger\ddagger}$	$(cQ^v)^{(TN/u)}$	$(cQ^v)^{(TN/u)}((N^2TRv/u)+NT)$

‡ In every row of $\mathbf{H}_{r,t}$, only N_{Ch} out of N elements are non-zero.
‡‡ In ψ, only NTv/u complex elements are nonzero.

Table 5.4 : Summary of the computational complexity of three different receiver structures.

Receiver	Complexity (CMs)
MMSE	$\sim \mathscr{O}\left(N^3(T^3+2T^2R)\right)$
MMSE-QRD	$\sim \mathscr{O}\left(N^3(2T^3+2T^2R)\right)$
ML	$(cQ^v)^{(TN/u)}((N^2TRv/u)+NT)$

Table 5.5 : System parameters used for numerical analysis.

Description	Parameter	Value
Number of subcarriers	K	128
Number of subsymbols	M	5
Pulse shaping filter	g	RC
Roll-off factor	a	0.5
Length of cyclic prefix	N_{CP}	32
Number of channel taps for EPA channel	N_{Ch}	7

SMX-GFDM-IM scheme with MMSE-QRD detection achieves 4.5 dB better BER performance than SMX-OFDM and SMX-GFDM schemes with MMSE-QRD detection. The performance improvement of SMX-GFDM-IM scheme with MMSE-QRD detection with respect to SMX schemes arises from the coding gain due to enhanced distance spectrum of IM. On the other hand, for SMX-GFDM-IM scheme, MMSE-QRD detection method provides 3.5 dB better BER performance than MMSE detection. The performance improvement of MMSE-QRD detection method with respect to MMSE method is the result of the joint MIMO detection, GFDM and IM demodulation of the active subcarrier indices and the data symbols in a near-optimal manner. In Fig. 5.5, for a 4×4 MIMO configuration, while BER performance gain of the SMX-GFDM-IM scheme with MMSE-QRD detection with respect to SMX-OFDM and SMX-GFDM schemes with MMSE-QRD detection is approximately the same with BPSK transmission, BER performance gain of the SMX-GFDM-IM scheme with MMSE-QRD detection with respect to SMX-GFDM-IM scheme with MMSE detection is increased to 6 dB. The reason behind this improvement is the increased diversity order of the MMSE-QRD detector with the number of receive antennas. Table 5.7 shows the number of CMs required to implement the configurations given in Figs. 5.4 and 5.5. From Table 5.7, it is observed that SMX-GFDM-IM receiver with ML detection has infeasible computational complexity as expected and the BER performance improvement of the

Table 5.6 : A look-up table example for $u = 4, v = 2$ and $p_i = 2$.

Bits	Indices	subblocks
[0 0]	{1,2}	$[s_\chi \quad s_\zeta \quad 0 \quad 0]^{\mathrm{T}}$
[0 1]	{2,3}	$[0 \quad s_\chi \quad s_\zeta \quad 0]^{\mathrm{T}}$
[1 0]	{3,4}	$[0 \quad 0 \quad s_\chi \quad s_\zeta]^{\mathrm{T}}$
[1 1]	{1,4}	$[s_\chi \quad 0 \quad 0 \quad s_\zeta]^{\mathrm{T}}$

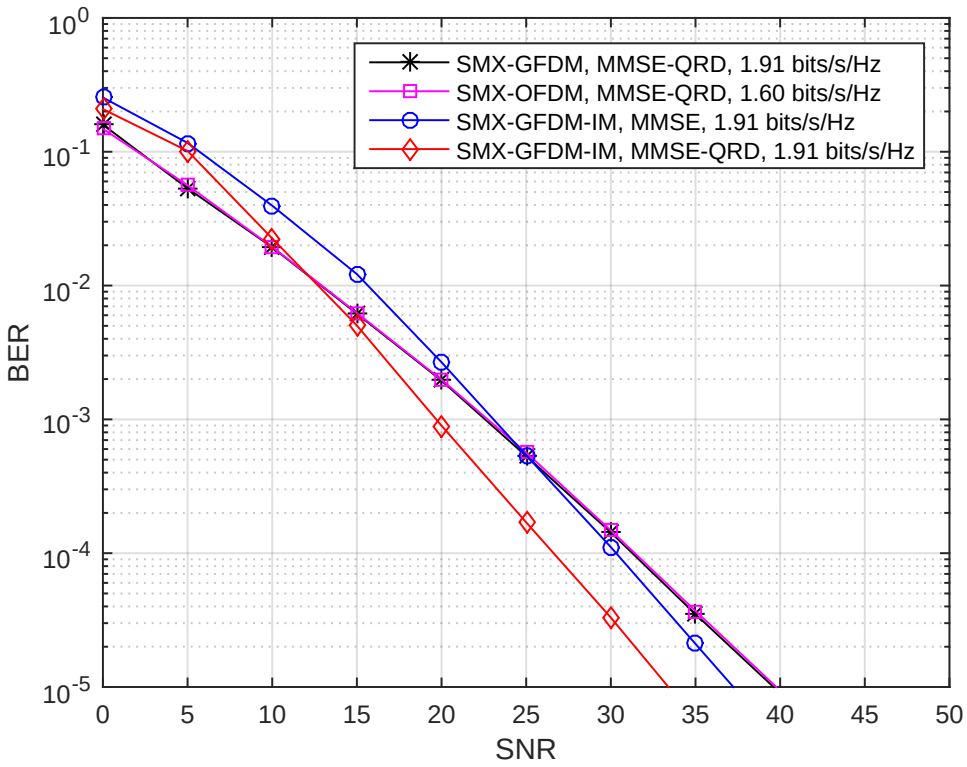

Figure 5.4 : Uncoded BER performance of MMSE and MMSE-QRD detection methods for 2×2 SMX and SMX-IM schemes using BPSK transmission.

MMSE-QRD detector with respect to MMSE detector is provided with negligible increase in computational complexity.

In GFDM, a single CP is used for entire block consisting K subcarriers with M timeslots on each of it. Therefore, GFDM provides a higher spectral efficiency with respect to OFDM due to reduced overhead of CP. For the configurations in Figs. 5.4 and 5.5, GFDM schemes provide 19% spectral efficiency with respect to OFDM schemes. Here, the spectral efficiency of SMX-IM schemes is given by $p/(N+N_{\mathrm{CP}})$, and the spectral efficiency of SMX schemes is given by $N\log_2(Q)/(N+N_{\mathrm{CP}})$.

Fig. 5.6 shows the OOB emission comparison of SMX and SMX-IM schemes using RC pulse shaping filter with a roll-off factor of 0.5 for BPSK transmission. From Fig.

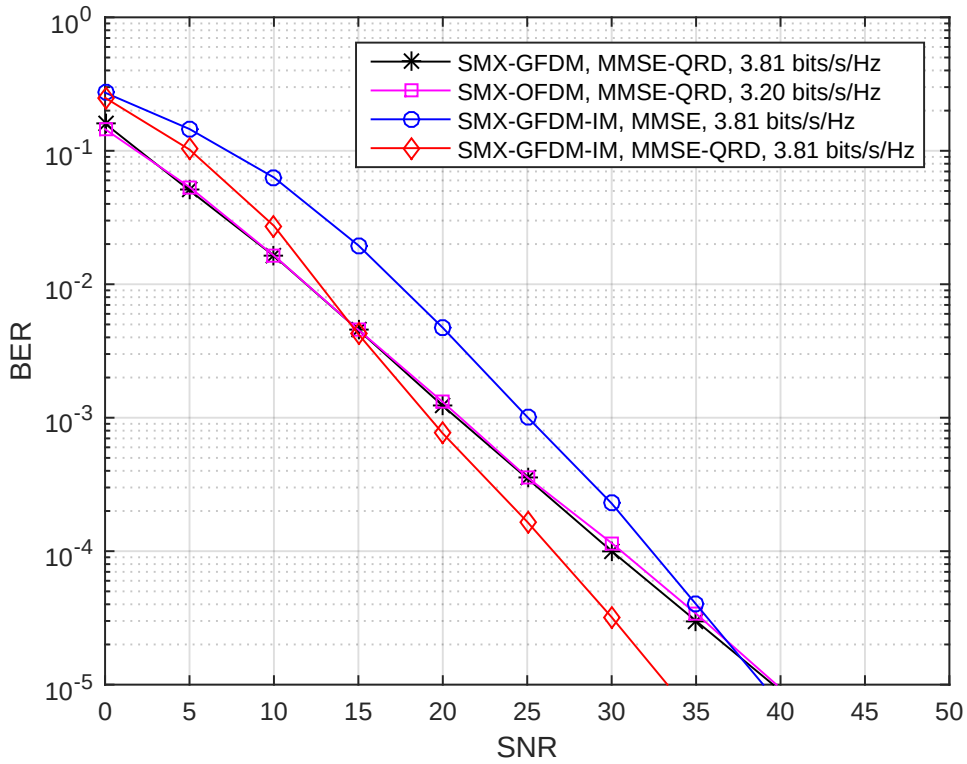

Figure 5.5 : Uncoded BER performance of MMSE and MMSE-QRD detection methods for 4×4 SMX and SMX-IM schemes using BPSK transmission.

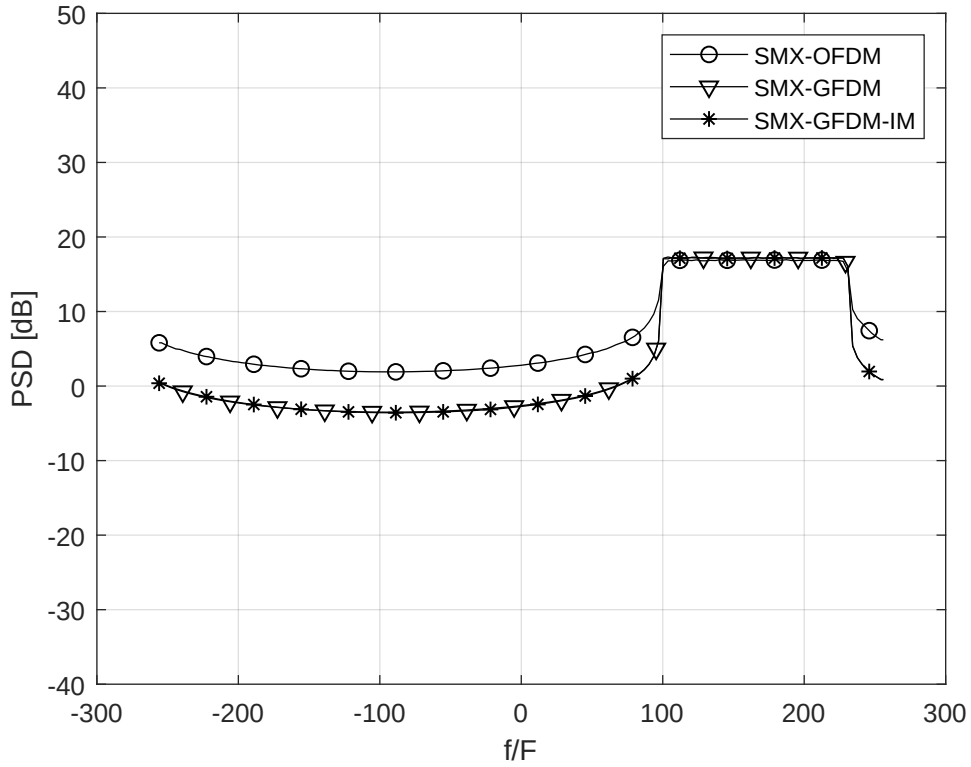

Figure 5.6 : OOB emission comparison of SMX and SMX-IM schemes using RC pulse shaping filter with a roll-off factor 0.5 for BPSK transmission.

Table 5.7 : The total number of CMs for SMX-GFDM-IM receivers using BPSK.

Ant. Config.	MMSE	MMSE-QRD	ML
2×2	6.31×10^{9}	8.40×10^{9}	3.64×10^{487}
4×4	5.04×10^{10}	6.72×10^{10}	2.95×10^{1162}

Table 5.8 : A look-up table example for $u = 4, v = 3$ and $p_i = 2$.

Bits	Indices	subblocks
[0 0]	$\{1,2,3\}$	$\begin{bmatrix} s_\chi & s_\zeta & s_\delta & 0 \end{bmatrix}^{\mathrm{T}}$
[0 1]	$\{1,2,4\}$	$\begin{bmatrix} s_\chi & s_\zeta & 0 & s_\delta \end{bmatrix}^{\mathrm{T}}$
[1 0]	$\{1,3,4\}$	$\begin{bmatrix} s_\chi & 0 & s_\zeta & s_\delta \end{bmatrix}^{\mathrm{T}}$
[1 1]	$\{2,3,4\}$	$\begin{bmatrix} 0 & s_\chi & s_\zeta & s_\delta \end{bmatrix}^{\mathrm{T}}$

5.6, it is observed that GFDM schemes provides 6 dB OOB emission suppression with respect to OFDM scheme due to pulse shaping of each subcarrier with RC filter. Note that, there is not any difference on OOB emission of SMX-GFDM and SMX-GFDM-IM schemes as expected.

Figs. 5.7 and 5.8 show the uncoded BER performance of the SMX-GFDM-IM schemes along with the SMX-OFDM and SMX-GFDM schemes for 2×2 and 4×4 MIMO configurations, respectively, using 4-QAM transmission. Here, the active subcarrier indices are determined using the look-up table in Table 5.8. From Figs. 5.7 and 5.8, it is observed that the BER performance gain of the SMX-GFDM-IM schemes with MMSE-QRD detection with respect to other schemes are decreased compared to the gains in BPSK transmission. The reason behind this decrease is the decrease of the p_i/p_q ratio from 1 to 0.33. On the other hand, the number of CMs required to implement the configurations given in Figs. 5.7 and 5.8 are given in Table 5.9. From Table 5.9, it is observed that ML detector has the highest computational complexity as in the BPSK case and the computational complexity of MMSE-QRD detector is higher than the computational complexity of MMSE detector with a negligible level.

Fig. 5.9 compares the coded BER performance of the SMX-GFDM-IM scheme with SMX-OFDM and SMX-GFDM schemes for 4×4 MIMO configuration using

Table 5.9 : The total number of CMs for SMX-GFDM-IM receivers using 4-QAM.

Ant. Config.	MMSE	MMSE-QRD	ML
2×2	6.31×10^{9}	8.40×10^{9}	1.14×10^{873}
4×4	5.04×10^{10}	6.72×10^{10}	1.92×10^{1933}

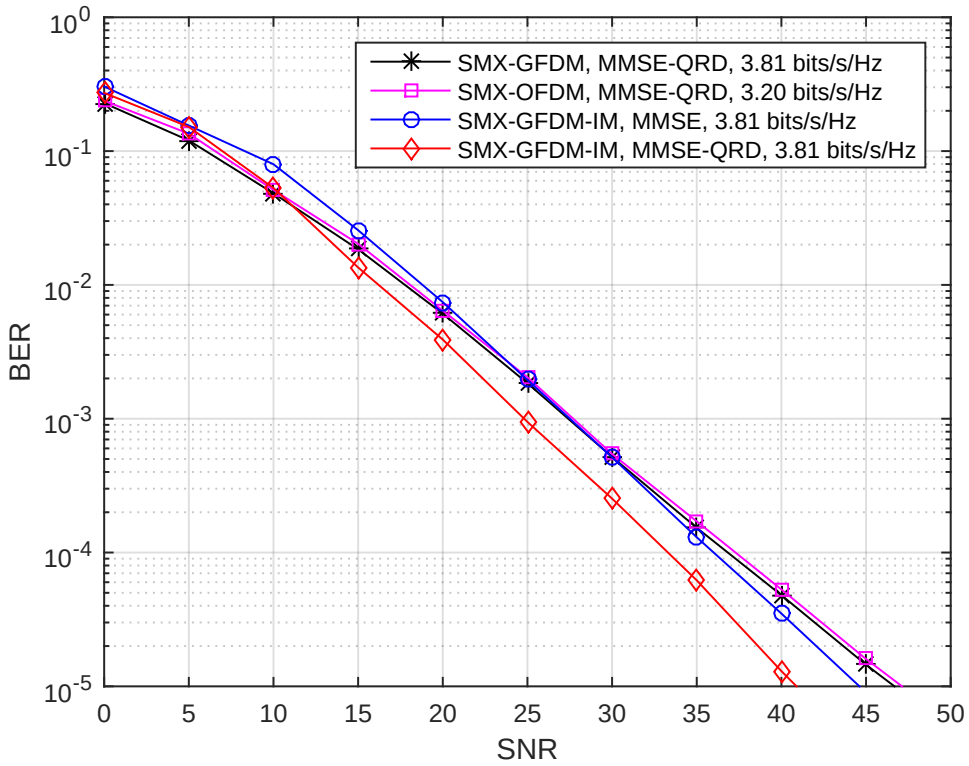

Figure 5.7 : Uncoded BER performance of MMSE and MMSE-QRD detection methods for 2×2 SMX and SMX-IM schemes using 4-QAM transmission.

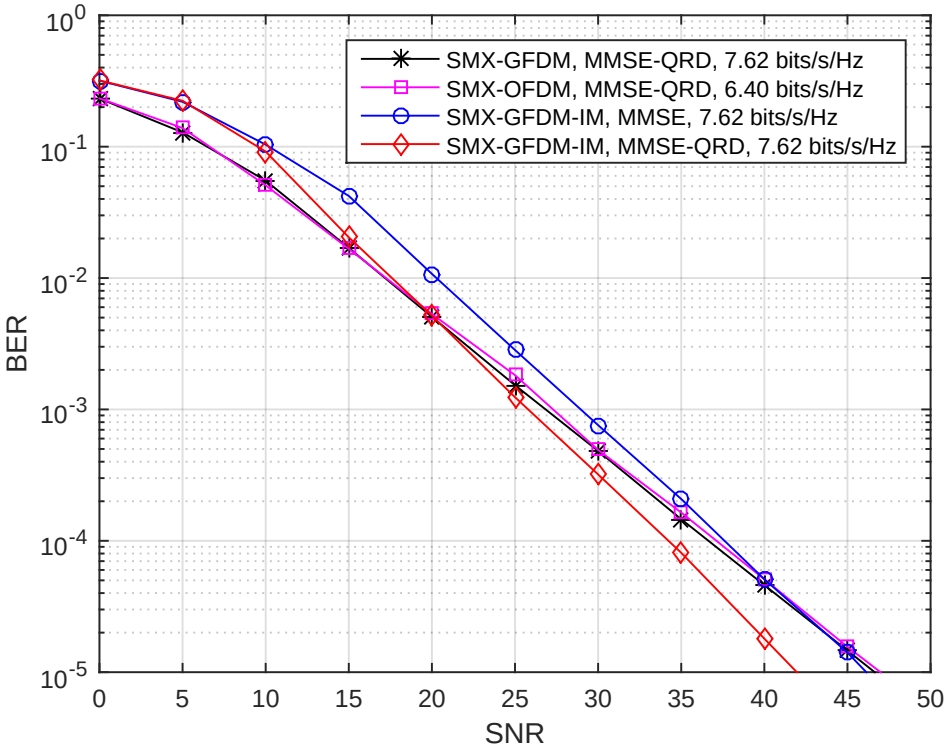

Figure 5.8 : Uncoded BER performance of MMSE and MMSE-QRD detection methods for 4×4 SMX and SMX-IM schemes using 4-QAM transmission.

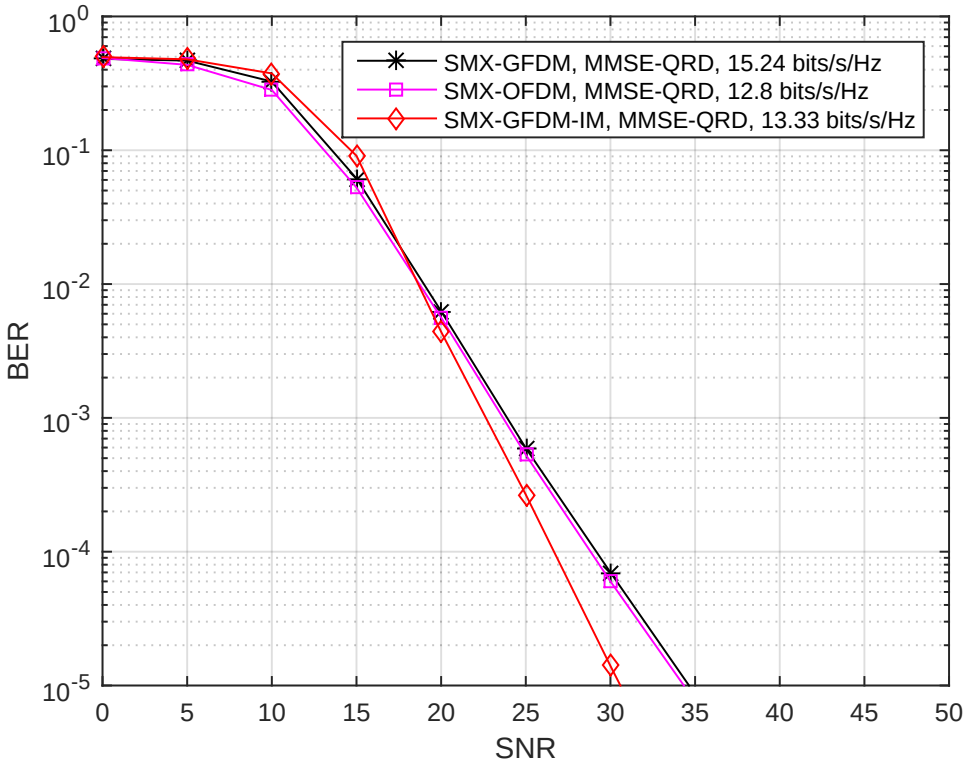

Figure 5.9 : Coded BER performance of 4×4 SMX and SMX-IM schemes using 16-QAM transmission.

16-QAM transmission. For the channel code, the rate 1/3 convolutional code with generator sequence $q = [133, 171, 165]$ is chosen [90]. In order to select the active subcarrier indices, the look-up table in Table 5.8 is used. From Fig. 5.9, at a BER value of 10^{-4}, it is observed that the SMX-GFDM-IM scheme achieves 2.5 dB better BER performance than SMX-OFDM and SMX-GFDM schemes. Here, since the p_i/p_q ratio is decreased to 0.16, BER performance improvement of the IM scheme is decreased with respect to BPSK and 4-QAM schemes. Therefore, it can be stated that the BER improvements of the IM scheme is directly proportional with the amount of information bits conveyed by the indices of the transmit entities as expected. Besides, considering Figs. 5.5, 5.8 and 5.9, it is observed that channel coding improves the BER performance of the SMX-GFDM-IM scheme. Note that, for the system configuration given in Fig. 5.9, while spectral efficiency of SMX-GFDM-IM scheme is slightly lower than SMX-GFDM scheme due to unused subcarriers, it has still higher spectral efficiency with respect to SMX-OFDM scheme due to reduced overhead of CP.

6. CONCLUSIONS AND RECOMMENDATIONS

In this thesis, the combination of MIMO and IM techniques with GFDM has been investigated and innovative novel transceiver structures, optimized in terms of energy, spectral and computational efficiency, have been introduced in order to fulfill the diverse requirements of future wireless networks.

In the first stage of the thesis, a GFDM-IM scheme, which uses flexible IM numerology along with the near-optimum detector, is proposed to improve OOB emission, error performance and computational complexity of the GFDM scheme. As a first attempt in the literature, the GFDM-IM system model is constructed and sparse IM numerology is applied to the edge GFDM subsymbols to jointly optimize OOB emission, spectral efficiency and latency of the GFDM scheme. Besides, in order to enhance the error performance and reduce the computational complexity of the scheme, a ML-SIC based near-optimum detector is developed for the SISO GFDM scheme considering the flexible IM numerology, and its theoretical error performance is analyzed. Furthermore, a new system model, which enables multi-layer transmission through IM-bits and QAM-bits, is presented. Thanks to this system model, the proposed scheme provides different error performances and spectral efficiencies for QAM and IM bits, and further benefits from enhanced distance spectrum of IM. The BLER, OOB emission and computational complexity of the proposed GFDM-IM scheme are evaluated via computer simulations. According to obtained simulation and theoretical results, it is observed that the proposed GFDM-IM scheme achieves better BLER performance than the plain GFDM-IM, OFDM-IM, GFDM and OFDM schemes at the same spectral efficiency. In addition, ML-SIC technique provides 34% less complexity with respect to classical MMSE detector.

As a continuation of the first stage, an FIM framework, which combines GFDM with space and frequency IM schemes, has been proposed and novel transmitter and receiver schemes for MIMO-GFDM applications have been presented in the second stage. The proposed framework has an FIM transmitter, which is capable

of generating six different SFIM schemes using single transmitter structure. For the receiver part, a near-optimum detection scheme, which is based on ML detection with SIC, has been proposed. The FIM receiver provides different levels of BER performances and computational complexities by the proposed ML-SIC detection scheme and the ZF-SDD and MMSE-JDD detection schemes. Thanks to the proposed FIM transmitter and receiver structures, transmission scheme and the detection method can be determined according to desired level of complexity, transmit power and spectral efficiency of the use cases. Besides, switching between different IM schemes according to channel conditions can be possible using a single transceiver structure. Furthermore, FIM framework provides a multi-layer scheme by means of different levels of BER performances and spectral efficiencies and enables to support different use cases by using common space, frequency and time resources at the same time. It has been shown that GFDM-FIM has a strong potential to engineer the space-frequency structure according to channel conditions and use cases as well as it provides a great flexibility, which can be easily tuned to address the required performance criterion.

In the third stage, SMX and IM techniques have been combined with GFDM in order to provide higher data rates while benefiting energy efficiency of the IM. At the transmitter side, each transmit antenna transmits its own GFDM-IM block, and at the receiver side, GFDM-IM blocks are detected and demodulated using a novel MMSE-QRD-based near-optimum detector. We have investigated the error performance, OOB emission, spectral efficiency and computational complexity of the proposed scheme via computer simulations. It has been demonstrated that the proposed SMX-GFDM-IM scheme achieves better error performance with respect to classical SMX-OFDM and SMX-GFDM schemes and has a lower OOB emission and better spectral efficiency advantages with respect to SMX-OFDM scheme because of digitally pulse shaping of each subcarrier and reduced overhead of cyclic prefix.

Although radically new PHY technologies and modulation formats have been explored to fulfill the challenges of 5G wireless networks, it was decided that none of the waveform alternatives were able to address all the requirements at the same time, thus, an expanded version of OFDM with multiple numerologies has been selected as fundamental PHY signal structure for Release 15, which is the first 5G specification of 3GPP. However, considering the diverse applications of future

wireless networks, there is a paradigm shift from orthogonal to non-orthogonal structures in terms of both waveform and multiple access schemes. As a first attempt to benefit from non-orthogonal schemes, non-orthogonal multiple access (NOMA) has been studying under the scope of the Release 16 specification of 3GPP. For the waveform side, potential support of non-orthogonal waveform would come into question for later releases of 3GPP to evolve and expand the wireless communication ecosystem due to attractive properties of non-orthogonal waveforms such as low OOB emission and tolerance to time and frequency synchronization errors. Amongst these non-orthogonal waveforms, as mentioned earlier, GFDM comes into prominence by providing advantages in terms of OOB emission, spectral efficiency and latency due to digitally pulse shaping of each subcarrier, reduced overhead of cyclic prefix and block-based structure, respectively. By integrating GFDM with promising MIMO and IM techniques in a skilled framework released in this thesis, GFDM has been gained significant advantages in terms of spectral and energy efficiency, thus, it can be considered a promising PHY layer technique for future wireless networks.

Throughout this thesis, it is assumed that perfect synchronization is ensured, wireless channel remains constant within one GFDM-IM block and the channel state information is perfectly known at the receiver. As a future work, performance analysis of integration of GFDM with MIMO and IM techniques under highly time-varying channels with imperfect synchronization and incomplete channel state information can be studied. Furthermore, optimum detection techniques with low computational complexity exploiting the block circularity of the GFDM modulation matrix can be examined.

The studies conducted in this thesis have been published as two international journal papers and three international conference papers. In addition, one US patent application and one international journal paper were submitted. The proposed techniques in this thesis have recently attracted significant attention from the researchers and these mentioned papers got more than thirty citations in two years.

REFERENCES

[1] **Zaidi *et. al.*, A.A.** (2016). Preliminary study on waveform candidates for 5G mobile radio communications above 6 GHz, *IEEE 83rd Vehicular Technology Conference (VTC Spring)*.

[2] **Michailow, N.**, **Matthe, M.**, **Gaspar, I.**, **Caldevilla, A.**, **Mendes, L.**, **Festag, A. and Fettweis, G.** (2014). Generalized frequency division multiplexing for 5th generation cellular networks, *IEEE Trans. Commun.*, *62*(9), 3045–3061.

[3] **Basar, E.** (2016). Index modulation techniques for 5G wireless networks, *IEEE Commun. Mag.*, *54*(7), 168–175.

[4] **Andrews *et. al.*, J.G.** (2014). What will 5G be?, *IEEE J. Sel. Areas Commun.*, *32*(6), 1065–1082.

[5] **ITU-R** (2015). *IMT Vision framework and overall objectives of the future development of IMT for 2020 and beyond*, *tech. rep. M.2083-0*.

[6] **3GPP** (2016). *Study on Scenarios and Requirements for Next Generation Access Technologies*, *tech. rep. 38.913*.

[7] **Wunder *et. al.*, G.** (2014). 5GNOW: Non-orthogonal, asynchronous waveforms for future mobile applications, *IEEE Commun. Mag.*, *52*(2), 97–105.

[8] **Banelli *et. al.*, P.** (2014). Modulation formats and waveforms for 5G networks: Who will be the heir of OFDM?: An overview of alternative modulation schemes for improved spectral efficiency, *IEEE Signal Process. Mag.*, *31*(6), 80–93.

[9] **3GPP** (2017). *NR, Physical layer, general description*, *tech. spec. 38.201*.

[10] **3GPP** (2018). *Study on new radio (NR) access technology*, *tech. spec. 38.912 V15.0.0*.

[11] **Abdoli *et. al.*, J.** (2015). Filtered OFDM: A new waveform for future wireless systems, *IEEE Int'l. Wksp. Signal Processing Advances Wireless Commun.*, Stockholm, Sweden, pp.66–70.

[12] **Zhang *et. al.*, X.** (2015). Filtered-OFDM - Enabler for flexible waveform in the 5th generation cellular networks, *IEEE GLOBECOM Workshops*, San Diego CA, USA.

[13] **Bala, E.**, **Li, J. and Yang, R.** (2013). Shaping spectral leakage: A novel low-complexity transceiver architecture for cognitive radio, *IEEE Veh. Technol. Mag.*, *8*(3), 38–46.

[14] **Bellanger *et. al.*, M.**, (2010), FBMC physical layer: a primer, `http://www.ict-phydyas.org`.

[15] **Farhang-Boroujeny, B.** (2011). OFDM versus filter bank multicarrier, *IEEE Signal Process. Mag.*, *28*(3), 92–112.

[16] **Vakilian, V.**, **Wild, T.**, **Schaich, F.**, **ten Brink, S. and Frigon, J.F.** (2013). Universal filtered multi-carrier technique for wireless systems beyond LTE, *IEEE Globecom Workshop*, Atlanta, GA, USA, pp.223–228.

[17] **Matthe, M.**, **Mendes, L.L. and Fettweis, G.** (2014). Space-time coding for generalized frequency division multiplexing, *20th Eur. Wireless Conf.*, Barcelona, Spain, pp.1–5.

[18] **Matthe, M.**, **Mendes, L.L.**, **Gaspar, I.**, **Michailov, N.**, **Zhang, D. and Fettweis, G.** (2015). Widely linear estimation for space-time-coded GFDM in low latency applications, *IEEE Trans. Commun.*, *63*(11), 4501–4509.

[19] **Matthe, M.**, **Mendes, L.L.**, **Gaspar, I.**, **Michailov, N.**, **Zhang, D. and Fettweis, G.** (2015). Multi-user time-reversal STC-GFDMA for future wireless networks, *EURASIP J. Wireless Commun. Netw.*, *2015*(1), 1–8.

[20] **Zhang, D.**, **Mendes, L.L.**, **Matthe, M.**, **Michailov, N. and Fettweis, G.** (2016). Expectation propagation for near-optimum detection of MIMO-GFDM signals, *IEEE Trans. Wireless Commun.*, *15*(2), 1045–1062.

[21] **Zhang, D.**, **Mendes, L.L.**, **Matthe, M. and Fettweis, G.** (2015). A Markov chain Monte Carlo algorithm for near-optimum detection of MIMO-GFDM signals, *IEEE Personal, Indoor and Mobile Radio Commun., (PIMRC'15)*, Hong Kong, pp.1–5.

[22] **Zhong, J.**, **Chen, G.**, **Mao, J.**, **Dang, S. and Xiao, P.** (2018). Iterative frequency domain equalization for MIMO-GFDM systems, *IEEE Access*, *6*, 19386–19395.

[23] **Tunali, N.**, **Wu, M.**, **Dick, C.**, **Studer, C. and Jose, S.** (2015). Linear large-scale MIMO data detection for 5G multi-carrier waveform candidates, *Asilomar Conf. on Signals, Systems, and Computers*, California, USA, pp.1–5.

[24] **Matthe, M.**, **Gaspar, I.**, **Zhang, D. and Fettweis, G.** (2015). Near-ML detection for MIMO-GFDM, *82nd IEEE Veh. Technol. Conf. Fall*, Boston, USA.

[25] **Matthe, M.**, **Zhang, D. and Fettweis, G.** (2016). Sphere-decoding aided SIC for MIMO-GFDM: coded performance analysis, *Int. Symp. on Wireless Commun. Systems (ISWCS)*, Poznan, Poland, pp.165–169.

[26] **Matthe, M.**, **Zhang, D. and Fettweis, G.** (2016). Iterative detection using MMSE-PIC demapping for MIMO-GFDM systems, *IEEE European Wireless (EW'16)*, Oulu, Finland.

[27] **Matthe, M.**, **Zhang, D. and Fettweis, G.** (2018). Low-complexity iterative MMSE-PIC detection for MIMO-GFDM, *IEEE Trans. Commun.*, *66*(4), 1467–1480.

[28] **Zhang, D.**, **Matthe, M.**, **Mendes, L.L. and Fettweis, G.** (2017). A study on the link level performance of advanced multicarrier waveforms under MIMO wireless communication channels, *IEEE Trans. Wireless Commun.*, *16*(4), 2350–2365.

[29] **Mesleh, R.**, **Haas, H.**, **Sinanovic, S.**, **Ahn, C.W. and Yun, S.** (2008). Spatial modulation, *IEEE Trans. Veh. Technol.*, *57*(4), 2228–2241.

[30] **Mesleh, R.**, **Ikki, S. and Aggoune, H.** (2015). Quadrature spatial modulation, *IEEE Trans. Veh. Technol.*, *64*(6), 2738–2742.

[31] **Basar, E.**, **Aygölü, Ü.**, **Panayırcı, E. and Poor, H.V.** (2013). Orthogonal frequency division multiplexing with index modulation, *IEEE Trans. Signal Process.*, *61*(22), 5536–5549.

[32] **Abu-alhiga, R. and Haas, H.** (2009). Subcarrier-index modulation OFDM, *IEEE Int. Sym. Personal, Indoor and Mobile Radio Commun.*, Tokyo, Japan, pp.177–181.

[33] **Tsonev, D.**, **Sinanovic, S. and Haas, H.** (2011). Enhanced subcarrier index modulation (SIM) OFDM, *IEEE GLOBECOM Workshops*, pp.728–732.

[34] **Mao, T.**, **Wang, Z.**, **Wang, Q.**, **Chen, S. and Hanzo, L.** (2016). Dual-mode index modulation aided OFDM, *IEEE Access*, *PP*(99), 1–1.

[35] **Wen, M.**, **Basar, E.**, **Li, Q.**, **Zheng, B. and Zhang, M.** (2017). Multiple-mode orthogonal frequency division multiplexing with index modulation, *IEEE Trans. Commun.*, *65*(9), 3892–3906.

[36] **Basar, E.** (2015). OFDM with index modulation using coordinate interleaving, *IEEE Wireless Commun. Lett.*, *4*(4), 381 – 384.

[37] **Fan, R.**, **Yu, Y.J. and Guan, Y.L.** (2015). Generalization of orthogonal frequency division multiplexing with index modulation, *IEEE Trans. Wireless Commun.*, *14*(10), 5350 – 5359.

[38] **Wen, M.**, **Zhang, Y.**, **Li, J.**, **Basar, E. and Chen, F.** (2016). Equiprobable subcarrier activation method for OFDM with index modulation, *IEEE Commun. Lett.*, *20*(12), 2386 – 2389.

[39] **Wen, M.**, **Ye, B.**, **Basar, E.**, **Li, Q. and Ji, F.** (2017). Enhanced orthogonal frequency division multiplexing with index modulation, *IEEE Trans. Wireless Commun.*

[40] **Zhang, H.**, **Yang, L.L. and Hanzo, L.** (2016). Compressed sensing improves the performance of subcarrier index-modulation-assisted OFDM, *IEEE Access*, *4*, 7859 – 7873.

[41] **Basar, E.** (2015). Multiple-input multiple-output OFDM with index modulation, *IEEE Signal Process. Lett.*, *22*(12), 2259 – 2263.

[42] **Datta, T.**, **Eshwaraiah, H.S. and Chockalingam, A.** (2016). Generalized space-and-frequency index modulation, *IEEE Trans. Veh. Technol.*, *65*(7), 4911–4924.

[43] **Basar, E.** (2016). On multiple-input multiple-output OFDM with index modulation for next generation wireless networks, *IEEE Trans. Signal Process.*, *64*(15), 3868–3878.

[44] **Zheng, B.**, **Wen, M.**, **Basar, E. and Chen, F.** (2017). Multiple-input multiple-output OFDM with index modulation: Low-complexity detector design, *IEEE Trans. Signal Process.*, *65*(11), 2758 – 2772.

[45] **Basar *et. al.*, E.** (2017). Index modulation techniques for next-generation wireless networks, *IEEE Access*, *5*(1), 16693–16746.

[46] **Chang, Y.K. and Ueng, F.B.** (2018). A novel turbo GFDM-IM receiver for MIMO communications, *International Journal of Electronics and Communications*, *87*, 22–32.

[47] **Yuzgecoglu, M. and Jorswieck, E.** (2018). Transceiver design for GFDM with index modulation in multi-user networks, *WSA 2018, 22nd International ITG Workshop on Smart Antennas*, pp.43–48.

[48] **Ozturk, E.**, **Basar, E. and Cirpan, H.** (2016). Spatial modulation GFDM: A low complexity MIMO-GFDM system for 5G wireless networks, *4th IEEE Int. Black Sea Conf. Commun. Networking*, Varna, Bulgaria.

[49] **Ozturk, E.**, **Basar, E. and Cirpan, H.** (2016). Generalized frequency division multiplexing with index modulation, *IEEE GLOBECOM Workshops*, Washington DC, USA.

[50] **Ozturk, E.**, **Basar, E. and Cirpan, H.** (2017). Generalized frequency division multiplexing with space and frequency index modulations, *5th IEEE Int. Black Sea Conf. Commun. Networking*, Istanbul, Turkey.

[51] **Ozturk, E.**, **Basar, E. and Cirpan, H.** (2017). Generalized frequency division multiplexing with flexible index modulation, *IEEE Access*, *5*, 24727 – 24746.

[52] **Ozturk, E.**, **Basar, E. and Cirpan, H.** (2018). Generalized frequency division multiplexing with flexible index modulation numerology, *IEEE Signal Process. Lett.*, *25*(10), 1480–1484.

[53] **Ozturk, E.**, **Basar, E. and Cirpan, H.** (2018). Multiple-input multiple-output generalized frequency division multiplexing with flexible index modulation, *PCT Patent Application Number: PCT/TR2018/050341*.

[54] **Sklar, B.**, (2001). *Digital Communications, Fundamentals and Applications*, Prentice Hall, Inc., Upper Saddle River, NJ., 2. edition.

[55] **Proakis, J. and Salehi, M.**, (2002). *Communications Systems Engineering*, Prentice Hall, Inc., Upper Saddle River, NJ., 2. edition.

[56] **Rappaport, T.**, (2002). *Wireless Communications: Principles and Practice*, Prentice Hall, Inc., Upper Saddle River, NJ., 2. edition.

[57] **Huawei** (2016). *5G Waveform: Requirements and design principles*, *R1-162151, 3GPP TSG RAN WG1 Meeting 84bis*.

[58] **Qualcomm** (2016). *Waveform requirements*, *R1-162198, 3GPP TSG RAN WG1 Meeting 84bis*.

[59] **Berardinelli *et. al.*, G.** (2014). On the potential of OFDM enhancements as 5G waveforms, *IEEE 79th Vehicular Technology Conference (VTC Spring)*.

[60] **Zhang, X.**, **Chen, L.**, **Qiu, J. and Abdoli, J.** (2016). On the waveform for 5G, *IEEE Communications Magazine*, *54*(11), 74–80.

[61] **Sjoberg, F.**, **Nilsson, R.**, **Isaksson, M.**, **Odling, P. and Borjesson, P.O.** (1999). Asynchronous zipper, *IEEE International Conference on Communications (ICC)*, p.231–235.

[62] **Matz, G.**, **Schafhuber, D.**, **Grochenig, K.**, **Hartmann, M. and Hlawatsch, F.** (2007). Analysis, optimization, and implementation of low-interference wireless multicarrier systems, *IEEE Transactions on Wireless Communications*, *6*(5), 1921–1931.

[63] **Huemer, M.**, **Hofbauer, C.**, **Onic, A. and Huber, J.B.** (2014). Design and analysis of UW-OFDM signals, *International Journal of Electronics and Communications*, *68*(10), 958–968.

[64] **Huemer, M.**, **Hofbauer, C. and Huber, J.B.** (2010). The potential of unique words in OFDM, *Proceedings International OFDM Workshop*.

[65] **Vakilian, V.**, **Wil, T.**, **Schaich, F.**, **Brink, S.T. and Frigon, J.F.** (2013). Universal-filtered multi-carrier technique for wireless systems beyond LTE, *IEEE Globecom Workshops (GC Wkshps)*.

[66] **Wild, T.**, **Schaich, F. and Chen, Y.** (aug). 5G air interface design based on universal filtered (UF-)OFDM, *19th International Conference on Digital Signal Processing (DSP)*, p.699–704.

[67] **Qualcomm** (2016). *Waveform candidates*, *R1-162199, 3GPP TSG RAN WG1 Meeting 84bis*.

[68] **Berardinelli, G.**, **Tavares, F.**, **Sorensen, T.**, **Mogensen, P. and Pajukoski, K.** (2013). Zero-tail DFT-spread-OFDM signals, *IEEE Globecom Workshops (GC Wkshps)*, p.229–234.

[69] **Sahin *et. al.*, A.** (2016). Flexible DFT-S-OFDM: Solutions and challenges, *IEEE Communications Magazine*, *54*(11), 90–98.

[70] **Wylie-Green, M.**, **Perrins, E. and Svensson, T.** (2011). Introduction to CPM-SC-FDMA: A novel multiple-access power-efficient transmission scheme, *IEEE Transactions on Communications*, *59*(7), 1904–1915.

[71] **Svensson, T. and Svensson, A.** (2009). Design and performance of constrained envelope continuous phase modulation, *2009 International Waveform Diversity and Design Conference*, p.312–316.

[72] **Svensson, N.** (1995). On differentially encoded star 16QAM with differential detection and diversity, *IEEE Transactions on Vehicular Technology*, *44*(3), 586–593.

[73] **Reyhani, A.R.**, **Farhang, A. and Farhang-Boroujeny, B.** (2015). Circularly pulse shaped waveforms for 5G, *Proc. IEEE GLOBECOM*.

[74] **Michailow, N. and Fettweis, G.** (2013). Low peak-to-average power ratio for next generation cellular systems with generalized frequency division multiplexing, *Proc. Int. Symp. ISPACS*, p.651–655.

[75] **Fettweis, G.** (2014). The tactile Internet: Applications and challenges, *IEEE Veh. Technol. Mag.*, *9*(1), 64–70.

[76] **Di Renzo, M.**, **Haas, H.**, **Ghrayeb, A.**, **Sugiura, S. and Hanzo, L.** (2014). Spatial modulation for generalized MIMO: Challenges, opportunities, and implementation, *Proc. IEEE*, *102*(1), 56–103.

[77] **Yang, P.**, **Di Renzo, M.**, **Xiao, Y. Li, S. and Hanzo, L.** (2015). Design guidelines for spatial modulation, *IEEE Commun. Surveys Tutorials*, *17*(1), 6–26.

[78] **Wen, M.**, **Cheng, X.**, **Ma, M.**, **Jiao, B. and Poor, H.V.** (2016). On the achievable rate of OFDM with index modulation, *IEEE Trans. Signal Process.*, *64*(8), 1919–1932.

[79] **Alamouti, S.** (1998). A simple transmit diversity technique for wireless communications, *IEEE J. Sel. Areas Commun.*, *16*(8), 1451–1458.

[80] **Tarokh, V.**, **Seshadri, N. and Calderbank, A.** (1998). Space-time codes for high data rate wireless communication: Performance criterion and code construction, *IEEE Trans. Inf. Theory*, *44*(2), 744–765.

[81] **Viswanath, P.**, **Tse, D. and Anantharam, V.** (2001). Asymptotically optimal water filling in vector multiple-access channels, *IEEE Trans. Inf. Theory*, *47*(1), 241–267.

[82] **Raleigh, G. and Cioffi, J.** (1998). Spatio-temporal coding for wireless communication, *IEEE Trans. Commun.*, *46*(3), 357–366.

[83] **Foschini, G.J.** (1996). Layered space-time architecture for wireless communication in a fading environment when using multi-element antennas, *Bell Labs Tech. J.*, *1*(2), 41–59.

[84] **Wolniansky, P.**, **Foschini, G.**, **Golden, G. and Valenzuela, R.** (1998). V-BLAST: An architecture for realizing very high data rates over the richscattering wireless channel, *Proc. URSI ISSSE*, p.295–300.

[85] **Wubben, D.**, **Bohnke, R.**, **Kuhn, V. and Kammeyer, K.** (2003). MMSE extension of V-BLAST based on sorted QR decomposition, *IEEE 58th Vehicular Technology Conference*, pp.508–512.

[86] **Wubben, D.**, **Bohnke, R.**, **Rinas, J.**, **Kuhn, V. and Kammeyer, K.** (2001). Efficient algorithm for decoding layered space-time codes, *IEE Electron. Lett.*, *37*(22), 1348–1350.

[87] **Yan, Z.**, **Wong, K.M. and Luo, Z.Q.** (2005). Optimal diagonal precoder for multiantenna communication systems, *IEEE Trans. Signal Process.*, *53*(6), 2089–2100.

[88] **Matthe, M.**, **Michailov, N.**, **Gaspar, I. and Fettweis, G.** (2014). Influence of pulse shaping on bit error rate performance and out of band radiation of generalized frequency division multiplexing, *Communications Workshops (ICC), 2014 IEEE International Conference on.*, pp.43–48.

[89] **3GPP** (2017). *Base station (BS) radio transmission and reception*, *tech. spec. 36.104 V14.4.0*.

[90] **3GPP** (2017). *Multiplexing and channel coding*, *tech. spec. 36.212 V14.3.0*.

CURRICULUM VITAE

Name Surname: Ersin ÖZTÜRK

Place and Date of Birth: Kartal, 02.09.1973

E-Mail: eozturk@netas.com.tr

EDUCATION:

- **B.Sc.:** 1995, Yıldız Technical University, Faculty of Electrical and Electronics Engineering, Electronics and Communication Engineering Department
- **M.Sc.:** 1998, Istanbul Technical University, Graduate School of Science Engineering and Technology, Electronics and Communication Engineering Programme

PROFESSIONAL EXPERIENCE AND REWARDS:

- 1995-1998 Universal Comm., Hardware Design Engineer.
- 1999-... NETAS Telecommunication, R&D Director

PUBLICATIONS, PRESENTATIONS AND PATENTS ON THE THESIS:

- **Ozturk E.**, Basar E., Cirpan H. A., 2017. Generalized Frequency Division Multiplexing with Flexible Index Modulation. *IEEE Access*, 5, 24727-24746.
- **Ozturk E.**, Basar E., Cirpan H. A., 2018. Generalized Frequency Division Multiplexing with Flexible Index Modulation Numerology. *IEEE Signal Processing Lett.*, 26(10), 1480-1484.
- **Ozturk E.**, Basar E., Cirpan H. A., 2018. Multiple-Input Multiple Generalized Frequency Division Multiplexing with Index Modulation, submitted to journal of *Physical Communication*.
- **Ozturk E.**, Basar E., Cirpan H. A., 2017. Generalized Frequency Division Multiplexing with Space and Frequency Index Modulation. *5th Int. Black Sea Conf. Commun. Netw. (IEEE BlackSeaCom)*, June 5-8, 2017, Istanbul, Turkey.
- **Ozturk E.**, Basar E., Cirpan H. A., 2016. Generalized Frequency Division Multiplexing with Index Modulation. *IEEE GLOBECOM Workshops*, December 4-8, 2016, Washington, DC, USA.
- **Ozturk E.**, Basar E., Cirpan H. A., 2016. Spatial modulation GFDM: A Low Complexity MIMO-GFDM System for 5G Wireless Networks. *4th Int. Black Sea Conf. Commun. Netw. (IEEE BlackSeaCom)*, June 6-9, Varna, Bulgaria.

- **Ozturk E.**, Basar E., Cirpan H. A., 2018. Multiple-Input Multiple-Output Generalized Frequency Division Multiplexing with Flexible Index Modulation. PCT Patent Application Number: PCT/TR2018/050341.

OTHER PUBLICATIONS, PRESENTATIONS AND PATENTS:

- Kazoglu A., **Ozturk E.**, Aydin O., 2018. Combining GPS and GLONASS Range Observations for Joint Position, Velocity and Time Calculation. *18th Mediterranean Microwave Symp. (MMS'18)*, October 31-November 2, 2018, Istanbul, Turkey.

- Aydin T., Aydin O., **Ozturk E.**, Ozdemir V., 2018. RF Front End and Baseband Integration Considerations for Single Board GNSS Software Defined Receivers. *18th Mediterranean Microwave Symp. (MMS'18)*, October 31-November 2, 2018, Istanbul, Turkey.

- Kazoglu A., Balsuzen S., **Ozturk E.**, Aydin O., 2018. Clocks Source Effects on Sinyal Tracking for Software Defined Global Navigation Satellite System Receivers. *Electrical, Electronics and Biomedical Engineering Conf. (ELECO'18)*, November 29-December 1. 2018, Bursa, Turkey.

- Mercan M. S., **Ozturk E.**, 2013. Through Wall Imaging Based on MIMO UWB Radar With A Fast Image Reconstruction Method. *10th European Radar Conf. (EuRAD'13)*, October 9-11, Nurnberg, Germany.

- Eren K., **Ozturk E.**, Cirpan H. A., 2013. Bayesian Learning Approach For Sparse Channel Estimation in IEEE 802.11p Based V2V Communication Systems. *9th Int. Conf. on Technical and Physical Problems of Electrical Engineering (ICTPE'13)*, September 9-11, 2013, Istanbul, Turkey.

- Mercan M. S., Caliskan A., **Ozturk E.**, 2013. Through-Wall Imaging with MIMO UWB Radar. *21th Signal Processing and Communications Applications Conf. (SIU'13)*, April 24-26, 2013, Haspolat, Turkey.

- **Ozturk E.**, Atli A. V., Mercan S. M., Caliskan A., Erer I. Y., 2012. Clutter Reduction Methods in Ultra Wideband (UWB) Radar and Time-Performance Evaluation on ARM Processors. *20th Signal Processing and Communications Applications Conf. (SIU'12)*, April 18-20, 2012, Mugla, Turkey.

- Mercan M. S., Atli A. V., **Ozturk E.**, 2012. A Through-Wall Imaging Approach Based on Ultra Wideband Radar", 20th Signal Processing and Communications Applications Conf. (SIU'12), Apr. 2012, Mugla, Turkey.

- Atli A. V., **Ozturk E.**, 2011. Non-invasive Respiratory Motion Tracking Using M-Sequence UWB Radar. *3rd Int. Cong. on Ultra Modern Telecommunications and Control Systems and Workshops (ICUMT'11)*, October 5-7, 2011, Budapest, Hungaria.

- **Ozturk E.**, Acikgoz A. U., 2010. Fault Sensing and Recovering Tools for Real-Time Embedded Systems. *2nd Symp. on Software Quality and Software Development Tools*, December 2010, Istanbul, Turkey.

- **Ozturk E.**, Aygolu U., 2001. A Combined Interleaving Technique for Trellis Coded MPSK Systems in Rayleigh Fading Channels. *Wireless Personal Communications*, 16(3), 245-247.

- **Ozturk E.**, Aygolu U., 1998. A Combined Interleaving Technique for Trellis Coded Systems. *6th Signal Processing and Communications Applications Conf. (SIU'98)*, May 1998, Ankara, Turkey.

- **Ozturk E.**, Ozerdogan G., Karadeniz M., 2016. A Generalized Monitoring Method for Embedded Systems", Turkish Patent Institute (TPE) Patent Pending, File No: 2016/16200.

- **Ozturk E.**, Asagidag F., 2016. An Efficient Message Distribution Method for Embedded Software Applications. Turkish Patent Institute (TPE) Patent Pending, File No: 2016/14552.

- **Ozturk E.**, Pataci M., Cetinkaya A. C., 2016. A Buffer Tracing Method for Embedded Software Applications. Turkish Patent Institute (TPE) Patent Pending, File No: 2016/14510.

- **Ozturk E.**, Kirkil A., 2016. A Software Deadlock Detection Method for Embedded Systems. Turkish Patent Institute (TPE) Patent Pending, File No: 2016/15171.

- **Ozturk E.**, Kazoglu A., Pataci M., Tuncay S., 2014. A Detection Method For Frequency Synchronization in RF Communication Systems. Turkish Patent Institute (TPE) Patent Pending, File No: 2014/11774.

- **Ozturk E.**, Kazoglu A., Pataci M., Tuncay S., 2014. A Method for Local Carrier Look-Up Table Generation. Turkish Patent Institute (TPE) Patent Pending, File No: 2014/13500.

- **Ozturk E.**, Kazoglu A., Pataci M., Tuncay S., 2014. A Detection Method for Symbol Synchronization. Turkish Patent Institute (TPE) Patent Pending, File No: 2014/11141.

- **Ozturk E.**, Koc B. Y., Acikgoz A. U., Kazoglu A., Caliskan A., Zavalsiz S., 2013. Through The Wall Imaging Method. Turkish Patent Institute (TPE) Patent Pending, File No: 2013/11497.